Plant Glucosylceramides and Mosquito Repellent Essential Oils Loaded Nano Carriers for Topical Applications: Formulation, Optimization and *In Vitro* Release Studies

A Dissertation Presented in Partial Fulfillment of the Requirements for the Degree of Doctor of Philosophy (PhD) in Pharmaceutics

Admassu Assen Adem (B.Pharm, MSc. Pharmaceutics)

Advisors: Prof. Dr. Tsige Gebre-Mariam
Prof. Dr. Dr. h.c. Reinhard H.H. Neubert
Dr. Anteneh Belete

September, 2023

Addis Ababa, Ethiopia

Addis Ababa University

College of Health Sciences, School of Pharmacy

Department of Pharmaceutics and Social Pharmacy

PhD Program in Pharmaceutics

Plant Glucosylceramides and Mosquito Repellent Essential Oils Loaded Nano Carriers for Topical Applications: Formulation, Optimization and *In Vitro* Release Studies

A PhD Dissertation submitted to the Department of Pharmaceutics and Social Pharmacy, School of Pharmacy, College of Health Sciences, Addis Ababa University, Presented in Partial Fulfilment of the Requirements for the Degree of Doctor of Philosophy (PhD) in Pharmaceutics

By: Admassu Assen Adem (B.Pharm, MSc. Pharmaceutics)

Advisors: Prof. Dr. Tsige Gebre-Mariam

Prof. Dr. Dr. h.c. Reinhard H.H. Neubert

Dr. Anteneh Belete

September, 2023

Addis Ababa, Ethiopia

Addis Ababa University

School of Pharmacy, College of Health Sciences

Department of Pharmaceutics and Social Pharmacy

Approval by the examining board

This is to certify that the Dissertation titled 'Plant Glucosylceramides and Mosquito Repellent Essential Oils Loaded Nano Carriers for Topical Applications: Formulation, Optimization and *In Vitro* Release Studies' is prepared by Admassu Assen Adem, and submitted in partial fulfilment of the requirements for Doctor of Philosophy (PhD) in Pharmaceutics, and complies with the regulations of the University and meets the accepted standards with respect to originality and quality.

Examiners:

External Signature: _____ Date: _____

Internal Signature: _____ Date: _____

Advisors:

Prof. Dr. Tsige Gebre-Mariam Signature: _____ Date: ____

Prof. Dr. Dr. h.c. Reinhard H.H. Neubert Signature: _____ Date: ____

Dr. Anteneh Belete Signature: _____ Date: _____

_____

Chair of Department or Graduate Program Coordinator

Declaration of academic integrity

With this statement I declare that I have independently completed the above PhD Dissertation titled 'Plant Glucosylceramides and Mosquito Repellent Essential Oils Loaded Nano Carriers for Topical Applications: Formulation, Optimization and *In Vitro* Release Studies'. The thoughts taken directly or indirectly from external sources are properly marked as such. This Dissertation was not previously submitted to another academic institution and has also not yet been published elsewhere.

Admassu Assen Adem _____

Addis Ababa, Ethiopia

September, 2023

Dedicated to my Father, Assen Adem Shifaw

Acknowledgments

First and for most, thanks to the Almighty God, for his mercy and righteousness in helping me to complete this PhD research work.

I would like to extend my heartfelt gratitude and appreciation to my advisor Prof. Tsige Geber-Mariam, for his scientific guidance, constructive comments and support he provided me with throughout the research work. I always remain grateful to you for providing me the chance to join the DAAD funded TRI-Sustain project and also covering my two months research stay in Germany from your Alexander von Humboldt research award fund (Georg Forster Research Award).

I am indebted to my advisor Prof. Reinhard Neubert for supervising the work, hosting me in his laboratory and connecting me to a number of experts in different departments of Martin-Luther University during my stay at IADP/Skinomics, Martin-Luther University (MLU), Halle (Saale), Germany. The work would not be possible without your involvement.

My countless appreciation goes to my advisor Dr. Anteneh Belete, for his scientific guidance, constructive feedbacks and support he provided me with throughout the research work.

Prof. Peter Imming and Dr. Lucie Mueller are acknowledged for facilitating my stay in Germany as part of the Tri-Sustain project. I would like to express my heartfelt gratitude to Prof. Imming for providing me an office to stay and allow me work in his lab during the COVID-19 close down. 'AG Imming' members are also acknowledged for their kind support whenever needed, special thanks go to Markus.

I am thankful to Dr. Andrej Frolov and Ms. Alena Soboleva, Leibniz Institute of Plant Biochemistry, for conducting LC-HRMS experiment of plant GlcCERs. Dr. Gerd Hause, Biozentrum, MLU, Dr. Albrecht Petzold, Institute of Physics, MLU, and Ms. Heike Rudolf, Institute of Pharmacy, MLU, are acknowledged for taking TEM images of the nanoemulsions, viscosity measurements and FTIR spectrometric analysis, respectively. I always remain thankful to Ms. Anke Nies, Ms. Claudia Bruneh and Dr. Fabio Strati for their excellent technical assistance and supports.

Prof. Dr. Johannes Wohlrab is acknowledged for his scientific contribution in the work and allowing his lab to perform skin homogenate hydrolysis experiment.

My special thanks go to Prof. Kaleab Asres and Dr. Julia Chuttke for their kind support in getting essential oils, and facilitating FTIR analysis, respectively.

I greatly acknowledge the financial support provided by TRI-Sustain Project (funded by the German Academic Exchange Service (DAAD) and Federal Ministry of Education and Research (BMBF)). CDT-Africa is also acknowledged for the financial support to cover my two months research stay at IADP/Skinomics, Germany. Addis Ababa University and Wollo University are acknowledged for sponsoring my PhD study.

I would like to thank members of IADP/Skinomics, MLU, Halle-Wittenberg, Germany.

Dr. Efrem Nigussu, is appreciated for making my stay in IADP/Skinomics, MLU, Halle (Saale) lively and fruitful.

I would like to thank Department of Pharmaceutics and Social Pharmacy, School of Pharmacy and all the staffs for their support throughout the study. Special thanks goes to Dr. Nisha M. Joseph, Mr. Abrham Temesgen and Mr. Muluken Nigatu for sharing me their office and to Dr. Bruck Messele for his kind support.

I am grateful to Wondim Melkam and Hana for their kind and unreserved support during lupin seed and plant collection.

Ethiopian Agricultural Institute, Holleta Research Center and Amhara Research Institute, Kemisse Research Center are acknowledged for supplying naked barley seed and mung bean plant for botanical identification, respectively.

Prof. Anna Dailey and her group are acknowledged for allowing me lab access and assisting me when a need arises.

Prof. B. Junker and Dr. Manish Raorane are acknowledged for providing me lab access to perform GC-MS analysis of essential oils and providing me excellent technical assistance during the experiment.

I am indebted to my whole family for their kind support, encouragement and understanding throughout this study. My beloved wife Seada Endris and My lovely children Harun and Yunus, are appreciated for scarifying their family time. My wife gave up her professional career for me. I thank you for being in my life.

Title

Plant Glucosylceramides and Mosquito Repellent Essential Oils Loaded Nano Carriers for Topical Applications: Formulation, Optimization and *In Vitro* Release Studies

Admassu Assen Adem,
Addis Ababa University; September 2023.

Abstract

Skin protects the body against the invasion of external pathogens, allergens, and chemical substances. It is considered that most of the skin barrier function resides in the epidermis, particularly in its outermost layer, *stratum corneum* (SC). The SC is composed of corneocytes embedded in a lipid-enriched intercellular matrix. Ceramides (CERs), free fatty acids (FFAs), and cholesterol are the major components of the lipid matrix in an approximately 1:1:1 molar ratio. The unique molecular organization and the equi-molar ratio are considered crucial in barrier function and semipermeable nature of the SC. Compositional and organizational changes in SC lipids such as CERs cause defective skin barrier function in relation with ageing and skin disorders partly due to altered enzymatic activity. However, the glucocerebrosidase enzyme responsible for the conversion of glucosylceramides (GlcCERs) to CERs is not affected by ageing. It has been shown that direct topical replacement of depleted native skin CERs has beneficial effects in improving skin barrier function and skin hydration. CERs are obtained from animal, plant and synthetic sources. Plants are more reliable sources of CERs, as animal and synthetic CERs have safety/ethical issues and affordability challenge, respectively. Though plants are preferred, most of the plant sphingolipids (SPLs) are available in a complex form with a polar head group attached to the CERs. It requires an economical and effective method of hydrolysis to produce CERs from dominant SPLs such as GlcCERs. Moreover, the poor solubility and permeability of CERs on top of normal SC barrier property make the delivery of topical CERs challenging using conventional formulations.

While GlcCERs/CERs are intended to be delivered to the upper layer of the skin, the present study also considered formulating essential oils having mosquito repellent activity for topical application. The mosquito repellent potential of plant materials has been exploited for centuries using different means, including applying essential oils on the skin

and clothes to combat transmission of malaria. However, due to the volatile nature of essential oils, the protection against mosquitoes is short-lived.

Therefore, the objectives of this PhD work were to explore potential GlcCER plant sources, investigate suitable chemical and enzymatic methods of hydrolysis of plant GlcCERs into CERs and develop an optimized nanoemulgel formulation for topical delivery of the plant GlcCERs as well as to formulate citronella oil (CO) (*Cymbopogon nardus)* and palmarosa oil (PO) (*C. martini)* in the form of nanoemulgel (NEG) to delay the volatility of the essential oils upon application.

GlcCERs were isolated from lupin bean (*Lupinus albus*), mung bean (*Vigna radiate*) and naked barley (*Hordium vulgare*). The GlcCERs were identified using ultra high-performance liquid chromatography hyphenated with atmospheric pressure chemical ionization-high resolution tandem mass spectrometer (UHPLC/APCI-HRMS/MS) and quantified with validated automated multiple development-high performance thin layer chromatography (AMD-HPTLC) method. The GlcCERs were hydrolyzed into CERs with mild acid hydrolysis (0.1N HCl) following treatment with an oxidizing agent, $NaIO_4$, and reducing agent, $NaBH_4$. After securing ethical clearance, excised human skin was employed to investigate the enzymatic hydrolysis of plant GlcCERs. Homogenized epidermis in citrate phosphate buffer was incubated with lupin GlcCERs. The total lipid was extracted with MeOH/$CHCl_3$/H_2O solvent mixture and the unhydrolyzed lupin GlcCERs in the extract was quantified using a UHPLC-QqQ-MS/MS method in MRM (multiple ion reaction monitoring) mode (*m/z* 714.5 →696.54→ 262.25). Formulations of GlcCERs were developed for topical delivery. The Nanoemulsion (NE) components were screened and pseudo-ternary phase diagrams were constructed at different hydrophilic-lipophilic balance (HLB) values of surfactant-co-surfactant mixture (S_{mix}). Extreme vertices mixture design was developed to investigate the impact of percentage compositions of the independent variables; oil mixture (2-3%), S_{mix} (15-18%) and aqueous component (79-83%) on the globule size of the NEs. NEG was prepared from optimized 0.25% lupin GlcCER NE and Carbopol 980 gel. The membrane penetration depths of GlcCERs loaded optimized NEs and NEGs were measured.

NE for both essential oils were also prepared using ultrasonication technique following suitable HLB selection of S_{mix} and phase diagram development. NEGs were formulated by mixing NEs and Carbopol 934 gel. Physicochemical characterizations, including i*n vitro* release and permeation studies were carried out. The Gas chromatography hyphenated mass spectrometry method for identification and quantification of essential oils was validated.

GlcCERs with 4,8-sphingadienine, 8-sphingenine and 4-hydroxy-8-sphingenine sphingoid bases linked with C14 to C26 α-hydroxylated FAs were identified from all the three plants. Single GlcCER (*m/z* 714.5520) was dominant in lupin and mung beans, while five major GlcCERs species (*m/z* 714.5520, *m/z* 742.5829, *m/z* 770.6144, *m/z* 842.6719 and *m/z* 844.56875) were obtained from naked barley. The GlcCERs contents of the three plants were comparable. However, lupin bean contained predominantly a single GlcCER (*m/z* 714.5520). CER species bearing 4,8-sphingadienine and 8-sphingenine sphingoid bases attached to C14 to 24 FAs were found after mild acid hydrolysis. CER species with *m/z* 552.4992 was the main component in the beans while CER with *m/z* 608.5613 was dominant in the naked barley. However, CERs with 4-hydroxy-8-sphingenine sphingoid base were not detected with UHPLC-HRMS/MS. Following skin enzyme hydrolysis investigation, the characteristic signals of GlcCER fragments (*m/z* 696.54, 552.49 and 534.48) due to in-source fragmentation were detected in the MS spectra of the skin extract. The MS2 fragmentation of the dominant fragment (*m/z* 696.54) ion provided the target product ion (*m/z* 262.25) which was integrated to quantify GlcCER. The LC-MS method was selective, precise and accurate. It was also free from matrix and carryover effects. The unhydrolyzed lupin GlcCER amount decreased with time suggesting hydrolysis of GlcCERs by the skin enzymes. An optimized NE formulation was prepared. The HLB values of 13.5 and 12 provided broader NE regions for Miglyol and isopropyl myristate, respectively. The analysis of variance of the quadratic model showed suitability of the model with R^2 of 99.80% and non-significant lack of fit (F value= 17.06). The optimized percentage compositions of oil phase, S_{mix} and aqueous phase were 2.15%, 16.39% and 81.46%, respectively, with predicted globule size of 23.96 nm. Accordingly, the optimized NE globule size, polydispersity index and zeta potential were 23.93 ± 0.25 nm, 0.069 ± 0.017 and 23.95± 1.20 mV, respectively. The oil globules were spherical and distributed

uniformly without aggregation. The NE exhibited Newtonian flow with a viscosity of 6.75 mPa.s, while NEGs showed non-Newtonian flow with shear thinning property. The amount of lupin GlcCER released and penetrated into each model membrane layer at different time points was in the order of NEs > basic cream > NEGs. After 180 min, 51%, 84% and 96% of lupin GlcCER was released and penetrated into the model membrane layers from NEG, basic cream and NEs, respectively.

The formulation developed for the topical application of essential oils employed CO and PO as the oil components. Tween 80, Transcutol P and distilled water with 40% glycerol were selected as surfactant, co-surfactant and aqueous components of the NE, respectively. HLB values of 11 and 12 were found to be appropriate for CO and PO NEs preparation, respectively. Clear CO and PO NEs with an average globule size of 131.34 nm and 120.77 nm, respectively, were obtained. The NEG preparations of both essential oils were kinetically stable, and the formulation components were chemically compatible with each other.

In conclusion, considering affordability, GlcCER content and yield, lupin bean would be the preferred alternative commercial source of GlcCERs. The mild acid hydrolysis method is economical and effective, mainly for plant GlcCERs carrying dihydroxy sphingoid bases. Plant GlcCER hydrolysis in skin homogenate, being investigated for the first time, the findings pave the way for a new mode of skin barrier function enhancement modality. Taking into account the drawbacks of animal and synthetic CERs on top of enzymatic and chemical methods of plant GlcCER hydrolysis limitations, topical administration of plant GlcCER to enhance skin barrier function would be the preferred alternative. The NEG formulation developed for dermal delivery of lupin GlcCERs prolonged the release and slowed down the penetration of GlcCER into the multilayer membrane model which is crucial to limit its penetration into the epidermal skin layer. Therefore, NEGs could be considered as an option for the delivery of plant GlcCER into the upper part of the skin after further *ex-vivo* investigation, as the study is the first of its kind.

Regarding formulations of the essential oils, NEGs prolonged the release of both CO and PO up to 24 h and significantly reduced the percentage permeation via cellulose acetate

membrane as compared to NEs. Therefore, NEG could be an alternative formulation to prolong the mosquito repellent effect of essential oils.

Key Words: Ceramide, Glucosylceramide, *Lupinus albus*, *Vigna radiate*, *Hordium vulgare*, Mild acid hydrolysis, Enzyme hydrolysis, LC-HRMS/MS, Structural characterization, Method validation, Topical delivery, Nanoemulsion, Nanoemulgel, Optimization, Extreme vertices mixture design, Mosquito repellent, Essential oil, *Cymbopogon nardus, Cymbopogon martini*, Ultrasonication.

Table of Contents

Acronyms and abbreviation

AD	Atopic Dermatitis
AFP	Atomic Force Microscope
AMD	Automated Multiple Development
APCI	Atmospheric Pressure Chemical Ionization
CER	Ceramide
CID	Collision Induced Dissociation
d18:0	dihydrosphingosine
d18:1	8-sphingenine
d18:2	4, 8-sphingadienine
DEET	N, N-diethyl-3-methylbenzamide
DHCer	Dihydroceramide
DLS	Dynamic Light Scattering
DMSO	Dimethyl sulfoxide
DS	Dihydrosphingosine
ELSD	Evaporative Light-Scattering Detection
ESI	Electrospray Ionization
FDA	Food and Drug Authority
FFA	Free Fatty Acid
FT-ICR	Fourier Transform-Ion Cyclotron Resonance,
FTIR	Fourier Transform Infrared
GC-MS	Gas Chromatography Coupled with Mass Spectrometer
GIPC	Glycosyl Inositolphosphoceramides
GlcCER	Glucosylceramide
GRAS	Generally Regarded as Safe
h16:0	α-hydroxy palmitic acid
h18:0	α-hydroxy stearic acid
h20:0	α-hydroxy arachidic acid
h24:0	α-hydroxy lignoceric acid
h24:1	α-hydroxy nervonic acid

HLB	Hydrophilic-Lipophilic Balance
HPH	High Pressure Homogenizers
HPTLC	High Pressure Thin Layer Chromatography
IRS	Indoor Residual Spray
ITN	Insecticide Treated Net
LCB	Long Chain Base
LC-MS	Liquid Chromatography Coupled with Mass Spectrometer
LIT	Linear Ion Trap
LLIN	Long-Lasting Insecticide Treated Net
LOD	Limit of Detection
LOQ	Limit of Quantification
MALDI	Matrix Assisted Laser Desorption Ionization
MS	Mass Spectrometer
MS/MS	Tandem Mass Spectrometry
NE	Nanoemulsion
NEG	Nanoemulgel
O/W	Oil-in-Water
PCS	Photon Correlation Spectroscopy
PDI	Poly Dispersity Index
PhytoCER	Phytoceramide
RPLC	Reversed-phase liquid chromatography
SAA	Surface Active Agents
SB	*Stratum Basale*
SC	*Stratum Corneum*
SD	4, 14-sphingadiene
SEM	Scanning Electron Microscope
SG	*Stratum Granulosum*
S_{mix}	Surfactant Mixture
SPL	Sphingolipid
SPT	Serine Palmitoyl-Transferase
SS	*Stratum Spinosum*

t18:1	4-hydroxy-8-spingenine
TEM	Transmission Electron Microscope
TLC	Thin Layer Chromatography
TOF	Time of Flight
UHPLC	Ultra High Performance Liquid Chromatography
W/O	Water-In-Oil

List of figures

List of tables

1 Introduction

1.1 The human skin

The skin is the largest organ of the body composed of three main layers, the hypodermis, the dermis and the epidermis. It mainly works as a permeability barrier that protects against the invasion of external pathogens, allergens, and chemical substances and prevents the loss of water and electrolytes from the body. It also plays a crucial role in thermoregulation, inflammatory and immune responses, and sensations of pain and touch [1–3]. The hypodermis contains blood vessels and adipocytes which is mainly responsible for thermoregulation and storage of energy. The dermis is composed of a vascular and nerve plexuses together with a fibroblasts and immune cells imbedded in a collagen and elastic fibers. The epidermis consists of four layers, the inner most layer, *stratum basale* (SB), the *stratum spinosum* (SS), the *stratum granulosum* (SG) and the *stratum corneum* (SC). It is considered that most of the skin barrier function resides in the epidermis, particularly in its outermost layer, *stratum corneum* (SC) [4,5].

The SC is composed of approximately 15-25 layers of protein-enriched flattened dead cells, corneocytes, embedded in a lipid-enriched, intercellular matrix. The corneocytes are surrounded by a cornified cell envelope made up of proteins, mainly loricrin and involucrin, and covalently bound to the hydroxyceramide molecules of a lipid envelope [6]. The lipids matrix, which accounts for about 15% of the SC weight, contains ceramides (CER), free sterols and sterolesters, cholesterol sulfate, and free fatty acids (FFA). Ceramides, FFAs and cholesterol are the major components in an approximately 1:1:1 molar ratio. The unique molecular organization into a bilayer units with alternating electron-dense and electron-lucent lamellae and the equimolar ratio are considered to be crucial in barrier function and semipermeable nature of the SC [7–9].

FFAs in the skin barrier are 14-34 carbons long, mostly saturated and unbranched. They mainly consist of palmitic (C16:0), stearic (C18:0), oleic (C18:1ω9), behenic (C22:0), lignoceric (C24:0) and cerotic (C26:0) acids. The last two species comprise approximately 50% of the SC FAs. Unsaturated and shorter FAs are available in the SC lipid membranes in minor quantities [8]. The primary sterol found in the SC is cholesterol (27%), though a

significant level of cholesterol esters (10%) and cholesterol sulfate (3%) are also observed [10].

1.1.1 Skin ceramide

CERs are a structurally heterogeneous and complex group of sphingolipids (SPLs) with a relatively small polar head that do not extensively hydrate. CER is composed of a long chain base (LCB) linked to a FA via an amide bond [2]. The structure of LCBs and FAs are depicted in Fig.1-1. There are five types of LCBs: dihydrosphingosine (DS), sphingosine (S), phytosphingosine (P), 6-hydroxysphingosine (H), and 4, 14-sphingadiene (SD). The Sphingosine and dihydrosphingosine bases are common in eukaryotic cells while phytosphingosine is found only in some human tissues. The 6-hydroxysphingosin and 4,14-sphingadiene are epidermis specific and recently identified bases, respectively [2,8]. The FA of human CERs are also four types: nonhydroxy (N), α-hydroxy (A), ω-hydroxy (O), and esterified ω-hydroxy (EO) FAs. Both the LCBs and FAs differ in their number and position of hydroxyl group, carbon chain length and degree of unsaturation [11,12].

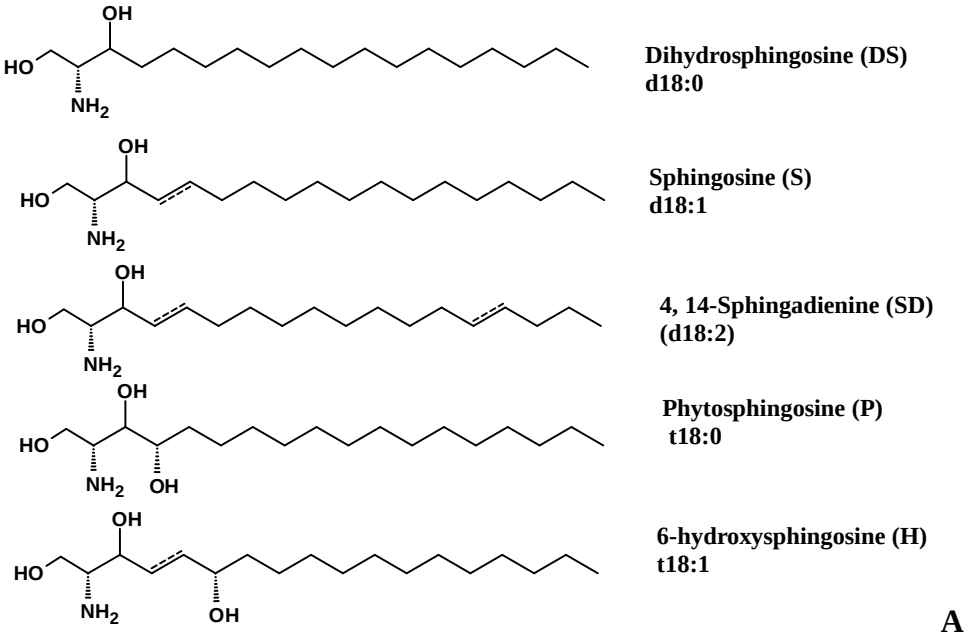

A

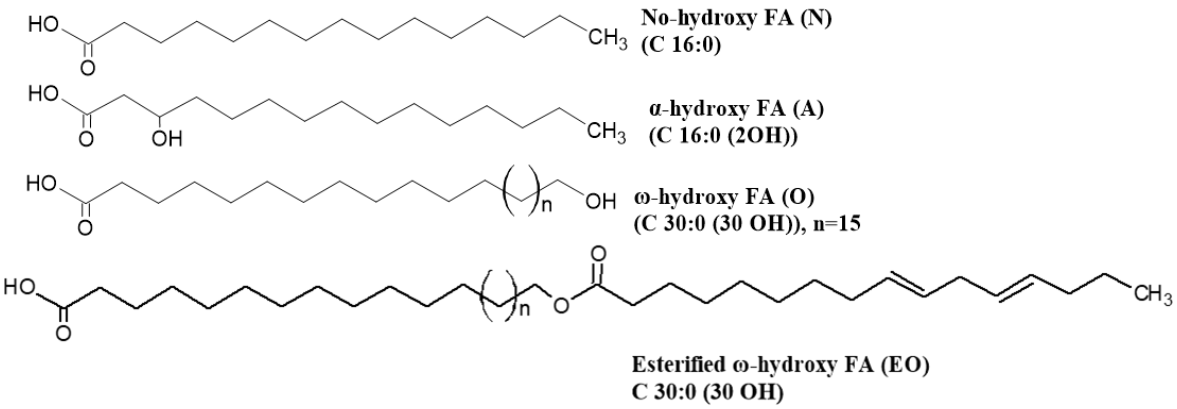

B

Figure 1-1: Structures of human CER LCBs (A) and FAs (B) [2]

There are currently 21 classes of human SC free CERs classified based on the combination of LCB and FA [2,8,13]. Each CERs class is represented using the abbreviations of its type of LCB and FA. The nomenclature of the CERs is presented in Table 1-1. It has also been reported that the CERs LCBs in the SC range from C16 to 26 of which C18 (28.6%) is the most abundant, followed by C20 (24.8%) and C22 (12.8%). The most abundant SC CER classes are NP (29.4%), NH (23.4%), NDS (11.3%), AH (9.1%), and EOS (7.7%) [2] while SD-type CERs levels are quite low (0.4%). [13].

Table 1-1: Nomenclature of human SC CER classes represented by a combination of their FA and LCB abbreviations.

LCB / FA	Dihydro-sphingosine (DS)	Sphingosine (S)	Phytosphingosine (P)	6-hydroxy-sphingosine (H)	4,14 Sphingadiene (SD)
Non-hydroxy (N)	NDS	NS	NP	NH	NSD
α-hydroxy (A)	ADS	AS	AP	AH	ASD
β-hydroxy (B)	-	BS	-	-	-
ω-hydroxy (O)	ODS	OS	OP	OH	OSD
Esterified ω-hydroxy (EO)	EODS	EOS	EOP	EOH	EOSD

1.1.1.1 Synthesis and organization

CERs and other skin SPLs are formed following the *de novo* synthesis or breakdown of a complex SPLs (salvage) pathways. The *de novo* pathway starts from the condensation of serine and palmitoyl CoA to form 3-ketodihydrosphingosine catalyzed by serine palmitoyltransferase (SPT) in the endoplasmic reticulum (ER) of a viable epidermis keratinocytes [14]. The reaction product is reduced, desaturated and acylated by 3-Keto-dihydrosphingosine reductase, dihydroceramide desaturase and ceramide synthases, respectively to provide CERs. CERs are then transported from the ER to the Golgi apparatus where they are converted to their polar precursor such as sphingomyelins and GlcCERs. The CER precursors are stored in lamellar granules together with catabolic enzymes. At the SG/SC interface, the lamellar granules migrate to the keratinocyte upper surface, merge with plasma membrane, and secrete their contents into the intercellular space. The enzymes, such as acid sphingomyelinase and beta-glucocerebrosidase are activated and convert sphingomyeline and GlcCERs into CERs, respectively [8,15].

CERs with other SC lipids form a periodic sheet of lipid lamellae. There are two forms of lamellar phases, short and long-periodicity phase, with a periodicities of ~6 and ~13 nm, respectively [16]. Within the lipid lamellae, the lipids are arranged in three types of lateral packing arrangements which differ in their rotational and translational mobilities[17]. The orthorhombic packing does not allow rotational or translational mobility as the lipid chains are organized in a rectangular crystalline lattice. The hexagonal packing allows some rotational mobility along their long axes with restricted translational mobility. The liquid-crystalline phase does not have lateral organization and the chains have both high rotational and high translational mobility [18]. The skin barrier lipids form an orthorhombic lattice with the exception of the most superficial layers in which hexagonal packing has been observed [8,10]. It has been reported that a tight orthorhombic packing is crucial in maintaining the permeability barrier of the SC and absence of proper lamellar organization has a greater impact on the skin barrier function [2,19–22].

1.1.2 Common skin disorder

Skin disease has an enormous impact on the health sector globally. It has been reported that skin diseases were the fourth leading cause of morbidity in 2010. Eczema (atopic

dermatitis) and psoriasis are the common skin diseases exhibiting skin barrier defect partly associated with SC CERs composition or organization problems, the former being among the top 50 globally [23,24].

1.1.2.1 Atopic dermatitis

Atopic dermatitis (AD) (also referred to as atopic eczema) is chronic, relapsing, inflammatory skin disorder characterized by dry skin, pruritus, increased total epidermal water loss, and decreased skin barrier function. Though, the pathogenesis of AD is not completely clear, complex interaction between skin barrier defect, infectious agents, and immune dysregulation contribute for the disorder [25]. It has been indicated that skin barrier problem in AD patients is associated with filaggrin gene mutation and epidermal lipid matrix composition and organizational disturbance [26]. A total amount of CERs and CERs to free sterols ratio decrease in SC of AD patients compared to healthy subjects. CERs (1and 3) and cholesterol are the most significantly reduced and increased SC lipids of AD patients, respectively[27]. The lateral and lamellar SC lipid organization are also changed as less lipids adopt orthorhombic packing while more lipids possess hexagonal packing [17].

1.1.2.2 Psoriasis

Psoriasis is a chronic inflammatory skin disease with a complex pathogenesis involving genetic, immune and environmental factors, and abnormal epidermal proliferation [28]. Impaired skin barrier function following disturbed process of keratinization is manifested[29]. Studies showed that lipids compositions and enzymatic expressions are affected in the SC of psoriatic patients. The percentage of a long chain CERs (NH and NP) with C24 or C26 FAs and ratio of CER NP to NS decreased in the SC of psoriatic patients [30,31]. Another report also inidcated that CER (AP), CER (NP) and CER (EOS) were reduced in 27%, 66% and 40%, respectively due to posriasis compared to normal skin [29]. The expression level of ceramide synthase 3 and activity of sphingomyelinase were reduced [31,32] and the level of ceramide synthesis was inversely correlated with the severity of mild to moderate psoriasis [33].

1.2 Plant sphingolipids

SPLs are an important structural membrane constituent of plants like other eukaryotes. They are also biologically active, involved in a number of activities such as in programmed cell death, signal transduction and response to low temperature and pathogen attack [34]. Free LCBs, CERs, glycosylceramides and glycosyl inositolphosphoceramides (GIPCs) are the main classes of plant SPLs. The chemical structure of LCBs, CERs and glycosylceramides are presented in Fig.1-2. Glycosylceramides are the predominant SPL in some plants [35] while free CERs are available in trace quantity. It is estimated that the CERs content of plant tissues is 10-20% of the glycosylceramides content [35–37].

The LCBs in plants are predominantly C18 amino alcohol characterized by the presence of a hydroxyl group at C1 and C3, an amine group at C2 and double bonds in the C4 or C8 positions (Fig. 1-2). The C4 double bond is found only in the *trans* configuration, while the C8 double bond can be found in either the *trans* or *cis* configurations. The C8-unsaturated LCBs are only found in plants [38,39]. The short hand notation of LCBs indicates the number of carbon, hydroxyl groups (d: 1, 3 dihydroxy, t: 1,3, 4 trihydroxy), the geometry and position of double bonds (E: trans, Z: cis) [40]. A LCB with 18 carbon containing 3 hydroxyl group and a double bond at C8 position in *cis* geometry is represented as $t18:1^{8}$. Plant SPLs LCBs are comprised of 4-hydroxysphinganine (t18:0) (phytosphingosine), (8E/Z)-4-hydroxy-8-sphingenine (t18:1), sphinganine (dihydrosphingosine) (d18:0), (E/Z)-sphing-8-enine (d18:1), 4-sphingenine (sphingosine) (d18:1) and 4,8-sphingadienine (d18:2) [34,36,41].

CER is the resulting molecule when a LCB is acylated at the 2-amino position and linked via an amide bond to a long-chain FA. Thus, N-acyl-sphingosine gives CERs, N-acyl-sphinganine gives dihydroceramide (DHCer), and 4-hydroxylated DHCer produces phytoceramide (phytoCER) [42]. The long chain FAs bonded to the LCB might be nonhydroxy FA, α-hydroxy FA or esterified ω-hydroxy FA, resulting in different CER subclasses. The basic CER structure can be further modified through changes in chain length, methylation, hydroxylation and/or degree of desaturation of both the LCB and FA moieties. Covalent linkage of the 1-hydroxyl group of CERs to a polar head group results in a complex SPLs which can be a phosphoryl group (ceramide-phosphates), mono- or

pluri-hexose (glycosphingolipids), and an inositol-phosphate group (IPC) (Fig.1-2) [40,43]. Most (90%) SPLs in plants are in a 'complex' form with a polar head group [44].

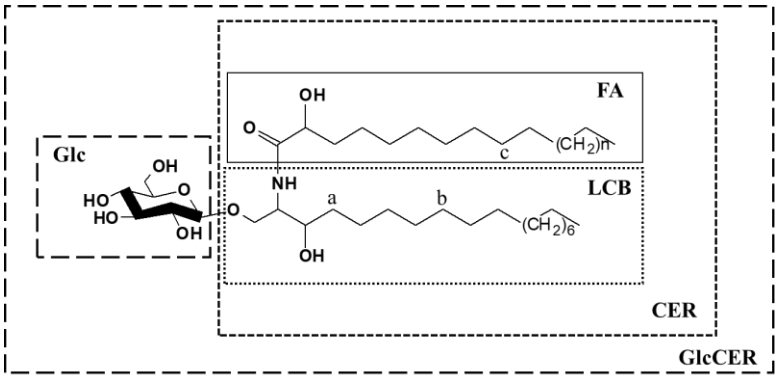

Figure 1-2: Chemical structure of plant SPLs LCB, CERs and GlcCERs.

Depending on the types of CERs, the LCBs are modified at C4 with hydroxyl group or double bond (a) and/or double bond at C8 (b). The FA chains can also be modified at C9 with double bond (c).

The simplest glycosphingolipid in plants is the GlcCER with a single glucose polar head group [45]. d18:1, t18:1, and d18:2 are the predominating LCBs in plant glycosylceramides. Plant glycosylceramides FAs are almost exclusively α -hydroxylated and vary in chain length from C14 to C26 with C16, C20, C22 and C24 FAs as major components. Saturated FAs predominate in plant glycosylceramides, whereas n-9 monounsaturated very long chain FAs from C22 to C26 occur in low amounts. The sugar moiety found in plant glycosylceramides is usually D-glucopyranose in β linkage to the C-1 hydroxy group of the SB. However, mannose can also be attached to the CER backbone, and higher homologues with up to four sugars as a linear chain were isolated from cereals [46–48].

1.2.1 Synthesis

SPLs can be formed following two pathways: the *de novo* and the salvage pathways [37]. The *de novo* synthesis begins in the endoplasmic reticulum (ER) with condensation of serine and palmitoyl-CoA by serine palmitoyl-transferase (SPT) to 3-ketosphinganine. The product is then reduced by ketosphinganine reductase (KSR) to sphinganine (d18:0) which is the simplest LCB in plants and other eukaryotes. In the modification process LCB

hydroxylase and desaturase enzymes are involved [48] which likely act before CER synthesis and on a more complex SPLs [36]. Addition of hydroxyl at C-4 produces the trihydroxy LCB, phytosphingosine (t18:0). LCBs may also be unsaturated to produce dihydroxy or trihydroxy LCB [34]. Sphinganine may also be phosphorylated to form sphinganine-1-phosphate; or hydroxylated to form 4-hydroxysphinganine [39].

CERs are formed from the LCBs following either using acyl-CoA as the acyl donor catalyzed by sphinganine N- acyltransferase or employing free FAs catalyzed by ceramide synthase [39,41]. The CERs can then be modified by addition of simple or multiple sugars at the C1 position to form complex SPLs such GlcCERs catalyzed by glucosylceramide synthase [47]. They can also be used as substrates for the synthesis of ceramide phosphates [49]. The salvage pathway include degradation of SPLs such as GlcCERs and CERs leading to the formation of CERs, free LCBs, FAs, sugar etc [36,37,48].

1.2.2 Extraction techniques

Extraction of plant SPLs is a complex process due to the presence of other lipid molecules such as sterols and triglycerides. Thus, it requires implementing suitable techniques depending on the sample type and complexity. In general, the protocol for this step should be efficient, simple, and reproducible [44,50,51].

Solvent extraction methods using organic solvent or their combination at different compositions are employed to extract SPLs. Chloroform–methanol (2:1, 1:2 or 1:1, *v/v*), sometimes in the presence of H_2O, NaCl or KCl, and hexane-isopropanol are the most common methods for SPLs extraction [45,52,53]. Propan-2-ol/hexane/water (55:20:25 v/v/v) is also reported to be preferable SPLs extraction method due to the lipase inhibiting nature of propan-2-ol, neutral pH of the solvent and better yield [45]. The use of methanol, ethanol and acetone, aqueous phenol or a mixture of butanol–ethyl acetate–hexane has also been reported [54,55].

Successful SPLs extraction technique requires consideration of factors affecting the yield and quality of the extract. Incomplete extraction and chemical instability due to enzymatic hydrolysis or oxidation are the main challenges during extraction. Thus, standardization for exhaustive extraction; short heat treatment to deactivate the released enzymes during homogenization; use of peroxide free solvents and suitable antioxidants, and avoiding

exposure to strong light should be considered to enhance the quality and yield of the SPLs extract [56].

After solvent extraction, the extracted lipids constitute a mixture of compounds which makes further purification of SPLs mandatory [51]. The purity of the extract can be enhanced by using either physical or chemical purification approaches. Liquid-liquid or solid phase extractions, thin layer chromatography (TLC), and preparative and semi-preparative liquid chromatography are the most common physical approaches to separate polar and non-polar portions of the extract. Alkaline hydrolysis to remove phospholipids and/or glycerolipids from SPLs is among the chemical methods employed [48,51,57].

1.3 Identification, separation and quantification of sphingolipids

1.3.1 Thin layer chromatography

TLC is a technique where compounds from a mixture are separated on a thin layer of stationary phase. Silica gel and alumina are the commonly used stationary phases. The particle sizes of TLC stationary phase range from 10 to 50 µm, while lower size (5 µm) stationary phases are employed in high performance TLC (HPTLC) to enhance separation efficiency [58].

TLC and HPTLC have long been indispensable tools for sphingolipidomics, as they constitute a simple, convenient, rapid, robust and economical technique that provides satisfactory purification of the sample, good resolution and a visual overview of the different classes of lipids. HPTLC has higher resolution than the typical TLC due to the smaller particle size and thickness of the layer. Additionally, HPTLC requires smaller sample amounts and can achieve better detection limits [59].

TLC is used for detection of SPLs when known standard compounds and suitable reagents are available. Reagents, such as orcinol or resorcinol solutions, iodine vapor, primuline, bromothymol blue or molybdenum blue and cupric sulfate in phosphoric acid are used to detect SPL fractions [51,59,60]. Nevertheless, it is difficult to confirm the homogeneity of the SPL species within a single TLC band which necessitates the use of other techniques for further structural elucidation [60,61].

Quantification by TLC is also possible through adding SPL standards to the TLC. However, due to lack of standard for all SPL classes semi-quantitative analysis is used to quantify SPLs using known standard possessing comparable migration distance with the analyte [62,63]. Densitometric scanning with incident light at a wavelength of 546, 550 and 580-620 nm using cupric sulfate, orcinol and resorcinol, respectively is carried out to quantify SPLs [59,60,64–66].

The development solvents used depend on the nature of the SPLs (acidic or neutral) of interest. A fresh mixture of different solvents such as chloroform, methanol, ethanol, *n*-hexane, isopropanol, ethyl acetate, acetone, acetic acid, or water with or without salt are used. Neutral SPLs are separated with chloroform, methanol and water (70:30:4 and 50:40:10, *v/v*). Chloroform, methanol (85:15, *v/v*) is a very common mobile phase for GlcCERs [59,63,67].

1.3.2 Liquid chromatography

Liquid chromatography (LC) is a frequently used technique for the separation and identification of SPLs. Both normal phase and reversed-phase LC (RPLC) are applied though the latter is preferable. Normal phase LC has limited application as it does not separate SPLs into a single component and the resins development is slow compared with the RPLC [68]. In RPLC, SPLs are separated based on the length and degree of unsaturation of the LCB and/or N-acyl FA. Moreover, RP-HPLC enables separation of GlcCER, possessing LCB in *cis* or *trans* configuration. The most commonly used reversed phases in sphingolipidomics are C18 and C8 [7,38,51,69].

HPLC application for SPLs analysis has been limited due to lack of UV chromophores or fluorescence and a tedious procedure to modify the amino group with chromophores or fluorescence such as ortho-phthaldehyde [70,71]. However, SPLs analysis without modification is currently possible with evaporative light-scattering detection (ELSD). GlcCERs, CERs and cerebrosides from wheat, rice and soyabean were quantified with HPLC-ELSD [35,72–74]**.** Yet, the technique fails to provide structural information of the analyte which requires additional instrument such as Mass spectrometry for better structural specificity [70,71,75,76].

1.3.3 LC-MS/MS based identification and quantification of sphingolipids

1.3.3.1 MS analysis of sphingolipids

Mass spectrometry (MS) is a powerful scientific technique with both qualitative and quantitative application to analyze SPLs. There are two possibilities for SPLs analysis, direct injection of a sample into the MS or by performing chromatographic separation prior to MS analysis. Though, direct infusion of SPLs requires short running time, identification of less abundant and isobaric SPLs is difficult due to complex spectra and high matrix effect [77]. The second technique involves either Gas chromatography (GC) or LC separation before MS analysis. LC-MS/MS is commonly employed as GC-MS requires derivatization of SPLs into a volatile form. LC separation enhances sensitivity, selectivity and reproducibility of the method [78,79]. The usefulness of the techniques arises from the less probability of different molecules to possess similar LC and MS ionization (fragmentation pattern and fragments) characteristics [77]. The effectiveness of the technique demands careful sample handling (extraction and separation), use of proper internal standard and selection of suitable MS techniques [80].

For the purpose of SPLs quantification, internal standards are mandatory to enhance precision and reproducibility of the method. Stable isotope labeled version of SPLs are ideal standards, however, the high number of SPL species makes the possibility unrealistic [81,82]. Moreover, difficulty of synthesis and less commercial availability of SPL standards compelled the scientists to look for standards possessing comparable behavior in HPLC elution, ionization and fragmentation. LCB, CERs, and GlcCERs were quantified using purified forms of plant CERs [83], uncommon chain length synthetic LCB (C17, sphingosine and sphinganine), C12 FA analogs of CERs and CER-1-Phosphate, [81,82] and using ‘eco-peak’ technique employing C12 FA analogs of CERs and C8 β-D-GlcCER. The eco-peak technique involves delayed injection of a standard compared to the sample to facilitate simultaneous elution and ionization of both samples [84].

The basic MS process include formation of ions from an injected sample, separation of ions based on their mass to charge ratio (*m/z*), detection and measuring the abundance of the ions [85]. In MS, only ions are detected and there are different methods of ionization including protonation, deprotonation and cationization [86]. The protonation or deprotonation methods of ionization are achieved via addition or removal of a proton to

and from a molecule, respectively. Protonation produces a net positive charge of 1 for every proton added while deprotonation provides a net negative charge of 1 after a proton is removed. Matrix assisted laser desorption ionization (MALDI), Electrospray ionization (ESI), and Atmospheric pressure chemical ionization (APCI) ion sources are suitable to ionize SPLs either positively or negatively [87]. Cationization helps to produce a positively charged complex by adding cation adduct other than proton such as alkali or ammonium. It is known to be useful with molecules unstable to protonation. Cationization is commonly achieved via MALDI, ESI, and APCI [86,87].

1.3.3.2 Ion sources

Though, there are a number of ionization sources, ESI, APCI and MALDI are the common ion sources to analyze SPLs [85] which provide excellent mass range and sensitivity [50,86]. These methods can be used both in positive and negative mode of ionization. Moreover, they are considered as "softer" methods, leading to a lower degree of fragmentation and analysis of larger charged molecules [51]. Other ionization techniques such as electron and chemical ionizations have limited application for SPLs analysis due to less sensitivity related with extensive fragmentation and time taking derivatization process [50].

In ESI, charged solvent droplets containing SPLs are formed and the solvent is removed in a vacuum with continuous pumping resulting in a formation of a charged SPLs in the gas phase. The technique is helpful to ionize high molecular weight samples, non-volatile molecules and liquids. ESI is helpful to obtain a major parent ions, with little or no fragmentation and product ions [45,51,86]. LCBs, CERs, GlcCERs, and GIPCs have been identified and quantified from a number of plants such *Brassicaceae* species [88], potato and sweet potato [84], coffee grounds and apple pomace [67], maize and rice [89] with LC-ESI-MS/MS. The drawback of this ionization method is poor sensitivity, low fragmentation and the source is unstable.

The process of APCI technique involves nebulization of the mobile phase with nitrogen gas and vaporization by heating it to relatively high temperature (above 400 °C). The resulting vapor is then subjected to a corona discharge electrode to create ions. APCI is a suitable ionization source for nonpolar lipids, which cannot form charged droplets in a

solution. Moreover, APCI is less susceptible to the effect of ionization suppression and salt buffer effects than ESI [85,90]. The ionization method has been applied to ionize neutral SPLs such as CERs and GlcCERs [66,67,91,92]. The process also causes some fragmentation of the precursor ion, especially at high voltage which can be considered an advantage to obtain additional structural information [85,93].

MALDI is an ionization technique for large and/or labile molecules such as peptides, proteins. The lipid identification using MALDI-MS has been limited, due to less likely existence of a proper matrix. The lipid signals with a molecular weight < 500 Da are suppressed due to photoreaction of the matrices. The samples are prepared by mixing solutions of the analyte and matrix at high concentration [77,86]. The matrices contain a moiety that can absorb the photonic energy of the laser that leads to vibrational excitation and volatilization into the gas phase with the analyte molecules. The analyte, matrix molecules and ions undergo charge exchange reactions resulting in ionization of the analyte as a singly charged species even if the analyte has multiple potentially ionizable moieties. In lipid studies 2,5-dihydroxybenzoic acid is predominantly used as a matrix [61,85]. MALDI has been used to identify different classes of SLPs including LCBs, CERs, monohexosylceramide and GIPC [94–96].

1.3.3.3 Mass analyzer

Mass analyzer is used to separate ions based on their *m/z* ratio. The performance of mass analyzer is measured based on accuracy, resolution, mass range, tandem analysis capabilities, and scan speed. Quadrupole (Q), Time of Flight (TOF), Fourier transform-ion cyclotron resonance (FT-ICR), Ion trap (linear LIT and Orbitrap) are employed for SPLs analysis [86,97]. Tandem (MS/MS or MS^n) SPLs analysis can be carried out in a spatial or temporal domain. Tandem MS employing two or more mass analyzer containing a collision cell in between is often called tandem in space MS. Triple quadrupole (QqQ) MS [63,91,98,99], QqTOF [58,100,101] and TOF-TOF MS are examples of tandem in space MS for SPLs analysis, the first being the most common. MS/MS that uses a single hardware for the selection of a precursor ion, collisionally activated dissociation, storage and scanning of a product ion at a different time interval stated as tandem in time MS [90,102]. FT-ICR, Quadruple ion trap (QIT) [66,103,104] and Orbitrap [105] are among the tandem in time MS used for SPLs analysis.

1.3.3.4 Fragmentation pattern and mode of scanning

Qualitative or quantitative analysis of SPLs using tandem MS include use of a standard for a target compound identification or quantification following mapping of its fragmentation pattern [68,85,102]. Either positive or negative ion modes can be used to study the fragmentation patterns of SPLs. Fragmentation of sphingosine, and its derivatives (CERs and GlcCERs) under suitable collision induced dissociation (CID) in positive mode (i.e., $[M+Y]^+$, Y=H, Li, Na, K) under acidic condition provides a product ion of $[M+Y-18]^+$, $[M+Y-36]^+$, $[M+Y-\text{head group}]^+$ (specific for GlcCERs) and a product ion indicative of the LCB type. The target *m/z* applied to identify LCBs; 4, 8-sphingadienine (d18:2), 8-sphingenine (d18:1), dihydrosphingosine) (d18:0) and 4-hydroxy-8-spingenine (t18:1) are 262, 264, 266 and 262/280, respectively [7,69,82]. Following fragmentation of SPLs either product ion scanning [82], precursor ion scanning [101,106], neutral loss or a combination thereof (selective ion monitoring, multiple ion monitoring) [89,99,107] are used for detection of the parent molecular ion and/or their respective fragments.

1.4 Oral and topical delivery of sphingolipids

SC lipids mainly CERs are known to play a crucial role in skin barrier function. Various skin disorder such as atopic dermatitis and psoriasis [29] and aging are related with SC lipid matrix organizational disturbance and compositional imbalance [17,27]. The problem is manifested in the form of skin dryness, inflammation, itching, loss of elasticity and increased roughness. A number of oral [108,109] and topical [110–112] preparations containing SPLs such as LCB, CERs, GlcCERs and other lipids (FAs and cholesterol) claiming to normalize a defective skin barrier function are available in the market.

1.4.1 Oral administration of sphingolipids

Enhancement of skin barrier function following oral administration of a plant GlcCERs has been reported in human and animal studies. Rice, wheat, konjac and sugar beet derived GlcCER extracts were prepared in the form of capsule (powder and oily solution) and suspension [108,109,113,114] for oral administration. Human clinical trial studies have shown that oral intake of GlcCERs resulted in increasing of skin hydration, elasticity and smoothness while the trans-epidermal water loss, roughness and wrinkledness reduced [108,113,115]. Animal studies also showed that defective skin barrier function induced by

UV irradiation and sodium dodecyl sulfate treatment was improved following oral intake of GlcCERs [114,116]. Though, the exact mechanism of skin barrier enhancement is not yet clear, SC CERs content increment [109], inhibition of inflammatory mediator [114,117], and activation of GlcCER synthase [115] have been reported in the literature. Orally administered rice GlcCER restored skin barrier function by increasing SC CERs content through enhancing GlcCER synthase and beta glucocerebrosidase enzymes and maturation of epidermis [115].

Plant GlcCERs are only slightly absorbed by the intestine and are metabolized in the intestinal lumen. Animal studies showed that the recovery of intact LCB (maize, 4, 8 sphingadienine) was extremely low in the lymph after oral administration [106], though radio labelled SPLs such as sphingosine were distributed into the epidermis [118,119].

1.4.2 Topical delivery of sphingolipids

Topical preparations containing either synthetic [112,120] or plant derived CERs [83] have been formulated aiming to restore native skin CER levels in order to improve skin barrier function. CERs alone [121,122] or in combination with other ingredients such as FAs, cholesterol, amino acid or others [121,123–125] were prepared in the form of cream, lotion, emulsion [120,126], liposomes [127,128] and nano carriers such nanoemulsion, cerosomes [129], nanocapsules [130], and polymeric nanoparticles [131]. Sphingomyeline, CER (3, 3B, 6), sphingosine, and phytosphingosine are among the commonly formulated SPLs [122,126,129,132,133]. Human and animal studies have been conducted to evaluate the effectiveness of the SPL loaded formulations through measuring skin hydration, total epidermal water loss (TEWL) or skin CERs level. The human studies involved both healthy volunteers and patients affected by AD [112,127,134], xerosis [120] or psoriasis [124]. Cultured human skin cell model [132,133,135], excised human skin [83,136] and animal (mice and rat) skin treated with detergents such as sodium laural sulfate, $CHCl_3$: MeOH were also employed to investigate the skin CERs level and its penetration [129,131,137]. The extent of CERs penetration into the different skin layers and its interaction with the other skin lipids are studied with suitable imaging technique such as IR imaging [110] and X-ray scattering (small and wind angle), respectively. Moreover, the skin CERs content

can be quantified using different analytical techniques such as HPTLC [62,63], HPLC [72,138] and LC-MS/MS [83,139].

Though, native skin CERs are crucial in maintaining skin barrier function, topically applied CERs have to penetrate the SC barrier and integrate into the lipid matrix structure in order to enhance the protective nature of a defective skin. However, poor solubility and permeability of CERs on top of normal SC barrier property make the delivery of topical CERs using conventional topical formulation challenging. It has been reported that topically applied perdeuterated CERs (NS, NP) in the form of oleic acid suspension showed limited penetration into the SC and most of the CERs were accumulated in the glyph region [110]. Thus, nano technology is being exploited to enhance topical delivery of CERs into the skin. It has been shown that topical application of CERs in the form of microemulsion, starch nanoparticle gel, liposomes and polylactic-glycolic acid (PLGA) nanoparticles enhanced penetration into the epidermis. Starch nanoparticles and ME gel were effective to concentrate CERs in the SC [83] while MEs and PLGA nanoparticles increased its penetration deep into the dermis layers [131,136]. Moreover, application of cerosomes (CER 3 and 6) [129] and liposomes (sphingomyelins, sphingosine) [132,133] on a porcine skin and cultured skin model enhanced skin barrier function and increased the level of different CER species, respectively. Nanocapsules loaded with CER 3B and tocopheryl linoleate also showed enhanced skin moisture content of AD patients [130].

A number of delivery systems are being investigated to overcome topical delivery challenge of lipophilic substance and lipid-based formulations are getting more attention including liposomes, niosomes, emulsions (micro/nano) and nanoemulgels (NEGs). Emulsion based formulations are preferred by considering industrial feasibility [140,141]. Thus, NEs and NEGs are covered in the next sections.

1.4.2.1 Nanoemulsions

NEs are clear, kinetically stable, isotropic colloidal systems composed of oil, water and surfactant/co-surfactant combination [142,143]. The mean droplet diameter ranges from 20 to 500 nm. Depending on their globule size, they may appear transparent, translucent (not larger than 200 nm) or sometimes milky (up to 500 nm) [144]. They can be in the form of oil-in-water (O/W) or water-in-oil, (W/O) or multiple emulsion types [145]. NEs are

thermodynamically unstable because of high free energy of formation than their phase separated state. Yet, they possess better long-term physical stability without apparent flocculation or coalescence due to better resistance toward droplet collisions induced by Brownian motion [146].

NEs improve the solubility of lipophilic drugs [144] which in turn enhance their therapeutic efficacy and render them suitabile for oral, parenteral, ocular and transdermal drug delivery [147]. NEs are being actively investigated for personal care, cosmetics and drug delivery applications due to their physical stability, better skin penetration capacity and less surfactant requirement [148,149].

1.4.2.1.1 Nanoemulsion composition

NE components selection usually considers solubility/miscibility of active ingredients in an appropriate dispersed phase, non-irritant nature and less sensitivity of excipients toward skin [150]. NE formulation requires four components: oil phase, water phase, surfactant and energy as the formation is not spontaneous [151,152].

Oil phase

The oil phase of NEs can be from various non-polar components, including triacylglycerols, diacylgycerols, monoacylglycerols, free FAs, FA esters (e.g., isopropyl myristate, isopropyl palmitate, ethyl oleate) [150,153,154], medium chain triglycerides, essential oils and mineral oils [155,156]. It has been reported that synthetic oils have higher solubilizing capacity than edible natural oils [157]. The physicochemical characteristics of the oil phase such as polarity, interfacial tension, viscosity, density and chemical stability affect the formation and stability of NEs. NEs of medium and long chain triacylglycerols are physically stable though the preparation is difficult because of their relatively low polarity, high interfacial tension and high viscosity [142,158]. To enhance the stability of NEs (O/W) weighing agents and ripening retarders are included in the oil phase of the formulation [159].

Surfactant/co-surfactant

Surfactants or surface active agents (SAAs) are surface-active molecules that are capable of adsorbing to droplets surface, facilitating droplets disruption, and protecting droplets against aggregation. The mechanism of barrier formation includes electrostatic repulsion,

creation of a 'bound' water layer, and steric hindrance [158,160,161]. Small molecule SAAs, which can be ionic, nonionic or zwitterionic, are highly effective in producing NEs, though phospholipids, proteins, and polysaccharides can also be used as SAAs. Safety and solubilizing capacity are crucial determinants of SAAs and co-SAAs selection [151,162,163]. Though it has been mentioned in the literature that 30 to 60% (*w/w*) SAA concentration is applicable in stable NEs formulation [163], high concentration of SAAs was also associated with skin irritation, toxicity and reduced drug release from the formulation [144]. In case of topical preparations for transdermal drug delivery, SAA concentration which provides maximum flux without causing skin toxicity should be selected [151].

An ionic SAAs are negatively charged which include citric acid ester of mono and diglyceride, ditartaric acid ester of mono and diglyceride [159], and sodium lauryl sulfate (SLS) [120,162]. Cationic SAAs are positively charged that include quaternary ammonium salts, such as hexadecyltrimethyl ammonium bromide and didodecyl ammonium bromide [141,163]. However, they have limited application due to their skin irritation potential [157,162]. Non-ionic SAAs are commonly employed for the preparation of NEs related with their less toxic, less irritant and low susceptibility to pH and ionic strength effects. They are also biocompatible and classified as generally regarded as safe (GRAS) by the FDA [157,164]. Nonionic SAAs include sugar ester (e.g., sorbitanmonooleate, sucrose monopalmitate), polyoxyethylene ether (POE) and ethoxylated sorbitan esters (e.g., Tweens and Spans), cremophor, miglyol, lauroyl macrogol- glycerides or lauroyl polyoxyl-glycerides [156,162,165–168].

The formation and stability of NEs can often be improved by using combinations of SAAs. Co-SAAs such as short- and medium-chain alcohols are also used in combination with SAAs in NEs preparation [169,170]. They are surface active with low emulsion stabilizing potential by themselves due to the small size of the polar head group. Co-SAAs provide the interfacial film with sufficient flexibility and help to reduce SAA concentration in the preparation. Polyols (PEG, 200, 400), glycerol, Transcutol P, plurol oleique [144,151,152,171,172] are among the commonly used co-SAAs in NEs formulation. The hydrophilic-lipophilic balance (HLB) value of SAAs is also a key factor to consider for the

formation of stable NE. HLB values of less than and greater than 10 are required to prepare stable W/O and O/W NEs, respectively**.** The right blend of low and high HLB SAAs leads to the formation of a stable NE [147,150,151].

1.4.2.1.2 Preparation techniques of nanoemulsions

Preparation of NEs requires energy generated either from mechanical device or chemical potential of the components consequently conventional emulsion preparation techniques are not suitable [147,173]. The preparation methods of NEs are generally classified as high- and low-energy emulsification. High energy methods usually employ less SAA concentration while low energy methods are energy efficient and require less sophisticated instruments [143,174,175].

High-energy preparation methods

Mechanical devices capable of generating energy that exceed the restorative forces holding the droplets into spherical shapes are employed. The NEs droplet size produced using high energy method depends on process related factor such as energy intensity, duration, and temperature and nature of formulation components including SAA type, oil viscosity, percentage and interfacial tension [147,176]. However, the method is not suitable for thermolabile drugs, proteins, peptide, enzymes and nucleic acid due to high temperature and pressure employed during the fabrication process [177]. High pressure homogenizers (HPHs) [178,179] and ultrasonicator [180] are among the commonly used devices for NEs preparation.

HPHs are mechanical devices that use 50 to 100 MPa (up to 350 MPa) pressure to produce NEs preferably from preexisting coarse emulsion. The device is capable of reducing droplet size into few nanometer size by applying an intense disruptive force (turbulence, shear and cavitation) [174,181]. Ultrasonicator utilizes high-intensity sound energy (> 20 kHz) to form small volume NEs either from preexisting course emulsion or from a separate NEs components [175,177]. Sound energy combining cavitation, turbulence and interfacial waves generates droplet size reduction to nano size range. To produce stable NEs with smaller droplet size controlling ultrasonic parameters such as sonication power, time, vessel geometry and viscosity and avoiding overprocessing (excess energy supply) are crucial [147,174,182].

Low-energy preparation methods

Low-energy approaches rely on the spontaneous formation of droplets within oil-water-SAA mixtures when either their composition or the environmental conditions are altered. The methods are energy efficient which need only gentle stirring to formulate NEs. The approach includes spontaneous emulsification (SE) [183] and phase inversion methods [146,162,184,185].

The spontaneous emulsification method is convenient to formulate NEs from aqueous phase, organic phase containing water miscible organic solvent such as ethanol or acetone and SAAs. The procedure includes adding aqueous phase into the organic phase consisting of SAA, oil and water miscible organic solvent at specific temperature or vice versa [153,175]. The mechanism of nano size droplet spontaneous formation is due to diffusion of water miscible component from the organic phase to the aqueous phase which creates large turbulent force and increases the oil-water interfacial area. Environmental conditions such as temperature and pH, mixing conditions such as stirring speed, rate of addition, and order of addition, and ratio of water miscible component with oil phase affect the droplet size and stability of the NE [162,183].

Phase inversion methods include phase inversion temperature (PIT) and phase inversion composition (PIC) (emulsion inversion point) techniques. The methods involve controlled transition of an emulsion from one type to another (e.g., W/O to O/W or vice versa) through an intermediate bicontinuous phase. PIT method depends on changes in solubility of the SAAs with changing the temperature [186,187]. Even though PIT is common to formulate pharmaceutical NEs, it has several limitations. Selection of SAAs, high concentration of SAAs, high polydispersity index (PDI) and challenge of identifying inversion temperature are among the limitations [146,147]. On the other hand, PIC approach involves NEs formulation by changing the composition of the two phases at a constant temperature [155]. The size of the droplets formed depends on process variables, such as the stirring speed and the rate of aqueous phase addition. The SAAs used in PIC are usually limited to small molecule surfactants that are able to stabilize both W/O emulsions (at least over the short term) and O/W emulsions (long term) [176].

1.4.2.1.3 Characterization of nanoemulsions

To ensure the quality of formulated NEs a number of physicochemical parameters are assessed. Measurement of particle size, PDI, zeta potential, surface morphology, viscosity, release and penetration studies are the commonly employed parameters. Droplet size, size distribution and zeta potential are among the crucial parameters to evaluate the stability of NEs. Photon correlation spectroscopy (PCS) [143,178,188] or dynamic light scattering (DLS) [170,189,190] is the most commonly used instrument to determine these characteristics of NEs. However, the instrument is not suitable to provide information about the droplet shape and surface morphology. Electron microscopes (TEM or SEM) are crucial to get information regarding the particle shape and surface morphology in addition to the size [147,164,168]. Atomic force microscope (AFP) also provides an indication about the shape and size of NEs droplet [191,192]. However, it has been suggested that the result has to be confirmed by other techniques such as DLS [187].

Other physicochemical characteristics such as thermodynamic stability, compatibility, pH, viscosity and *in vivo* and *ex vivo* penetration evaluation are also investigated. Thermodynamic stability is performed by exposing the formulation to different stress conditions such as heating-cooling cycle, freeze-thaw cycle and centrifugation. The test is recommended with the intention of identifying stable NEs from the metastable forms which take a long time to exhibit instability problems such as phase separation. Those NEs that survive the stress testing conditions, are considered stable and do not require frequent testing during storage [163,193]. The compatibility of formulation components and drug excipient interaction are investigated with FTIR [144,194]. The pH of topical preparation is a key consideration to avoid skin irritation due to acidity or alkalinity of the formulation. Moreover, formulation pH indicates stability as chemical reaction can result pH change [155]. It is recommended that the formulation pH should be close to the skin pH [164]. Formulation pH is measured using pH meter [160,188,195]. The viscosity and refractive index of NEs are usually measured using different kinds of rotational viscometer and refractometer, respectively [151,195,196]. Franz diffusion cell is used to investigate *in vitro* and *ex vivo* permeation studies. The *in vitro* release study can also be performed using artificial model membrane or dialysis membrane depending on the purpose of the active

ingredient loaded in the NEs [83,195,197]. *Ex-vivo* experiments are conducted using abdominal skin obtained from mice [188], rat [142,172] and guinea pig [166].

1.4.2.2 Nanoemulgels

Despite their attractive properties NEs have limited topical application due to low viscosity driven poor retention capacity on the skin. Currently, viscosity enhancement using a gel is being used as a strategy to widen the topical application of NEs. An amalgamated formulation of NEs and hydrogel is known as NEG [151,166]. NEGs exhibit the characteristics of both formulations and overcome the limitations of the respective components [198]. NEGs would have suitable viscosity to increase the formulation contact with the skin which enhances drug absorption and accumulation within the skin. The viscosity of the formulation could be adjusted by controlling the percentage of a gelling agent to modify the skin permeation profile [183]. NEG are non-greasy, easily spreadable, bio-friendly and translucent with agreeable appearance [198].

1.4.2.2.1 Preparation of nanoemulgels

NEG is prepared by incorporating NE into a hydrogel. Natural, semi-synthetic and synthetic gelling agents are used. Xanthan gum, Na-carboxymethylcellulose, Na-alginate, chitosan, different grade of Carbopol (934, 940, 980) are the common gelling agents applicable for NEG preparation. The percentage of the gelling agent varies (0.5 to 5% w/w) depending on the required viscosity of the formulation [185,196,199,200]. Hydrogel is formulated by soaking a suitable gelling agent in an aqueous or hydroalcoholic solvent with or without mechanical stirring. The pH is adjusted using either sodium hydroxide or triethanolamine. Then, the NE is slowly added into the hydrogel with moderate stirring until uniform NEG is formed [157,199]. NEGs loaded with active substances with anti-inflammatory, wound healing [150,152,194], antifungal [195], antioxidant [201] activities and plant extract [160,185,196] have been formulated.

1.4.2.2.2 Characterization of nanoemulgels

The suitability of NEG formulations are assessed for their color, uniformity, phase separation, stability, pH, rheology, spreadability and activity. Stability of NEG is tested after exposing the formulation to different stress conditions (heating-cooling, freeze-thaw and centrifugation) and pH change and phase separation are indicators of formulation

stability [161,185]. Accelerated stability study can also be conducted at different relative humidity and temperature for three months and checking for pH, spreadability, viscosity, and drug content [160,194]. The rheology of NEG is also measured using rheometer with cone and plate geometry to evaluate its flow property so as to enhance the formulation effectiveness [185].

While GlcCERs/CERs are intended to be delivered to the upper layer of the skin, the present study also considered formulating essential oils having mosquito repellent activity for topical application. The mosquito repellent potential of plant materials has been exploited for centuries using different means, including applying essential oils on the skin and clothes to combat transmission of malaria. However, due to the volatile nature of essential oils, the protection against mosquitoes is short-lived.

1.5 Malaria

Since time immemorial, malaria has been a curse on humanity, even in the modern world. Malaria is endemic in 87 countries and poses a risk of malarial infection for almost half of the world's population mostly in tropical and subtropical areas of the world, including regions in Africa, Asia and America. In 2015, an estimated 212 million cases of malaria occurred worldwide of which 90% were in Africa. During the same year, among 429 000 malaria deaths globally 92% were in Africa. Almost all deaths (99%) resulted from *P. falciparum* infection. In 2019, an estimated 229 million cases of malaria occurred worldwide of which 215 million cases were African [202,203]. There were 247 million malaria cases and 619,000 deaths worldwide in 2021 [204]. Children under five years of age accounted for 80% of the death. It continues to be a cause and consequence of poverty and inequality as it disproportionally affects the disadvantaged people in the world. Malaria is a preventable and curable disease though it is life threating without proper diagnosis and effective treatment. Pregnant women, children and people with compromised immunity are vulnerable [205,206].

1.5.1 Malaria prevention

There are efforts being implemented to eliminate malaria from the world. WHO developed a global technical strategy, ''ensure access to malaria prevention, diagnosis and treatment as part of universal health coverage'' being the first pillar. Vector control,

chemoprevention, diagnostic testing and treatment are considered as a prevention package in order to reduce malaria morbidity and mortality [205].

Implementation of more than one malaria prevention method has been found effective in reducing incidence and prevalence of malaria. The prevention strategies are use of insecticide treated net (ITN), indoor residual spray (IRS), repellents (topical and spatial), microbial larvicides, and house improvements [207]. The use of personal repellent with ITN has been reported to reduce prevalence of malaria. Topical repellents are also critical especially during the challenge to use other prevention methods. The use of repellent was associated with a significant reduction in *P. falciparum* infection incidence [206,208,209]. The effectiveness of topical repellents in Africa is indicated to be challenging due to unavailability of standardized formulation, lack of information/communication, less user compliance and short protection time of the repellent [209,210].

1.5.1.1 Synthetic mosquito repellents

Natural and synthetic repellents are available to prevent mosquito bites. Plant based repellents, commonly citronella, were widely used before the Second World War (WW II). A number of synthetic repellents were discovered primarily for military personnel after WW II [211,212]. N,N-diethyl-3-methylbenzamide (DEET), Permethrin, picaridin (Hydroxyethyl Isobutyl piperidine Carboxylate), IR3535 (3-[N- Butyl-N-acetyl]-aminopropionic acid), and N,N-diethyl-2-phenyl-acetamide (DEPA) are commercially available synthetic repellents. Repellents are applied on the skin, fabrics or other materials. Except permethrin, which is a skin irritant, the others are applied on the skin in the form of spray, cream, lotion or other forms. The duration of protection against mosquito bites depends on the concentration of the repellent and the species of the mosquito. DEET is the most effective and widely used repellent worldwide which was patented by the US Army and registered for use in 1957. It is available in different concentrations (5% to 100%) and forms including conventional and modified release preparations. The protection time also varies with the concentration, types of preparation and species of mosquito [213–215]. However, there are reports indicating the toxicity of DEET resulted from its permeation through the skin [207,216].

1.5.1.2 Plant based mosquito repellents

Mosquito repellents derived from plants have been practiced for a very long time. They are essential oils obtained from different parts of odoriferous plants. Due to their volatile nature the protection time is short-lived and demands frequent application. Several essential oils are reported to possess mosquito repellent activity. Citronella oil (CO) [186,217,218], palmarosa oil (PO), lemon grass oil, melissa oil [219–221], eucalyptus oil [222], cinnamon oil, peppermint oil, [156,223], clove oil [224], fennel oil [215], neem oil, hairy basil oil, vetiver oil [181] and citrus oil [225] are reported in the literature as mosquito repellent. The essential oils were formulated in the form of oil blend, cream, gel, patch, NEs, MEs, lipid nanoparticle, and MC while their effectiveness was verified against *Ae. Albopictus*, *Ae. Aegypti*, *Cx. Quinquefasciatus*, and *An. Sundaicus* [165,178,181,221,226,227].

Citronella (*Cymbopogon nardus*) and palmarosa (*Cymbopogon martini*), belong to Poaceae family and genus *Cymbopogon*, are sources of CO and PO, respectively. The essential oils are used in food, drink, cosmetics and pharmaceutical industry. It has been reported that both essential oils have mosquito repellent activity though their protection time varies. CO is composed of mainly monoterpenes and sesquiterpenes. Citronellal, citronellol, geraniol, limonene, citronellyl acetate and geranyl acetate are the main constituent of CO with varying percentage, citronellal being the major component [227,228]. The complete protection time of CO against mosquito bites varies from 9.5 min at 5% spray against *A. albopictus* [215] to 2.8 h at 20% NE against *A. aegypti* [178]. The protection time of 10% CO NE in the presence of 5% hairy basil oil and 5% vetiver oil was 4.7 h [181]. It has been shown that though CO protection time is shorter that DEET, it provides sufficient protection against mosquito bite [207].

PO contains monoterpenes, sesquiterpenes, and alcohols majorly geraniol and geranylacetate. The percentage of each constituents varies depending on the harvesting areas and season [229,230]. The complete protection time of pure PO was found to be 6 and 8 h against *An. sundaicus* [221]. Limited data is available regarding the mosquito repellent activity of PO.

1.6 The present study

The unique molecular organization and the equi-molar ratio of SC lipid matrix constituents are considered crucial for skin barrier function and semipermeable nature. Compositional and organizational changes in SC lipids such as CERs cause defective skin barrier function in relation to ageing and skin disorders due to partly altered enzymatic activity. However, the glucocerebrosidase enzyme responsible for conversion of GlcCERs to CERs is not affected by ageing. Several studies showed that topical application of CERs to animals and human volunteers with defective skin barrier, improved the barrier nature of the skin. However, there are limitations to avail CERs loaded topical products to clients. The first challenge is associated with CERs source reliability and affordability. CERs can be obtained from animals, plant and synthetic sources. However, animal CERs are associated with unintended disease transmission, such as encephalopathy and ethical issues. Synthetic CERs are also very expensive on top of the lengthy and cumbersome synthesis procedure. Thus, plants are currently getting more attention as a reliable source of CERs. CERs are not only available in trace amounts in plants but exist in complex forms such as GlcCERs. Suitable chemical or enzymatic method of hydrolysis is required to produce CERs from GlcCERs. Lupin bean (*Lupinus albus*. L), naked barley (*Hordium vulgare* L) and mung bean (*Vigna radiata* L.) were investigated as a potential source of GlcCERs. The second challenge was unavailability of economical and effective method of hydrolysis to produce CERs from abundant plant SPLs. Chemical (mild acid hydrolysis) and enzymatic hydrolysis within skin homogenate, which could be a critical milestone for direct topical delivery of GlcCERs, were investigated in this study. To the best of our knowledge, both methods are employed to hydrolyze plant GlcCERs for the first time. Even though, the above difficulties are addressed successfully, skin barrier recovery requires proper delivery of CERs/GlcCERs into the skin which demands careful formulation development due to the poor solubility and high molecular weight of CERs/GlcCERs and the permeability barrier nature of SC. An optimized GlcCER loaded nanoemulgel was developed and *in vitro* release and permeation experiments were conducted which is the first of its kind.

On the other hand, malaria poses a serious public health concern and requires an integrated prevention approach including implementation of well-studied malarial vector control strategies and effective treatment. Despite the availability of various vector control means,

personal mosquito repellents are vital in preventing mosquito bites when the other means are impractical to implement. Though plant-based mosquito repellents are preferred as compared to synthetic repellents due to environmental pollution and toxicity issues, their protection is short-lived since the essential oils are volatile. A number of essential oils, including citronella oil have been formulated in different forms, such as microcapsules to extend the release and protection against mosquito. CO and PO were formulated in the form of NEGs to further prolong the release for more than 12 h.

1.7 Research questions

- How efficient are the chemical methods of hydrolysis towards different species of plant glucosylceramide?
- How efficient are the skin epidermal enzymes to hydrolyze glucosylceramide?
- How effective are nanoemulgels to deliver plant-derived glucosylceramide/ceramides to the skin model membrane?
- How effective are nanoemulgels to prolong the *in vitro* release of essential oils with mosquito repellant activities?

1.8 Objectives

1.8.1 General objective

- To isolate, characterize and hydrolyse plant GlcCER and formulate nanoemulsion /nanoemulgel loaded with GlcCERs as well as essential oils with mosquito repellent activities.

1.8.2 Specific objectives

- To investigate the available GlcCER species in selected plants and develop a suitable chemical method of hydrolysis into ceramides,
- To investigate the possibility of GlcCER topical delivery to substitute depleted skin CER,
- To formulate, optimize and characterize nanoemulsion/nanoemulgel for topical delivery of plant derived GlcCERs, and
- To formulate, optimize and characterize nanoemulsion/nanoemulgel loaded with essential oils possessing mosquito repellent activities.

2 Structural characterization of plant glucosylceramides and the corresponding ceramides by UHPLC-LTQ-Orbitrap mass spectrometry

2.1. Introduction

The main function of skin is to form a barrier between the external hostile environment and the internal milieu of the host [231]. A major element of its defensive function is to maintain homeostasis by preventing the uncontrolled loss of water, ions and serum proteins from the organism into the environment [134]. This protective function mainly relies on *stratum corneum* (SC) which contains layers of corneocytes embedded in a lipid matrix. The composition and organization of the lipid matrix, which consists of mainly ceramides (CERs), free fatty acids (FFAs) and cholesterol, are essential for maintaining skin barrier function. CERs act as a water modulator and a permeability barrier by forming multi-layered lamellar structures with other lipids between cells in the SC layers [232]. Variation in composition and organization of SC lipids such as CERs leads to impaired skin barrier function and dryness. The problem is observed in the elderly and in association with several cutaneous disorders such as psoriasis and atopic dermatitis [231].

It has been shown that direct topical replacement of depleted native skin CERs has beneficial effects in improving skin barrier function and skin hydration [134,233]. The depleted CERs can potentially be replaced with similar CERs obtained from various sources such as animal, plant and synthesis [234]. Plants as source of CERs represent safe and low cost alternative compared to animal-based CERs due to their ethical and safety issues [233] and laborious and expensive synthetic procedure [89,235].

Plant CERs are a member of sphingolipids (SPLs), which are biologically active structural membrane constituent of plants like other eukaryotes [236]. They are composed of sphingoid bases (predominantly C18) esterified to long chain FAs or very long chain FAs (> 20 carbon chain). The sphingoid bases are characterized by the presence of a hydroxyl group at C1 and C3, an amine group at C2 and double bonds at the C4 and/or C8 positions. The C4 double bond is found only in the trans configuration, while the C8 double bond, which is widely available only in plants, exists in either trans or cis configuration [9]. Sphingoid bases in plants consist of 4,8-sphingadienine (d18:$2^{4,8}$), (8E/Z)-4-hydroxy-8-

sphingenine ($t18:1^8$), (E/Z) 8-sphingenine ($d18:1^8$), 4-hydroxysphinganine (phytosphingosine) (t18:0), sphinganine (dihydrosphingosine) (d18:0), and 4-sphingenine (sphingosine) ($d18:1^4$) among which the first three bases are dominant [39,45]. FAs of plant CERs are almost exclusively α-hydroxylated ranging from C14 to C26 chain length with C16, C20, C22 and C24 FAs as major components with small amounts of odd FAs having 21, 23, and 25 carbon atoms [48].

The basic CER structure is also modified through changes in chain length, hydroxylation and/or degree of desaturation of both the sphingoid base and FA moieties. Covalent linkage of the 1-hydroxyl group of CERs to polar head group results in a complex SPLs such as glycosphingolipids when mono or pluri-hexose is attached. The simplest and predominant SPL form in plants are the glucosylceramides (GlcCERs) with a single glucose head group [48,233,236].

GlcCERs are commercially available from legumes such as soya and cereals such as rice and wheat [84,236] which are consumed by majority of the world population. Plants which are cheap and less commonly consumed as food such as lupin and naked barley may provide alternative economic advantage as sources of GlcCERs. Lupin bean (*Lupinus albus*. L) or white lupine (locally known as *Gibto*) belongs to the genus *Lupinus* family Fabaceae which is rich in lipid like the other legumes. It is often grown as ornamental plant and animal feed. The amount of lupin bean used for food is estimated to be 5 to 10% of the total production worldwide [237]. In Ethiopia, it is very cheap and used as snack, animal feed and as a raw material in the preparation of local alcoholic drink '*Areki*' in northwestern Ethiopia [238]. Naked barley, hull-less variety of barley, (locally known as *Temej gebs*) belongs to the genus *Hordium* and grass family Poaceae. In Ethiopia, hull-less variety of barley is only used as snack in the form of '*kolo'* (the roasted form), and it is not preferred for other dishes [239]. Mung bean (*Vigna radiata* L.) (locally known as *Mashoo*) belongs to the genus *Vigna*, family Fabaceae. Cultivation and geographical distribution of mung bean is limited due to its sensitivity to cold [240]. Cold sensitive plants are known to have high level of GlcCERs with saturated FAs chain than cold resistant plants [39]. In this study, lupin bean, mung bean and naked barely have been investigated as alternative sources of GlcCERs. Characterization and quantification of GlcCER species in these plant species

have not been carried out so far.

As free CERs are less abundant in plants, a suitable method to transform GlcCERs into CERs is required. Though enzymes are available to hydrolyze GlcCERs into CERs, enzymatic hydrolysis is very expensive [45,48,67]. On the other hand, the classical acid/alkaline hydrolysis methods are associated with drawbacks such as converting CERs into different chemical entities, breaking the CERs amine linkage, and not effective towards all GlcCER species [63,241,242]. Thus, cheap and effective method of producing CERs from the most abundant plant SPL, GlcCERs [48] has economic benefit.

Therefore, in the current study, structural analysis (UHPLC-MS/MS and UHPLC-HRMS/MS) and quantification (AMD-HPTLC) of GlcCERs from the three plants were carried out. CERs were produced from GlcCERs with mild acid hydrolysis which would pave the way to employ plant CERs commercially for cosmetic and therapeutic applications. Periodate mediated hydrolysis of GlcCERs from these plants and characterization of the resulting CERs are performed for the first time.

2.2. Materials and methods

2.2.1. Materials

Soya bean GlcCER (Soy GlcCER) (Avanti Polar Lipids, AL, USA) and CER [AP] (Evonik-Industries, Essen, Germany) were used as a reference standard. Methanol (Fontenay-sous-bios, France) was purchased from VWR International. Chloroform, acetic acid, isopropyl alcohol, *n*-hexane, NaOH and HCl were supplied by Carl Roth (Karlsruhe, Germany). Ethylene glycol and formic acid were obtained from Sigma-Aldrich Chemie GmbH (Steinheim, Germany). $NaBH_4$, acetone, silica gel 60 (0.063 - 0.200 mm), TLC (silica gel 60, F254, 20 cm×20 cm) and HPTLC (silica gel 60 F254, 20 cm×10 cm) plates were purchased from Merck KGaA (Darmstadt, Germany). $NaIO_4$ was obtained from Aldrich Chemical Co. Ltd (Dorset, United Kingdom).

2.2.2. Methods

2.2.2.1. Plant materials collection and authentication

Lupin bean (*Lupinus albus* L) and mung bean (*Vigna radiate* L) seeds were purchased from local market in Bahir Dar and Addis Ababa, Ethiopia, respectively. The identification of

lupin bean (voucher number, AA002) and mung bean (voucher number, AA001) plants was performed at the National Herbarium (Ethiopia), Addis Ababa University [243]. The identified specimens were stored at the National Herbarium. The seeds of naked barley (*Hordium vulgare* L) were kindly donated by Ethiopian Agricultural Research Institute, Holleta Research Center.

2.2.2.2. Extraction and purification of GlcCERs

The GlcCERs-enriched lipid fraction (GELF) of lupin bean, mung bean and naked barley were extracted and purified as per the methods described elsewhere [45,67]. Briefly, the total lipid extracts of powdered lupin bean (L, 300 g), mung bean (M, 300 g) and naked barley seeds (N, 200 g) were extracted with 0.75, 0.75 and 0.60 L of isopropyl alcohol/*n*-hexane/water (55:20:25, *v/v/v*), respectively for 30 min with sonication and vacuum filtered. To exhaustively extract the lipids, the residues were treated two times with similar amount of solvent and composition for 3 h with frequent stirring (second extraction) and overnight (third extraction). The filtrates were pooled and evaporated to dryness in a rotary evaporator (90 rpm, 40 °C).

The dried total lipid extract was separated into polar and non-polar fractions using a mixture of $CHCl_3$/ MeOH/H_2O (1:1:1, *v/v/v*, L, 1.2 L; N and M, 0.75 L). The resulting aqueous and $CHCl_3$ extracts were washed with $CHCl_3$/MeOH (1:1 *v/v*, L, 0.2 L; N and M, 0.1 L) and MeOH/H_2O (1:1 *v/v*, L, 0.2 L; N and M, 0.1 L), respectively. The $CHCl_3$ extracts were combined and dried in a rotary evaporator (90 rpm, 40 °C).

The dried $CHCl_3$ extract was fractionated in a TLC-guided column chromatography packed with silica gel 60 (0.063 - 0.200 mm, sample to silica gel ratio, 1:25). The fractions were sequentially eluted with solvents with increasing polarity; the first elution, $CHCl_3$ (L, 1.1 L; N and M, 0.5 L), second elution $CHCl_3$/MeOH (9:1, *v/v*, L, 1.1 L; N and M, 0.5 L) and third elution $CHCl_3$/MeOH (8:2, *v/v*, L, 1.1 L; N and Mb, 0.5 L). Adequate volume of fractions (L, 50 mL; N and M, 30 mL) were collected and TLC was developed to identify GlcCERs containing fraction. TLC was run using $CHCl_3$/MeOH (85:15, *v/v*). The TLC plate was then treated with $CuSO_4$/H_3PO_4 solution (10 % $CuSO_4$ (*w/v*), 8 % phosphoric acid (*v/v*) and 5 % MeOH (*v/v*)) for 20 sec and oven-dried for 10 min at 150 °C. The band from the samples were compared with that of the Soy GlcCER standard and the flasks containing the GELFs were added up together and dried in a rotary evaporator. The

experiments were conducted in triplicate.

2.2.2.3. Structural characterization of GlcCERs by UHPLC-APCI-LTQ/Orbitrap-MS/MS

The high resolution (HR) MS analysis was performed on Dionex UltiMate 3000 UHPLC system (Thermo Fisher Scientific, Bremen, Germany) coupled on-line to a hybrid linear ion trap-orbital trap mass spectrometer LTQ-Orbitrap Elite (Thermo Fisher Scientific, Bremen, Germany) equipped with APCI ion source and operated in positive ion mode. The source parameters applied were as follows: ion spray voltage at 4 kV, source (discharge) current at 3.8 μA, capillary temperature at 275 °C, source vaporizer temperature at 450 °C, sheath gas pressure at 50 psig, aux gas pressure at 25 psig and ion sweep gas pressure at 30 psig. The separation of GlcCER species was performed on YMC-Pack ODS-AQ column at 45 °C and flow rate of 0.3 mL/min. After sample injection (10 μL), elution was accomplished in linear gradient mode. Eluents A and B were water and methanol, both containing 0.1 % (*v/v*) formic acid. The injected sample was eluted isocratically at 90 % eluent B for 5 min, before sequential linear gradients to 95 and 100 % eluent B in 7 and 25 min, respectively. The post run equilibration time was 10 min. The HR-MS analysis relied on the Fourier transform (FT) full scan mode and Orbitrap mass analyzer. The spectra were acquired in the mass range of 220-1000 *m/z*, mass resolution of 60,000 and mass tolerance of 5 ppm. Data-dependent acquisition (DDA) experiments were accomplished according to doubly play algorithm, and comprised a survey FT-scan with mass resolution of 60,000 followed with dependent scans for the three most abundant signals selected in each survey scan. The MS/MS scans were acquired in the ion trap (IT) mode with isolation width of *m/z* 2. The dynamic exclusion duration was 20 s with one repeat count per hit, whereas mass tolerance for dynamic exclusion was 3 ppm. The isolated singly charged ions were fragmented under CID conditions with the activation time of 10 ms and 30% normalized collision energy. Chromatograms and spectra were evaluated with the Thermo Xcalibur software version 2.2 (Thermo Fisher Scientific, Bremen, Germany).

2.2.2.4. HPTLC method validation

To confirm the applicability of the automated multiple development (AMD)-HPTLC method for quantification of GlcCERs mentioned elsewhere [63]; linearity, limit of

detection (LOD), limit of quantification (LOQ), accuracy and precision were determined according to EMA guideline on validation of bioanalytical methods, 2012 [244]. The linearity of the response over the concentration range of 50 to 1000 ng/band was investigated using Soy GlcCER standard (n = 4). LOD and LOQ of the method were estimated using calibration curve of Soy GlcCER standard in $CHCl_3$/MeOH (1:1, *v/v*) solution (0.5 - 1.7 µL of 100 µg/mL of Soy GlcCER in $CHCl_3$/MeOH (1:1, *v/v*)) (n = 3). The standard deviation of the response (δ) and slope of the curve (S) were used to calculate LOD (LOD=3.3δ/S) and LOQ (LOD=10δ/S).

The within-run precision and accuracy of the method were estimated by analyzing sample of Soy GlcCER at four concentration levels (50, 100, 400 and 800 ng/band) five times for each on the same day. Similar concentration and determination levels were used to analyze between-run precision and accuracy in three different days. The relative standard deviation (RSD) and percentage recovery were used to estimate the precision and accuracy of the method, respectively.

2.2.2.5. Plant GlcCERs quantification with AMD-HPTLC method

Quantification of plant GlcCERs was carried out using an AMD-HPTLC system with a software CAMAG winCATS Planar Chromatography Manager (Camag, Muttenz, Switzerland) after validation. The standard Soy GlcCER solution (100 µg/mL) was prepared in $CHCl_3$/MeOH (1:1, *v/v*) mixture. Solutions containing GELFs (1 mg/mL) were also prepared with similar solvent composition to the standard. Chromatography was performed on precoated silica gel 60 F254 HPTLC plates (20 x 10cm). Prior to sample application, the HPTLC plate was prewashed (immersed in isopropanol for at least 2 h) and dried in an oven at 100 °C for 30 min. The plate was then cooled to room temperature and different volumes of Soy GlcCER standard solution (0.5, 1, 2, 4, 6, 8, and 10 µL) and 2 µL of GELF solutions were applied on the plate (positioned 8 mm from the bottom and 15 mm from the side edge) as 6 mm bands using a CAMAG Automatic TLC sampler 4 equipped with 25 µL syringe. Chromatographic developments were conducted three times using CAMAG AMD 2. $CHCl_3$/MeOH/HAc (95:4.5:0.5, *v/v/v*) was used as a mobile phase for the first two steps with 70 mm migration distance and $CHCl_3$/MeOH/AC (76:20:4, *v/v/v*) for the last run of 30 mm migration distance. Before each step was run, the plate was

automatically vacuum dried for 1.5 min and then conditioned in an acetic acid (4 mol/L) atmosphere. The lipids were detected by immersing the HPTLC plate in aqueous $CuSO_4/H_3PO_4$ solution for 20 s using automatic dipping device and charring in an oven at 150 °C for 20 min. Then, the plate was scanned by a CAMAG TLC Scanner 3 in absorbance mode (λ = 546 nm). The retention factors and the peak areas of the standard were used to identify and quantify GlcCERs in the plants, respectively.

2.2.2.6. Alkaline hydrolysis of plant GlcCERs

Alkaline hydrolysis of GlcCERs was carried out as follows: GELFs were prepared at two different concentrations (1 mg/mL and 2.5 mg/mL) in 1,4-dioxane. Then, 4 N NaOH was added to each solution (2:1 and 1:1, sample to NaOH ratio) and continuously stirred with magnetic stirrer for different duration of time at room temperature, 80 °C, 110 °C and 150 °C. The reaction time and temperature are presented in Table A1 (Appendix). The reaction temperatures were maintained in a water bath for the second reaction condition and in an oil bath for those above 100 °C. Then, the pH of the reaction mixture was neutralized with 1 N HCl after cooling the mixture below 30 °C. $CHCl_3$ was added into the reaction mixture and allowed for phase separation in a separatory funnel for 2 h. After removing the $CHCl_3$ phase, the aqueous phase was washed with 30 mL of $CHCl_3$. The $CHCl_3$ phases were mixed, washed with saturated NaCl solution overnight and dried with N_2 gas stream. The dried sample was solubilized in $CHCl_3$/MeOH (1:1, *v/v*) and TLC was developed using $CHCl_3$/MeOH (85:15, *v/v*) to detect GlcCERs and/or CERs. The standards, Soy GlcCER, CER [AP] and untreated GELFs of the respective plants were used for comparison.

2.2.2.7. Structural characterization of GlcCERs by UHPLC-QqQ-MS/MS

The structural analysis of GELF was carried out using UHPLC coupled on-line to a triple quadrupole (QqQ) MS (QqQ-MS, TSQ Quantum Ultra, Thermo Fisher Scientific, Bremen, Germany) equipped with an APCI source. GlcCER species separation was achieved on a YMC-Pack ODS-AQ column (150 × 2.0 mm, 3 µm particle size, 200 Å pore size, YMC Europe GmbH, Dinslaken, Germany) at 40 °C and flow rate of 0.3 mL/min. After sample injection (10 µL), elution was accomplished in linear gradient mode. Eluents A and B were water and methanol, both containing 0.1 % (*v/v*) formic acid. The injected sample was eluted isocratically at 90 % eluent B for 5 min, before sequential linear gradients to 95 and

100 % eluent B in 5 and 20 min, respectively. The post run equilibration time was 10 min. The APCI/MS parameters were set as follows: discharge voltage +4.5 kV, source (discharge) current of 6 μA, capillary temperature 275 °C, source vaporizer temperature 450 °C, sheath gas pressure of 55 psig, and ion sweep gas pressure of 30 psig. Tandem mass spectrometric (MS/MS) analysis was accomplished in the product ion mode using collision-induced dissociation (CID) at the collision potential of 15-35 eV. The GlcCER species were analyzed in the positive ion mode by Q1 scan (100 - 1000 *m/*z). Chromatograms and spectra were evaluated with the Thermo Xcalibur software version 2.2 (Thermo Fisher Scientific, Bremen, Germany) [234].

2.2.2.8. Mild acid hydrolysis of plant GlcCERs

A method employed elsewhere to study Gaucher spleen cerebroside was modified and used to produce CERs from plant GlcCERs [245]. Briefly, 0.1 - 1 % (*w/v*) GELFs solutions (10 mL) in $CHCl_3$/EtOH (1:3, *v/v*) were prepared and 1 mL of 0.2 M $NaIO_4$ was added to the solution. The mixture was covered with aluminum foil and allowed to oxidize for 24 h at room temperature. Then, equal volume of water containing two drops of ethylene glycol was added. The aqueous phase was washed two times with 13 mL of $CHCl_3$ each. The $CHCl_3$ phases were combined, mixed with equal volume of MeOH and its pH was adjusted to 9 with aqueous 4 N NaOH. Then, 1 mL of 2.5 mg/mL $NaBH_4$ in 0.1 N NaOH was added drop wise to the solution and left for 24 h at room temperature. The reduction was terminated by neutralizing the solution with addition of 6 mol/L HCl. Acidic hydrolysis was carried out by adding 0.75 mL of 6 mol/L HCl and allowed to stand for 24 h. The reaction mixture was diluted with 20 mL of $CHCl_3$ and 25 mL of H_2O. The aqueous phase was washed with $CHCl_3$/MeOH (1:1, *v/v*) two times. The $CHCl_3$ phases, which contain the ceramide enriched fraction (CEF), were mixed together, washed with H_2O/MeOH (1:1, *v/v*) two times and dried with N_2 gas stream.

2.2.2.9. Preparative TLC

CEF was dissolved in $CHCl_3$/MeOH (1:1, *v/v*) and applied with a syringe on preparative TLC (PTLC) glass plate (20 cm x 20 cm) along the line marked 2 cm from the bottom and 1 cm from side edge of the plate. The standards (Soy GlcCER and CER [AP]) and the sample were applied on the second PTLC glass plate (20 cm x 20 cm) at similar position

to the first plate (1 cm band width for each). Both plates were immersed into TLC chamber at the same time and developed using $CHCl_3$/MeOH (85:15, *v/v*) until the solvent front reached 4 cm mark from the top. Then, post chromatographic derivatization was performed on the second plate. The area of the first plate, parallel to the bands of CER [AP] and plant CERs on the reagent treated plate, was marked, scrapped with spatula and added to $CHCl_3$/MeOH (85:15, *v/v*) solvent mixture. It was sonicated for 2 min, filtered with № 1 filter paper and 0.45 µm cartridge filter and dried under N_2 gas stream.

2.2.2.10. Structural characterization of CERs by UHPLC-LTQ-Orbitrap-MS/MS

The structure of CERs obtained from mild acid hydrolysis was confirmed with UHPLC-APCI/LTQ-Orbitap-MS/MS using similar procedure mentioned under section 2.2.2.3.

2.3. Results and discussion

2.3.1. Extraction and purification

Extraction of plant lipids from the complex biological system requires efficient, simple and reproducible protocol. Though, the most frequently used lipid extraction method is $CHCl_3$/MeOH (2:1, 1:2 or 1:1, *v/v*) [51]; in the present study, isopropanol/*n*-hexane/water (55:20:25, *v/v/v*) was employed as it has been recommended for SPLs extraction in relation with lipase inhibiting property of isopropanol and neutral pH of the solvent [45].

Plants from Fabaceae family (lupin bean and mung bean) and Poaceae family (naked barley) were screened for GlcCERs. GlcCERs were not detected on the TLC of total lipid extract of all the plants at the applied concentrations. Liquid-liquid extraction leads to partitioning of lipids, including neutral SLPs (such as GlcCERs) into the $CHCl_3$ phase and removal of more than 70% of the total lipid extract in the form of polar fraction [67]. Purification with column chromatography resulted in the appearance of GlcCERs bands on TLC plates of the investigated plant extracts. The TLC chromatograms of the three plants and Soy GlcCER are shown in Fig. A1 (Appendix). The GELFs were collected from the last gradient ($CHCl_3$/MeOH (8:2, *v/v*)). As it can be seen in Table 2-1, the total lipid extract (14.00 g/100 g of seed, dry weight) and $CHCl_3$ lipid extract (4.07 g/100 g of seed, dry weight) of lupin bean were higher than the respective values of mung bean and naked barley. The amount of GELFs in the three plants were comparable albeit mung bean had

somehow the highest value (Table 2-1). In addition to the three plants, eucalyptus leaf and seed cover from Myrtaceae family were also screened for GlcCERs and negative results were obtained.

2.3.2. UHPLC-LTQ-Orbitrap-MS/MS characterization of GlcCERs

LC-MS/MS method has high selectivity and sensitivity for identification of GlcCERs, making it a powerful tool for analysis of complex SPLs in plants. LC coupled with MS using both electrospray ionization (ESI) and APCI sources has been applied for identification of plant SPLs. However, an APCI method has been found to be efficient for the analysis of polar lipids such as GlcCERs and CERs [63]. The GlcCER species of the three plants were screened by UHPLC-LTQ-Orbitrap-HRMS. The separation of GlcCERs species with UHPLC was based on the difference in structure of their FA chains.

All the GlcCERs species were identified as $[M+H]^+$ during HRMS analysis. In all cases the mass accuracy was < 2 ppm. Pairs of structurally specific product ions of sphingoid bases and their precursor ions were used for the identification of GlcCER species. The sugar moiety of the identified GlcCERs was considered as hexose group by considering the neutral loss (*m/z* 162). The target mass-to-charge ratio used for identification of 4, 8-sphingadienine (d18:2), 8-sphingenine (d18:1) and 4-hydroxy-8-spingenine (t18:1) were 262.2535, 264.2690 and 262.2535/280.2640, respectively [63].

HRMS spectra of GlcCERs of the investigated plants showed the ($[M+H]^+$) ion and fragment ions; $[M+H-H_2O]^+$, $[M+H-2H_2O]^+$, $[M+H-Glc]^+$) and $[M+H-Glc-H_2O]^+$ due to in-source fragmentation. It also revealed that $[M+H-H_2O]^+$ and $[M+H-Glc]^+$ signals were abundant for GlcCERs with dihydroxy (d18:2 and d18:1) and trihydroxy (t18:1) sphingoid bases, respectively. Similar in-source fragmentation of plant GlcCERs containing d18:2 (attributed to easily electron donating tendency of double bond at C 4) and t18:1 sphingoid bases have been reported elsewhere [63]. The three most intense signals, corresponding to ($[M+H]^+$, $[M+H-H_2O]^+$ and $[M+H-Glc-H_2O]^+$ for d18:2 and d18:1 based GlcCERs detected at specific retention time of full scan were subjected to HR-MS/MS fragmentation for the identification of product ions. Similarly $[M+H]^+$, $[M+H-Glc]^+$ and $[M+H-Glc-H_2O]^+$ were considered as precursor ions for the identification of t18:1 based GlcCERs.

Previous studies on plant GlcCERs employed either molecular ions ($[M+H]^+$) [233] or fragment ions ($[M+H-H_2O]^+$ and $[M+H-Glc]^+$) [63] signals with strong intensities during full scan MS for further analysis in MS/MS structural elucidation.

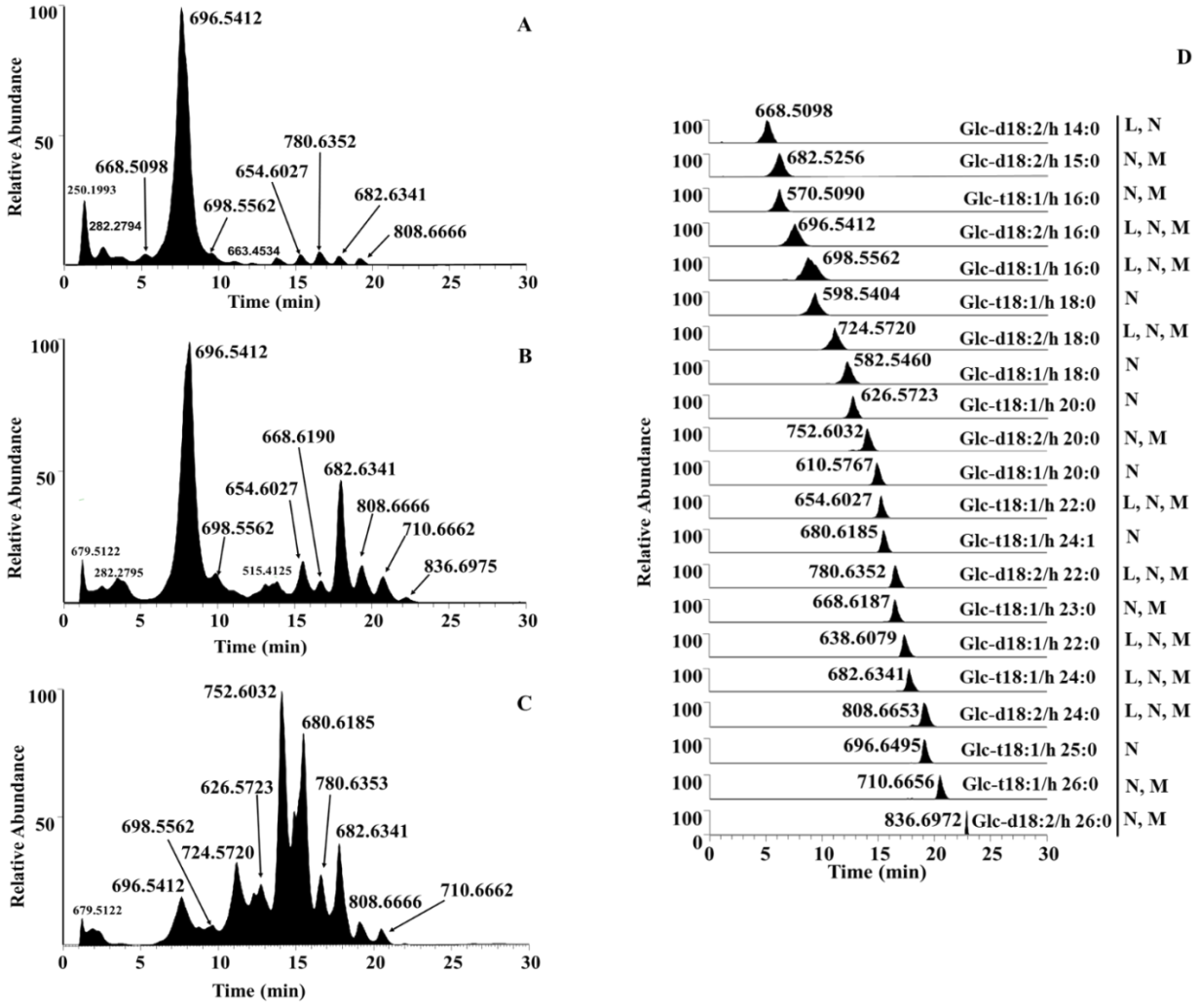

Figure 2-1: Base peak chromatograms (full scan: *m/z* 220 - 1000) of lupin bean (A), mung bean (B), naked barley (C) and extracted ion chromatograms (D) of GlcCER species identified from the three plants with UHPLC-LTQ-Orbitrap-MS. The letters (L: lupin bean, M: mung bean and N: naked barley) indicate the respective GlcCER species of each plants in the extracted ion chromatograms.

Table 2-1: Amount of total lipid extract, $CHCl_3$ lipid extract, GELFs and GlcCERs of lupin bean, mung bean and naked barley (n = 3).

Source	Total lipid extract (g/100 g)	$CHCl_3$ lipid extract (g/ 100 g)	GELFs (mg/ 100g)	GlcCERs (mg/100 g)
Lupin bean	14.00 ± 0.63	4.07 ± 0.23	77.47 ± 10.03	17.17 ± 0.77
Mung bean	8.71 ± 3.25	1.43 ± 0.07	80.24 ± 3.89	18.99 ± 0.97
Naked barley	7.10 ± 0.35	2.12 ± 0.01	71.66 ± 13.12	20.62 ± 2.85

The base peak and extracted ion chromatograms of the three plants are shown in Fig. 2-1A to D. A total of five dominant GlcCER species were found from the plants and identified in the form of an abundant ion in the full scan base peak chromatogram. Among them, signal at *m/z* 696.5412 was found in all of the investigated plants (Fig. 2-1A to C). While signal at *m/z* 682.6341 appeared in both mung bean and naked barley spectra (Fig. 2-1B and C), the rest three GlcCER species (*m/z* 724.5720, 752.6032 and 680.6185) existed as major species in naked barley (Fig. 2-1C). The full scan HRMS base peak chromatogram bearing *m/z* 696.5412 signal revealed that signals at *m/z* 714.5520, *m/z* 696.5412 and *m/z* 534.4883 were intense and therefore selected for HRMS/MS study. HRMS/MS study of $[M+H]^+$ ion (*m/z* 714.5520) provided $[M+H-H_2O]^+$ (*m/z* 696.5412), $[M+H-Glc]^+$ (*m/z* 552.4989), $[M+H-Glc-H_2O]^+$ (*m/z* 534.4883) and $[M+H-Glc-2H_2O]^+$ (*m/z* 516.4777) fragments. Similarly, the fragmentation of the ion at *m/z* 696.5412 resulted in appearance of the fragment ions at *m/z* 534.4883, *m/z* 516.4777 and *m/z* 262.2533 (weak signal). The third abundant ion fragmentation also yielded product ions at *m/z* 516.4777, 262.2533 and 272.2588. Among these the latter two signals represented d18:2 sphingoid base and α-hydroxy palmitic acid, respectively. Thus, the GlcCER could be annotated as Glc-d18:2/h16:0 (*m/z* 714.5520). Representative tandem mass spectrum of the main lupin bean GlcCER (*m/z* 714.5520) is depicted in Fig. 2-2.

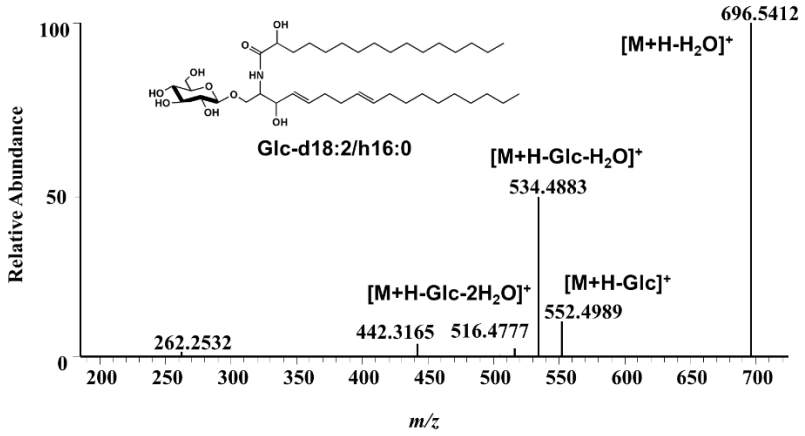

Figure 2-2: Tandem mass spectrum of lupin bean GlcCER (Glc-d18:2/h 16:0, *m/z* 714.5520) when $[M+H]^+$ ion (*m/z* 714.5520) was subjected to UHPLC-LTQ-Orbitrap-MS/MS under FT-IT scan mode (*m/z* 185 - 725).

The fragmentation patterns of the GlcCER species at *m/z* 724.5720 and 752.6032 were alike with Glc-d18:2/h16:0. The HRMS base peak chromatogram of the former signal showed that the signals at *m/z* 742.5829, 724.5720 and 562.5193 dominated at the spectrum and hence, subsequently fragmented. The tandem MS of both ions (*m/z* 724.5720 and 562.5193) showed appearance of signals at *m/z* 544.5089, 300.2899 and 262.2534. Among which the last two signals (*m/z* 262.2534 and 300.2899) represented d18:2 sphingoid base and α-hydroxy stearic acid, respectively which supports the annotation of the compound as Glc-d18:2/h 18:0. The HRMS base peak chromatogram of *m/z* 752.6032 signal indicated intense signals at *m/z* 770.6144, 752.6032 and 590.5510 and were fragmented. Product ions at *m/z* 262.2535 and *m/z* 328.3214 were detected which are the characteristic signals of d18:2 sphingoid base and α-hydroxy arachidic acid, respectively. The result allowed annotation these GlcCER species as Glc-d18:2/h 20:0. The possible fragmentation pattern of GlcCERs species with d18:2 sphingoid base and the product ions of d18:1 and t18:1 sphingoid bases are depicted in Fig. A2 (Appendix).

The species with *m/z* 680.6185 and 682.6341 followed a different fragmentation pattern unlike GlcCERs with d18:2 sphingoid base. The HRMS spectra of both species showed highly intense signals of the $[M+H]^+$, $[M+H\text{-}Glc]^+$, $[M+H\text{-}Glc\text{-}H_2O]^+$ ions and characteristics neutral loss due to in-source fragmentation and proceeded to undergo

fragmentation. $M+H\text{-}Glc]^+$ (*m/z* 680.6185) and $[M+H\text{-}Glc\text{-}H_2O]^+$ (*m/z* 662.6087) resulted in similar product ions with different signal intensities (strong signal from *m/z* 662.6087) in the tandem spectra. The product ion signals were at *m/z* 382.3682, 298.2744, 280.2639 and 262.2533. By the same token, four product ion signals at *m/z* 384.3844, 298.2744, 280.2639 and 262.2533 were identified from tandem spectra of $[M+H\text{-}Glc]^+$ (*m/z* 682.6341) and $[M+H\text{-}Glc\text{-}H_2O]^+$ (*m/z* 664.6241) ions. The similarity of the last three product ions of both species evidently implies sharing of sphingoid base of the same class which was found to be 4-hydroxy-8-sphingenine (t18:1). While signals at *m/z* 382.3682 and *m/z* 384.3844 represented α-hydroxy nervonic acid and α-hydroxy lignoceric acid, respectively. Hence, the compounds were annotated as Glc-t18:1/h 24:1 (*m/z* 842.6719) and Glc-t18:1/h 24:0 (*m/z* 844.6875). The other GlcCER species of the investigated plants were identified following similar procedure applied to the dominant GlcCER species. The identified GlcCER species of each plant and their structure are shown in Table 2-2 and Fig. 2-3, respectively.

From the current investigations, GlcCERs with d18:2, d18:1 and t18:1 sphingoid bases attached to C14 to C26 FAs were identified. Though, most of the α-hydroxylated FAs linked to the sphingoid base of GlcCERs had even number of carbon atoms, FAs having odd number of carbons (C15, 23, and 25) were also obtained. Similar sphingoid bases linked to α-hydroxy FAs were also reported in wheat, barley, rice, soya and maize [89,233,241]. Unsaturated FA (C24) linked with trihydroxy sphingoid base was found in naked barley. Unsaturated very long chain FAs in GlcCERs were found in wheat where the double bond was at position 9 [67]. GlcCERs with d18:2 and C16 FA (Glc-d18:2/h 16:0, *m/z* 714.5520) was highly abundant in plants from Leguminosae family such as lupin bean and mung bean. However, it was the only dominant species in lupin bean which is similar with commercial Soy GlcCER and haricot bean GlcCER [63]. Glc-d18:2/h16:0 is also available commercially from rice bran and wheat germ in the form of skin moisturizer [235]. GlcCERs containing d18:2 acylated to α-hydroxy FAs were reported as predominant species both in maize and rice [89]. FAs with mostly even number of carbons (C14 - 24 for lupin and C15 - 26 for mung bean), amide linked to d18:2, d18:1 and t18:1 sphingoid bases were identified. GlcCERs with odd number of carbon atoms in grass pea and oat grain

[63,234] and unsaturated FAs linked to t18:1 sphingoid base were reported in Ethiopian mustard [63].

Among the dominant GlcCERs species in naked barley three of them (Glc-d18:2/h 16:0, Glc-d18:2/h18:0 and Glc-d18:2/h20:0) were reported to be dominant in barley [233] and the commercially available rice GlcCERs mainly contain Glc-d18:2/h20:0 species [115]. Like that of the beans, naked barley showed similar types of sphingoid bases linked to mostly saturated and unsaturated FAs containing both even as well as odd number of carbon atoms. Unsaturated FAs with odd number of carbon atoms were found in GlcCERs bearing t18:1 sphingoid bases.

2.3.3. Quantification of GlcCERs

Quantification of plant SPLs continues to be challenging due to unavailability of internal standard and their structural complexity. Irrespective of the difficulties, limited number of articles are published on quantification of plant SPLs with TLC [69], HPTLC [234], HPLC [241], LC-ESI-MS [84]. MS-based quantification methods for specific sphingoid base, CER or GlcCER employed internal standards that are similar in structure, ionization and fragmentation characteristics for the categories of SPLs to be quantified. However, determination of whole plant GlcCERs remains difficult [81].

A three-step AMD-HPTLC method for the quantification of total GlcCERs was revalidated for accuracy, precision, LOD and LOQ and the results are shown in Table A2 (Appendix). The inter and intra-day precision and accuracy were within the acceptance range. LOD and LOQ values were estimated to be 17 and 50 ng per band, respectively. The calibration curve of Soy GlcCER (ranged from 50 to 1000 ng/band) was found to be non-linear beyond 200 ng/band. The best fit line to the data was selected based on the F-test values obtained for both linear and nonlinear (polynomial) curves on top of R^2 values. Calculated F-values were 3538.0 and 497.9 for polynomial (R^2 = 0.9997) and linear (R^2 = 0.9880) calibration curves, respectively. As high F-test value indicates best fit model, polynomial calibration curve was selected for the determination of accuracy and precision. The calibration curve of Soy GlcCER is presented in Fig. A3 (Appendix).

Table 2-2: GlcCER species identified from the three plants using UHPLC - LTQ-Orbitrap-MS/MS.

Source	GlcCERs species	Formula	t_R (min)	$[M+H]^+$	$[M+H-H_2O]^+$	$[M+H-Glc]^+$	$[M+H-Glc-H_2O]^+$	Target *m/z*
L, N	Glc-d18:2/h 14:0	$C_{38}H_{72}NO_9$	5.2	686.5193	668.5098		506.4567	262.2531
N, M	Glc-d18:2/h 15:0	$C_{39}H_{74}NO_9$	6.3	700.5364	682.5278		520.4730	262.2686
L, N, M	Glc-d18:2/h 16:0	$C_{40}H_{76}NO_9$	7.6	714.5520	696.5412		534.4883	262.2535
L, N, M	Glc-d18:2/h 18:0	$C_{42}H_{80}NO_9$	11.2	742.5829	724.5720		562.5193	262.2534
N, M	Glc-d18:2/h 20:0	$C_{44}H_{84}NO_9$	14.1	770.6144	752.6032		590.5510	262.2535
L, N, M	Glc-d18:2/h 22:0	$C_{46}H_{88}NO_9$	16.6	798.6459	780.6353		618.5821	262.2534
L, N, M	Glc-d18:2/h 24:0	$C_{48}H_{92}NO_9$	19.2	826.6767	808.6666		646.6138	262.2532
N, M	Glc-d18:2/h 26:0	$C_{50}H_{96}NO_9$	22.0	854.7076	836.6972		674.6447	262.2530
L, N, M	Glc-d18:1/h 16:0	$C_{40}H_{78}NO_9$	8.7	716.5677		554.5148	536.5040	264.2690
N	Glc-d18:1/h 18:0	$C_{42}H_{82}NO_9$	12.3	744.5989		582.5460	564.5354	264.2690
N	Glc-d18:1/h 20:0	$C_{44}H_{86}NO_9$	15.2	772.6303		610.5767	592.5665	264.2690
N	Glc-d18:1/h 22:0	$C_{46}H_{90}NO_9$	17.4	800.6614		638.6079	620.5976	264.2688
N, M	Glc-t18:1/h 16:0	$C_{40}H_{78}NO_{10}$	6.3	732.5621		570.5090	552.4985	262.2531/280.2636
N	Glc-t18:1/h 18:0	$C_{42}H_{82}NO_{10}$	9.4	760.5933		598.5404	580.5296	262.2532/280.2637
N	Glc-t18:1/h 20:0	$C_{44}H_{86}NO_{10}$	12.8	788.6252		626.5718	608.5613	262.2532/280.2637
L, N, M	Glc-t18:1/h 22:0	$C_{46}H_{90}NO_{10}$	15.3	816.6563		654.6027	636.5924	262.2533/280.2638
N, M	Glc-t18:1/h 23:0	$C_{47}H_{92}NO_{10}$	16.5	830.6721		668.6187	650.6083	262.2532/280.2637
N	Glc-t18:1/h 24:1	$C_{48}H_{92}NO_{10}$	15.5	842.6719		680.6185	662.6087	262.2534/280.2639
L, N, M	Glc-t18:1/h 24:0	$C_{48}H_{94}NO_{10}$	17.8	844.6875		682.6341	664.6241	262.2534/280.2639
N	Glc-t18:1/h 25:0	$C_{49}H_{96}NO_{10}$	19.1	858.7034		696.6495	678.6393	262.2532/280.2637
N, M	**Glc-t18:1/h 26:0**	**$C_{50}H_{98}NO_{10}$**	**20.5**	**872.7189**		**710.6656**	**692.6555**	262.2531/280.2637

L: lupin bean, M: mung bean, N: naked barley, t_R: retention time

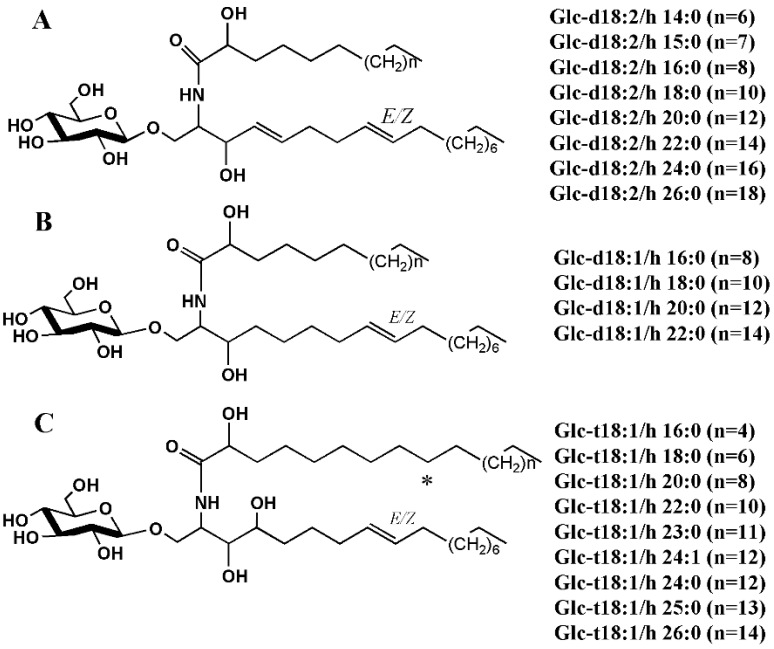

Figure 2-3: Structures of GlcCER species possessing 4, 8-sphingadienine (d18:2) (A), 8-sphingenine (d18:1) (B) and 4-hydroxy-8-sphingenine (t18:1) (C) sphingoid bases identified from lupin bean, mung bean and naked barley.

The three plants investigated had comparable GlcCERs content though the highest yield (20.6 mg/100 g of seeds, dry weight) was obtained from naked barley. Previous study on quantification of GlcCERs content of Ethiopian plants with HPTLC showed 19.1 mg (oat grain), 16.1 mg (haricot bean) and 13.0 mg (grass pea) per 100 g seeds, dry weight [63]. The current results are also comparable with soya cotyledon (0.2 mg/g of dry weight) [235] and different soya bean varieties (6 - 28 mg/100 g of dry weight) GlcCERs content [73]. The content of GlcCERs and other SPLs have been reported to vary with genotype, stage of maturity, growing location and the part of the plant [74].

Though the three plants showed comparable GlcCERs content, lupin has predominantly (> 98 %) of a single GlcCER species (Glc-d18:0/h16:0) which is similar to commercially available Soy GlcCER. On the other hand, naked barley GlcCERs mainly composed of d18:2 and t18:1 sphingoid bases are similar to the marketed rice GlcCERs. Further, both lupin bean and naked barley are affordable and have limited use as human food; making them the best alternative commercial source for GlcCERs. Though, GlcCERs content of

mung bean was comparable with the other plants, the seed is expensive in the local market.

2.3.4. Chemical methods for GlcCERs hydrolysis

Chemical method of hydrolysis (alkaline/acid) has been employed for long time for the purpose of investigating animal SPLs components such as sugar head group, sphingoid base and FAs [242]. HCl and trifluoroacetic acid/acetic anhydride were used to cleave the sugar moiety of SPLs [241,246]. However, use of concentrated HCl for hydrolysis of SPLs causes inversion of the secondary hydroxyl group on the sphingoid base thus, producing diastereoisomeric CERs and formation of O-methyl derivative of sphingoid base which make separation of pure CERs difficult. It was also mentioned that hydrolysis of GlcCERs in aqueous HCl resulted in cleavage of amine bond in d18:2 containing SPLs [241]. Similarly, the use of trifluoroacetic acid/acetic anhydride causes methylation of the resulting CERs which possess different chemical characteristics from CERs [246]. Tessema *et al*., [234] employed anhydrous non-methanolic HCl to hydrolyze oat GlcCERs and succeeded in obtaining only CERs with d18:1 sphingoid base [234]. All the aforementioned methods are not suitable for the current samples as the dominant GlcCER species identified constituted d18:2 sphingoid base.

On the other hand, alkaline (NaOH, KOH and $Ba(OH)_2$) treatment of animal SPLs at high temperature were used to study sphingoid bases by cleaving both amide and glycosidic linkages [241,242]. In this study, it was tested whether alkaline treatment at lower concentration and different temperature range would result in the cleavage of glycosidic bond and loss of sugar moiety so as to produce CERs.

Study on carbohydrate showed opening of sugar ring with appropriate oxidizing agent transforms the glycosidic bond into acetal bond which is susceptible for mild acid breakage [247]. Oxidation-reduction followed by acid hydrolysis were employed to open the hemiacetal structure and remove GlcCERs sugar head group. The method has been applied on animal SPLs study and it was modified and tested whether it would work for plant GlcCERs. To completely hydrolyze the susceptible GlcCER species different experimental conditions were tested by changing reaction time, temperature and stirring condition. The oxidation step was performed at 3, 6, 18 and 24 h duration. Reduction was carried out with stirring (250 rpm) and without stirring for 3, 6, 12 and 24 h at room temperature and 50 ˚C.

The final hydrolysis step was tested at 12, 18, 22 and 24 h, the first 4 h of which was with stirring at a speed of 250 rpm. Since stirring and high temperature resulted in appearance of new TLC bands, the reaction was carried out at room temperature without stirring.

2.3.4.1. Alkaline method of GlcCERs hydrolysis

The dominant GlcCERs species of all the three plants were detected during the UHPLC-QqQ-MS analysis of GELF samples treated with 4N NaOH but not CERs. Consequently, alkaline treated GlcCER species were not analyzed by HR-MS. The base peak chromatogram of lupin bean, mung bean and naked barley GlcCERs, obtained after alkaline treatment, are presented in Fig. A4 (Appendix). GlcCERs with d18:2 and t18:1 sphingoid bases, which mostly belong to mung bean and naked barley were identified and presented in Table A3 (Appendix). The minor GlcCER species were not detected in all the plants after alkaline treatment. Instead, new peaks with lower t_R were detected in the chromatograms. The MS spectra of these peaks showed signals at *m/z* 280.9, 281.2 and 283.1 which might probably be the sphingoid bases generated due to amid bond cleavage. It has been reported in the literature that alkaline treatment of SPLs at high temperature resulted in cleavage of both glycosidic and amine bonds [241].

2.3.4.2. Mild acid hydrolysis of pretreated GlcCERs

Plant CER species were annotated as $[M+H]^+$ ions with UHPLC-LTQ/Orbitrap-MS. A total of eight CER species from both d18:2 and d18:1 sphingoid bases were obtained. The base peak chromatogram of lupin bean and extracted ion chromatograms of the three plants CER species are depicted in Fig. 2-4A and B, respectively.

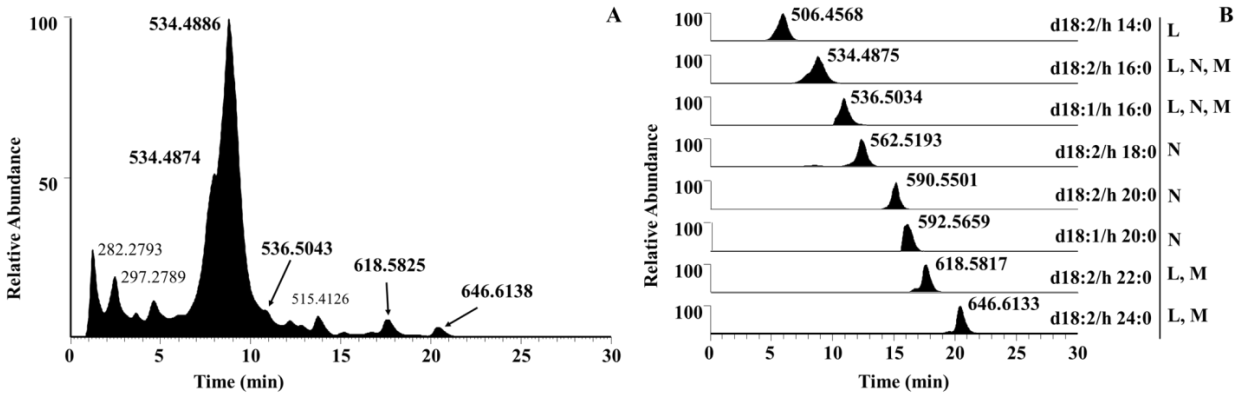

Figure 2-4: Base peak chromatogram (full scan: *m/z* 220 -1000) (A) of lupin CEFs and extracted ion chromatograms (B) of CER species obtained from the three plants after mild acid hydrolysis of pretreated GlcCERs by UHPLC-LTQ-Orbitrap-MS. The letters (L: lupin bean, M: mung bean and N: naked barley) indicate the respective CER species of each plants in the extracted ion chromatograms.

The full scan of lupin and mung beans CEFs showed base peak chromatograms possessing similar ion (*m/z* 534.4874 and 534.4886) with different t_R (7.6 and 8.8 min). The UHPLC-LTQ/Orbitrap-MS/MS analysis of *m/z* 714.5520 ($[M+H]^+$), *m/z* 696.5412 ($[M+H-H_2O]^+$) and *m/z* 534.4883 ($[M+H-Glc-H_2O]^+$) identified from the shoulder (with shorter t_R) granted the presence of GlcCER (Glc-d18:2/h16:0). The UHPLC-LTQ/Orbitrap-MS spectrum of the second base chromatographic peak (t_R 8.8 min) showed ion signals at *m/z* 552.4992, 534.4886 and 516.4781 which were successively fragmented and resulted in a similar product ion signal (*m/z* 262.2533). The species was identified as CER (d18:2/h16:0) as the spectra of the peaks showed signals at *m/z* 262.2533 and 272.2588. The tandem mass spectra of $[M+H]^+$ and $[M+H-H_2O]^+$ ions of lupin bean and dominant naked barley CERs are depicted in Fig. 2-5 A to F. From the result, it is evident that CER *(m/z* 552.4992) was obtained from two different sources. While the source of the former ion peak was in-source fragmentation of GlcCER (*m/z* 714.5520) and the latter ion peak was due to mild HCl hydrolysis of pretreated GELFs. As the removal of sugar moiety made it less polar, the acid-induced CER elutes after its GlcCER counterpart in reversed-phase liquid chromatography. Moreover, traces of other CER species possessing d18:2 and d18:1 sphingoid bases were identified (Table 2-3). On the contrary, neither CERs nor GlcCERs

were detected from t18:1 sphingoid base bearing and other trace GlcCER species. Instead a number of peaks appeared early in the chromatogram which might be the degradation products due to redox reaction and acid treatment. The structure of CERs from the three plants and possible mechanism of GlcCERs oxidation-reduction-hydrolysis process are depicted in Fig. 2-6 and 2-7, respectively.

Table 2-3: CER species identified, after $NaIO_4/NaBH_4/HCl$ treatment of GELFs of the three plants, using UHPLC-LTQ-Orbitrap-MS/MS.

Source	CER species	Formula	t_R (min)	$[M+H]^+$	$[M+H-H_2O]^+$	$[M+H-2H_2O]^+$	Target *m/z*
L	d18:2/h 14:0	$C_{32}H_{62}NO_4$	5.9	524.4675	506.4573	488.4461	262.2531
L, N, M	d18:2/h 16:0	$C_{34}H_{66}NO_4$	8.8	552.4987	534.4883	516.4778	262.2533
N	d18:2/h 18:0	$C_{36}H_{70}NO_4$	12.4	580.5302	562.5195	544.5093	262.2534
N	d18:2/h 20:0	$C_{38}H_{74}NO_4$	15.0	608.5613	590.5510	572.5405	262.2535
L,M	d18:2/h 22:0	$C_{40}H_{78}NO_4$	17.6	636.5927	618.5825	600.5720	262.2532
L,M	d18:2/h 24:0	$C_{42}H_{82}NO_4$	20.4	664.6240	646.6138	628.6033	262.2532
L, M	d18:1/h 16:0	$C_{34}H_{68}NO_4$	10.9	554.5145	536.5036	518.4937	264.2690
N	d18:1/h 20:0	$C_{38}H_{76}NO_4$	15.9	610.5774	592.5668	574.5563	264.2687

L: lupin bean, M: mung bean, N: naked barley, t_R: retention time.

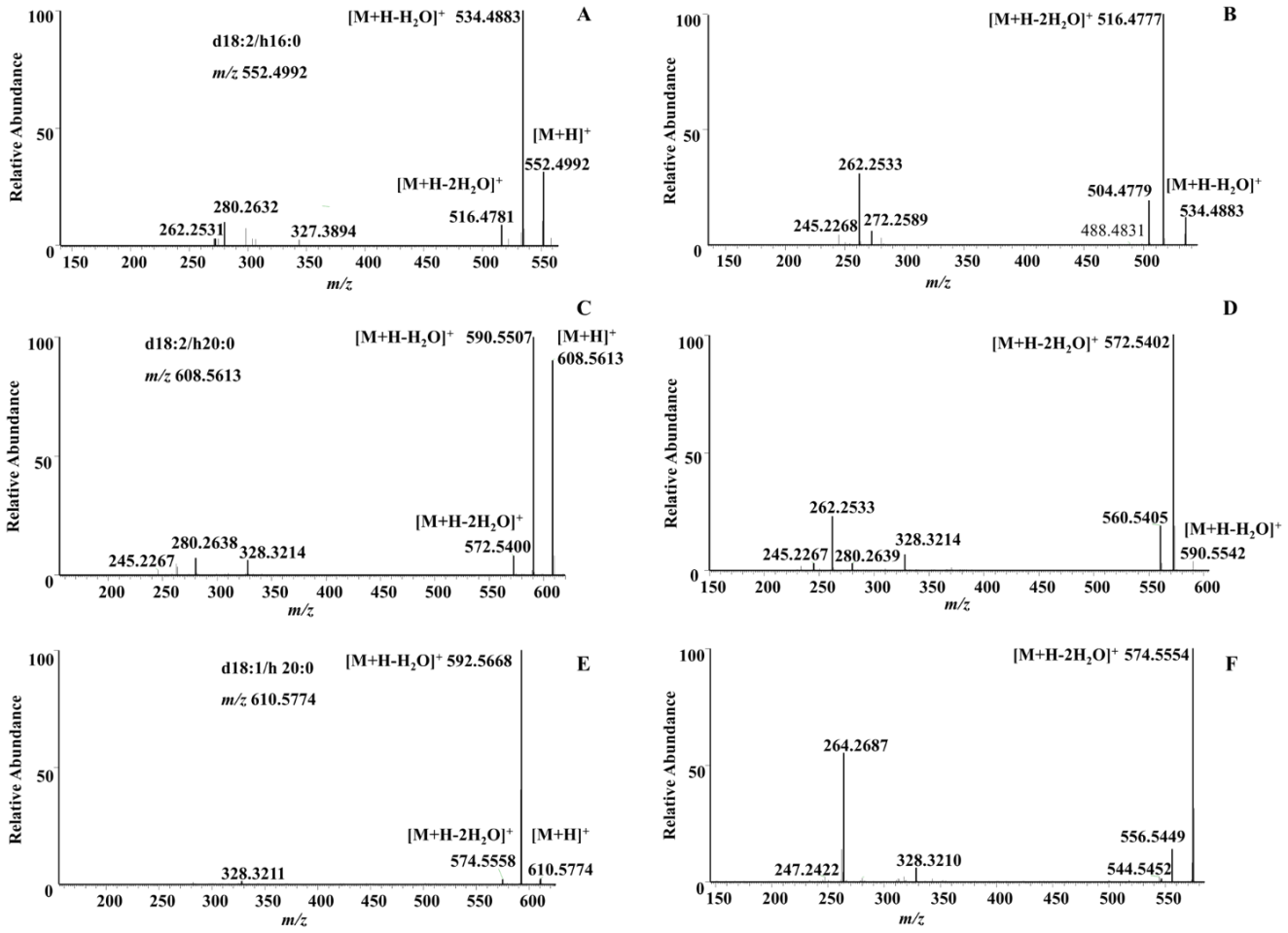

Figure 2-5: Tandem mass spectra of dominant ion signals of lupin CER (*m/z* 552.4992) (A and B) and naked barley CER species (*m/z* 608.5613 and 610.5774) (C-F) when $[M+H]^+$) and $[M+H-H2O]^+$ ions were subjected to UHPLC-LTQ-Orbitrap-MS/MS under FT-IT scan mode.

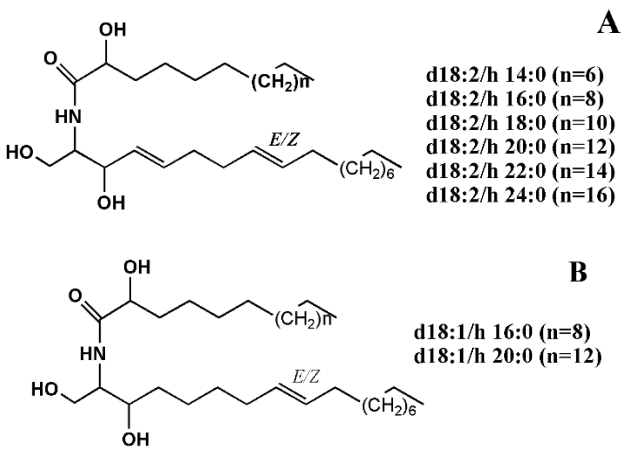

Figure 2-6: Structure of lupin bean, mung bean and naked barley CERs bearing 4, 8-sphingadienine (d18:2) (A) and 8-sphingenine (d18:1) (B) sphingoid bases.

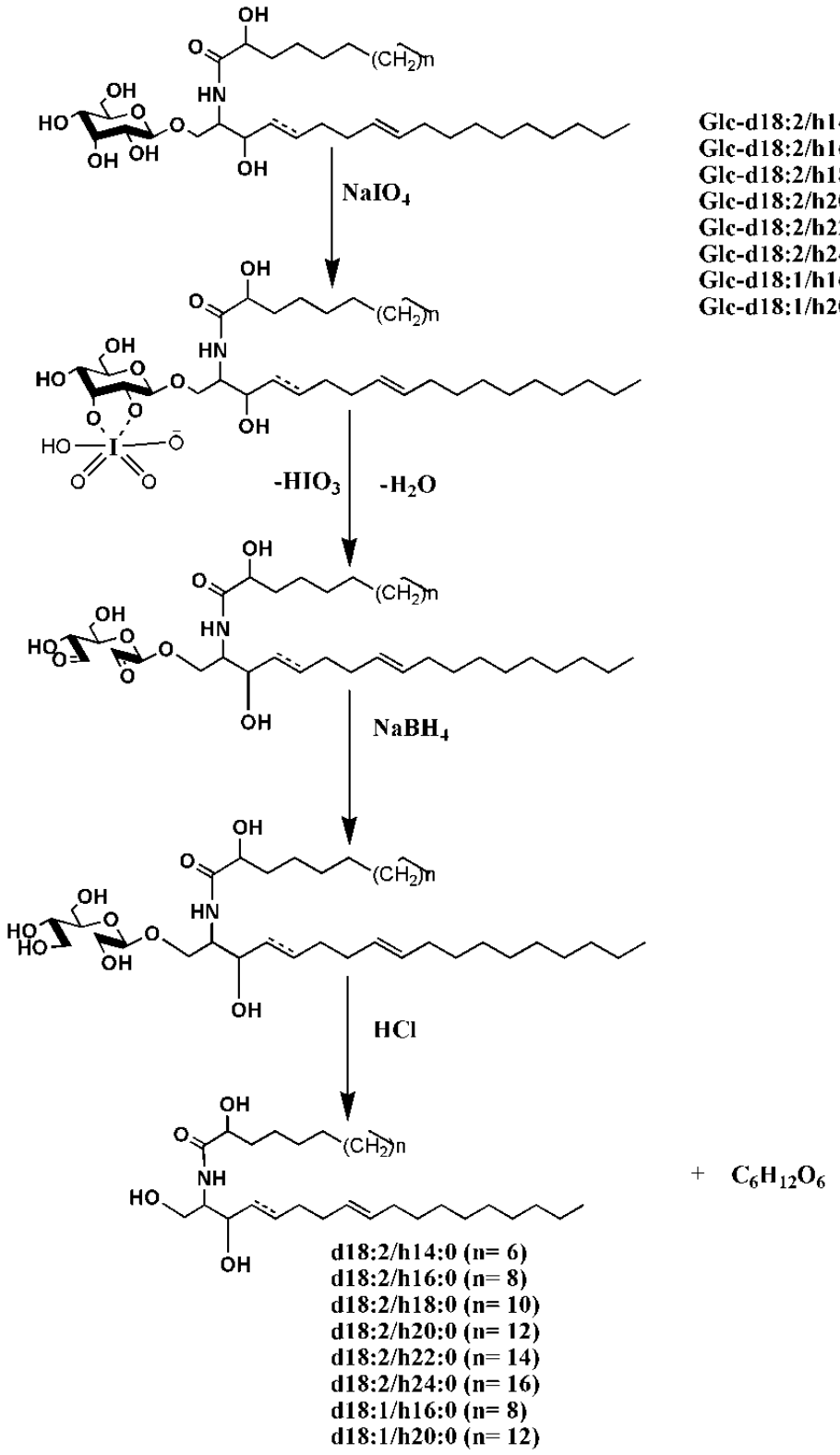

Figure 2-7: Proposed mechanism of GlcCERs oxidation-reduction-hydrolysis process to produce CER.

Likewise the UHPLC-LTQ-Orbitrap-MS analysis of naked barley CEFs showed a base peak chromatogram dominated with signals at *m/z* 534.4886, 562.5199, 590.5510 and 610.5774. The first signal at *m/z* 534.4886 was confirmed to be CER (d18:2/h16:0, *m/z* 552.4992) with similar annotation for lupin and mung beans CERs. The $[M+H]^+$, $[M+H-H_2O]^+$ and $[M+H-2H_2O]^+$ ions of the last three species detected by UHPLC-LTQ-Orbitrap-MS were selected for fragmentation. The tandem mass spectra acquired for the *m/z* 580.5302, 562.5195 and 544.5093 revealed the presence of product ion signals at the *m/z* 262.2534 and *m/z* 300.2899 with intensity difference (strongest signal intensity obtained from *m/z* 544.5093). The product ions were indicative for d18:2 sphingoid base and α-hydroxy stearic acid, respectively. Therefore, it was annotated as CER (d18:2/h 18:0, *m/z* 580.5302). As evidently seen from the tandem mass spectrum (Fig. 2-5C) of *m/z* 608.5613, ion signals at *m/z* 590.5504 and 572.5405 were obtained whereby their consecutive fragmentation (Fig. 2-5D) resulted in *m/z* 262.2533 and *m/z* 328.3214 representing d18:2 sphingoid base and α-hydroxy arachidic acid, respectively. Based on this, the CER species was identified as d18:2/h 20:0 (*m/z* 608.5613).

The HRMS/MS spectrum of the *m/z* 610.5774 showed appearance of *m/z* 592.5668 and 574.5563 signals (Fig. 2-5E). The product ion signals observed in the tandem mass spectra of both *m/z* 592.5668 and *m/z* 574.5563 were *m/z* 264.2687 and 328.3212 (Fig. 2-5F) which corresponds to d18:1 sphingoid base and α-hydroxy arachidic acid, respectively resulting in CER (d18:1/h 20:0, *m/z* 610.5774).

In mammalian cells, the most common sphingoid base is sphingosine (*trans*-4-sphingenine, d18:1) with lesser amounts of sphinganine (d18:0) and 4-hydroxysphinganine (t18:0) [92]. The number of hydroxyl groups in the head group of CERs is important for integrity of the SC barrier function by forming inter and intra hydrogen bond [231]. The CERs found in the current study constitute sphingoid bases (d18:2 and d18:1) having similar number of hydroxyl group with dominant skin CERs which might be considered as possible substituents to reinforce the barrier nature of SC.

Preparing CERs with mild acid hydrolysis of plant GlcCERs is economical in comparison with enzymatic method and effective method for dihydroxy sphingoid bases (both d18:2

and d18:1) bearing GlcCERs in contrast to the method employed by Tessema et al., which was effective only for d18:1 based GlcCERs [5]. It will also play a major role in exploring plants enriched with dihyroxy sphingoid bases containing GlcCERs, such as legumes, as reliable sources of CERs and foster commercialization of plant CERs loaded topical products.

2.4. Conclusions

The UHPLC-LTQ-Orbitrap-MS/MS analysis of GlcCERs species from lupin bean, mung bean and naked barley have shown three types of sphingoid bases (d18:2, d18:1 and t18:1) linked to C14 to C26 FAs. The UHPLC- LTQ-Orbitrap-MS and HPTLC experiments revealed that lupin bean contains Glc-d18:2/h 16:0 (> 98%) and showed comparable yield with commercial GlcCERs plant sources, respectively. Hence, it would be an alternative commercial source of GlcCERs and selected for further study.

Alkaline treatment of GELFs of the plants produced no CERs under the condition employed in the current study. Unlike the alkaline method, plant GlcCERs were effectively hydrolyzed into CERs after mild acid treatment of pretreated GELFs. CERs species with d18:2 and d18:1 sphingoid bases attached to C14 to 24 FAs were obtained from HRMS/MS study. However, CERs from the GlcCER species with t18:1 sphingoid base were not detected in the study. The method worked well for GlcCERs having dihydroxy sphingoid bases (d18:2 and d18:1) and hence, would play vital role in producing CERs from plants rich in these kind of GlcCERs such as legumes and their commercialization.

3 Investigation of plant glucosylceramides hydrolysis within the skin epidermis using a validated quantitative LC-HRMS/MS method

3.1. Introduction

Human skin forms a barrier between the external environment and the internal body. This barrier function serves multiple purposes including prevention of uncontrolled water loss, ions and serum proteins and protection from foreign insult. It is considered that most of the skin barrier function resides in the epidermis, particularly in its outermost layer, *stratum corneum* (SC) [4,232]. The unique composition and organization of SC contributes for its barrier nature. It is composed of dead keratinized corneocytes surrounded by lipid matrix. The lipid matrix is constituted mainly from ceramides (CERs), cholesterol and fatty acids. CERs in SC play a prominent role in the barrier and permeability properties or water barrier functions of the skin [248,249]. SC CERs and other lipids are produced by the living keratinocytes from the granular layer and processed at the junction of SC and *stratum granulosum* (SG) [250,251].

Variation in composition and organization of SC lipids especially CERs which is observed in the elderly and in association with several cutaneous disorders, such as psoriasis and atopic dermatitis, leads to impaired skin barrier function and dryness [252,253]. It has been reported that the activity of glucocerebrosidase/glucosidase enzymes responsible for conversion of glycosylceramides to CERs was not affected by ageing unlike sphingomyelinase and ceramidase which showed reduced and enhanced activity with age, respectively[254]. The activities of the latter two enzymes are considered to be among the reasons for skin CERs reduction with ageing [254]. On the other hand, beta glucosidase enzymatic action was shown to be enhanced in atopic dermatitis[255].

It has been shown that direct topical replacement of depleted native skin CERs has beneficial effects in improving skin barrier function and skin hydration [123,256]. The depleted CERs can potentially be replaced with similar CERs obtained from various sources such as animal, plant and synthesis [234]. Though, plants are preferred [233] free CERs are less abundant in plants, rather exist in the form of GlcCERs [45]. Enzymatic and chemical methods of hydrolysis are available to produce CERs. However, these approaches are not without limitations, the former one is highly expensive [67] and the second has

limited range of effectiveness towards specific types of GlcCER species in addition to its low recovery yield [257]. A suitable, effective and economical method to transform GlcCERs into CERs is still lacking.

Considering the unchanged activity of glucosidase epidermal enzyme, topical administration of plant GlcCERs into the skin might be a potential alternative to replenish the depleted native skin CERs. To this end, hydrolysis of plant GlcCERs in excised human skin epidermis homogenate and validation of the quantitative analytical method for the hydrolysis process using LC-HRMS/MS were investigated.

3.2. Materials and methods

3.2.1. Materials

Fresh human skin was obtained from surgery in the University Hospital, Halle (Saale), Germany. Methanol and disodium hydrogen phosphate dihydrate (Fontenay-sous-bios, France) were purchased from VWR International. $CHCl_3$, sodium taurocholate, citric acid, NaCl, NaOH and HCl were supplied by Carl Roth (Karlsruhe, Germany). Formic acid was obtained from Sigma-Aldrich (Steinheim, Germany). Soya bean GlcCER (Soy GlcCER) (Avanti Polar Lipids, AL, USA) was used as a reference standard. Lupin GlcCER was extracted and purified based on the procedure stated elsewhere [257].

3.2.2. Methods

3.2.2.1. Skin sample processing

Human *ex vivo* skin from surgery was obtained from University Hospital. The skin sample was sliced into appropriate sizes with scalpel blade and immersed into 1N NaCl solution at 4 ˚C for 48 h. Then, the epidermal layer was pulled off from the dermis with tweezers [258].

3.2.2.2. Skin epidermis homogenization and incubation with GlcCERs

The skin epidermal layer was sliced into small pieces with blade and scissors. The homogenized epidermal layer (10-20 mg) was added to 100 µL citrate-phosphate buffer (pH= 5.6) containing 0.2% w/v sodium taurocholate in 5 mL glass tube with teflon lined cap and sonicated for 10 min [259]. Lupin GlcCERs (250 µg) and sodium taurocholate (200 µg) were dissolved in chloroform: methanol (2:1, v/v) and the solvent was evaporated

to dryness under nitrogen gas stream. Citrate-phosphate buffer (100 µL) was then added to the dried mixture to form a dispersion which was added to the homogenized epidermis and incubated for different duration of time (0, 30, 60, 90, 120 and 180 min) at 37 ˚C [260]. Homogenized epidermis with pure buffer (without GlcCERs) was treated in the same way at 120 min [250]. The experiment was carried out using Soy GlcCER with similar procedure. The experiments were performed in triplicate.

3.2.2.3. Glucosylceramide recovery

The percentage recovery of lupin and Soy GlcCERs was determined following similar procedure mentioned under section 3.2.2.2 except the skin epidermal layer was immersed in a boiled water for 10 min to inactivate the enzymes [261] and the lipid extraction was performed immediately after GlcCER was added into the homogenate.

3.2.2.4. Total lipid extraction

The total lipid extraction was carried out following Bligh & Dyer method [53]. Methanol (500 µL) and $CHCl_3$ (250 µL) was added to the incubated epidermis-GlcCERs mixture and sonicated for 5 min. Then, $CHCl_3$ (250 µL) was added, sonicated for 1 min. Afterwards, phase separation was induced by adding 250 µL of distilled water and sonicated for 1 min. The mixture was filtered with 0.45 µm syringe filter and allowed to form clear phase separation. The lower organic phase was pipetted out and the aqueous phase was rinsed two times with 500 µL $CHCl_3$. The syringe and the filter were rinsed with $CHCl_3$: MeOH (2:1, v/v). The organic phases were combined, dried with N_2 gas stream and kept in freezer until use. The samples without GlcCER were extracted following similar procedure and employed as a matrix for method validation.

3.2.2.5. Method development

Dionex UltiMate 3000 UHPLC system (Thermo Fisher Scientific, Bremen, Germany) coupled on-line to a hybrid linear ion trap-orbital trap mass spectrometer LTQ-Orbitrap Elite (Thermo Fisher Scientific, Bremen, Germany) equipped with APCI (atmospheric pressure chemical ionization) ion source was used for development and validation of the analytical method. The source parameters applied were as follows: ion spray voltage at 4 kV, source (discharge) current at 3.8 µA, capillary temperature at 275 °C, source vaporizer temperature at 450 °C, sheath gas pressure at 50 psig, aux gas pressure at 25 psig and ion

sweep gas pressure at 30 psig. The separation of GlcCER from other skin lipids was carried out in YMC-Pack ODS-AQ column (150 × 2.0 mm, 3 µm particle size, 200 Å pore size, YMC Europe GmbH, Dinslaken, Germany) at 45 °C and flow rate of 0.3 mL/min. After sample injection (5 µL), elution was accomplished in linear gradient mode. Eluents A and B were water and methanol, respectively, both containing 0.1 % (*v/v*) formic acid, respectively. The injected sample was eluted isocratically at 90 % eluent B for 5 min, before sequential linear gradients to 95 and 100 % eluent B in 5 and 10 min, respectively. The post run equilibration time was 10 min. The HR-MS analysis relied on the Fourier transform (FT) full scan mode and Orbitrap mass analyzer. The spectra were acquired in the mass range of 220-1000 *m/z*, mass resolution of 60,000 and mass tolerance of 5 ppm. The MS was run in the positive ion mode using multiple ion reaction monitoring (MRM, *m/z* = 714.5 to 696.4 then 262.2). The MS/MS scans were acquired in the ion trap (IT) mode with isolation width of *m/z* 2. The dynamic exclusion duration was 20 s with one repeat count per hit, whereas mass tolerance for dynamic exclusion was 3 ppm. The isolated singly charged ion was fragmented under CID (collision induced dissociation) conditions with the activation time of 10 ms and 35% normalized collision energy. Chromatograms and spectra were evaluated with the Thermo Xcalibur software version 2.2 (Thermo Fisher Scientific, Bremen, Germany).

3.2.2.6. Method validation

The UHPLC-QqQ-MS/MS method was validated with respect to linearity, limit of detection (LOD), limit of quantification (LOQ), accuracy, precision, selectivity, matrix effects and carry-over effect as per EMA guideline on validation of bioanalytical methods [244].

3.2.2.6.1. Linearity

Soy GlcCER was solubilized in $CHCl_3$: MeOH (1:1, *v/v*) and 10 µg/mL of stock was prepared. Then, different concentrations of Soy GlcCER (100, 200, 400, 600, 800, 1000, 2000 and 4000 ng/mL) in the matrix were prepared. The linearity of the response over the concentration range of 100-4000 ng/ml was investigated using Soy GlcCER (n = 4). The standard in the matrix was analyzed using LTQ-Orbitrap MS/MS, in MRM mode (*m/z*,

714→696→262). The corresponding chromatogram peak area of the daughter ion (*m/z* 262) was integrated and a calibration curve was drawn.

3.2.2.6.2. Limit of detection and limit of quantification

Limit of detection (LOD) and limit of quantification (LOQ) were calculated from a separate calibration curve drawn using five levels of Soy GlcCER concentration (100, 150, 200, 250 and 300 ng/mL) (n=3) including blank. The concentrations were equally spaced, LOQ being the lowest level. The standard deviation of the response (δ) and slope of the curve (S) were used to calculate LOD (LOD = 3.3 δ/S) and LOQ (LOQ = 10δ/S).

3.2.2.6.3. Matrix effect

Post-column infusion experiment was carried out to evaluate matrix effects using a syringe pump attached with a T-connector and LC-pumps. The mobile phase was delivered by the LC pumps using a regular gradient program to define the base line. A standard Soy GlcCER solution was continuously infused into the ionization source using the syringe pump while the matrix was injected into the column. Soy GlcCER standard was also infused while pure blank was injected in to the column. The resulting extracted ion chromatograms of the target product ion (*m/z* 262) was evaluated for suppression or enhancement region of signals within the retention time of the analyte [262].

3.2.2.6.4. Accuracy and precision

The within-run accuracy and precision of the method were estimated by analyzing sample of Soy GlcCER at four concentration levels (100 (lower limit of quantification (LLOQ)), 300 (3 x LLOQ), 2000 (50 % of upper limit of quantification (ULOQ)) and 3000 (75 % of ULOQ) ng/mL) in $CHCl_3$: MeOH (1:1, *v/v*) five times for each on the same day. Similar concentration and determination levels were used to analyze between-run accuracy and precision in two different days. The percentage recovery and relative standard deviation (RSD) were used to estimate the accuracy and precision of the method, respectively.

3.2.2.6.5. Carryover effect

The carryover effect was tested by injecting blank (methanol and pure matrix), after high concentration of Soy GlcCER at 4000 ng/ml was run. The experiment was conducted in triplicate.

3.2.2.6.6. Selectivity

The selectivity of the method was determined using skin epidermal homogenate extract passed through similar procedure of skin processing and lipid extraction under section 3.2.2.1-3.2.2.4. The interference of the extract constituents in the analysis of GlcCERs was evaluated by spiking the standard Soy GlcCER at low (300 ng/mL) and high (4000 ng/mL) concentrations.

3.2.2.7. GlcCER quantification by UHPLC-QqQ-MS/MS

The dried total lipid extracts were reconstituted in 2.5 mL $CHCl_3$: MeOH (1:1, *v/v*) and dilution was carried out to make the concentration within the calibration curve range. The extracts were then analyzed as per the method mentioned under section 3.2.2.5 using UHPLC-QqQ-MS/MS in MRM mode.

3.3. Results and discussion

3.3.1. Skin epidermal layer processing

Histologically, the skin consists of the epidermis, dermis and hypodermis. The epidermis, which is the outermost layer of the skin, protects the human body from the external environment [232,249]. Skin layer separation into dermal and epidermal component is an important technique in epidermis related investigation. Epidermis and dermis are attached by epidermal-dermal junction which is mainly composed of collagen and heparan sulfate proteoglycan [263]. A number of epidermal separation techniques such as mechanical removing, heating, chemical treatment, ultrasonication and enzyme treatment are reported in the literature [264–268]. Even though, selection of a specific method depends on the purpose of the experiment, preserving the structure and function of epidermis are crucial during separation. In this study, the epidermis of the skin was separated from underlying layers after NaCl treatment. Incubation in 1N NaCl is among the reproducible, convenient and reliable methods in providing complete epidermis-dermis separation [258,269].

3.3.2. Total lipid extraction

Lipids have multiple structural and functional roles such as signaling and maintenance of membrane structure in different human tissues and organs including the skin. Analyzing lipids in biological samples requires efficient extraction technique. Solvent or solvent mixture is used to extract biological lipids which must be adequately polar to remove lipids

from their association with cell membranes and tissue constituents. The extraction solvent system has to be selected in a way to minimize lipid degradation/oxidation or contamination from non-lipid components, such as sugars, peptides and amino acids [270]. The traditional Folch, and Blyer and Dyer lipid separation methods are common. The lipids are partitioned into the lower organic phase in a biphasic mixture of chloroform, methanol and water [52,53]. MTBE-methanol extraction method was also developed employing similar principle with the two original methods which showed equivalent lipid extraction efficiency with Blyer and Dyer method [271]. In this study, Blyer and Dyer method was employed to extract unhydrolyzed GlcCERs from skin homogenate mixture.

3.3.3. Method validation

The method for GlcCERs isolation reported in our pervious article [257] was slightly modified and employed. Base line separation of GlcCERs from other total skin lipid extract was obtained using H_2O/MeOH (0:100 to 10:90 ratio) with 0.1% (*v/v*) formic acid in both solvents. The separation was accomplished with isocratic elution of MeOH (0.1% formic acid) at 90% for 5 min before sequential linear gradients to 95 and 100 % MeOH in 5 and 10 min, respectively.

3.3.3.1. Linearity

The response was found to be linear over a concentration range of 100 to 4000 ng/ml. The slope and intercept of the equation were 93279.95 and -22061.07, respectively with R^2 value of 0.9996. The calibration curve of Soy GlcCER (ng) against peak area is presented in Fig. 3-1. Demonstrating linearity of calibration curve using optimum number of replicates at each concentration level decreases the uncertainty and produces a uniform prediction region for quantification [272]. Published articles and guidelines propose different concentration levels (5 to 7 levels) and replicates (3 to 6 replicates) at each level to develop calibration curve [262,273–275]. A minimum of five concentration levels in triplicates has also been mentioned as a reasonable test of linearity [276]. The reliability of LC-MS based calibration data depends on calibration strategy, standard selection, solution preparation and reduction of calibration data. Use of certified reference standard, preparation of calibration solution in a matrix and employing appropriate statistical data analysis are among the preferred techniques to enhance method reliability [262].

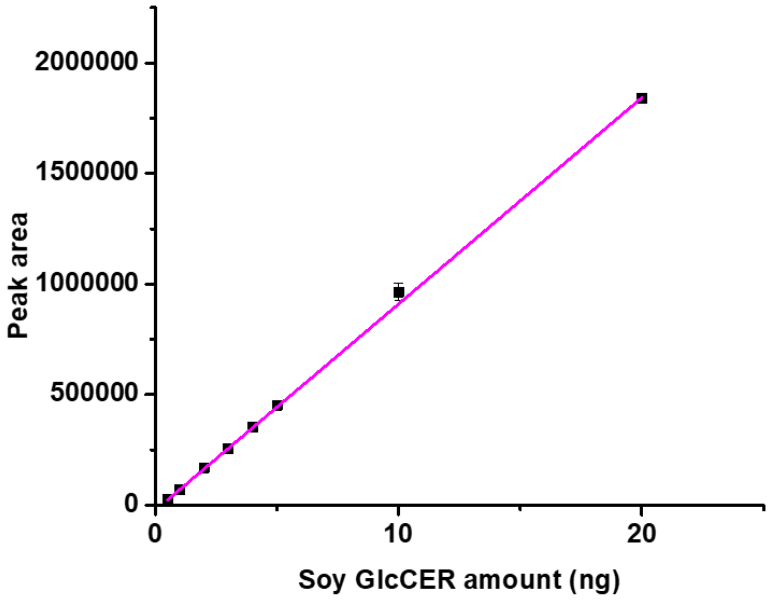

Figure 3-1: Calibration curve of Soy GlcCER in skin epidermis extract (matrix) quantified using UHPLC-QqQ-MS/MS.

3.3.3.2. Limit of detection and limit of quantification

The LOD and LOQ values were 34 and 100 ng, respectively which were determined based on calibration curve approach. The slope (S) of the graph and standard deviation of the response (δ) were used to calculate LOD (LOD = 3.3 δ/S) and LOQ (LOQ = 10δ/S). There are two common approaches for the determination of both LOD and LOQ. The first approach is comparing measured signals of blank and a samples with known low concentration. The second approach employs standard deviation of the response and slope of specific calibration curve drawn other than the main calibration curve [275,277].

3.3.3.3. Accuracy and precision

Analytical method accuracy determination is crucial in method validation and follows different techniques depending on the existing conditions. Use of known concentration of a reference standard is a common practice. Working standards can also be used when pure reference standards are not available [244,273,277]. The accuracy and precision of the method are presented in Table 3-1.

Table 3-1: Inter and intraday precision and accuracy of UHPLC-LTQ-Orbitrap-MS/MS based GlcCER quantification method (n = 5).

	Inter day			Intra day		
	Accuracy		Precision	Accuracy		Precision
Nominal amount (ng)	calculated amount	% recovered	RSD	calculated amount	% recovered	RSD
100	98.02	98.02	10.44	98.18	98.18	11.38
300	270.31	90.11	3.92	270.98	90.32	5.52
2000	1801.94	90.17	3.42	1805.23	90.26	4.26
3000	2869.65	95.65	5.11	2975.73	99.19	4.25

RSD: relative standard deviation.

As per the recommendation of different guidelines [244,273] calculated mean within 15% (within 20% for LLOQ) of the nominal value for accuracy and RSD not exceeding 15% (not exceeding 20% for LLOQ) for precision are considered as acceptance criteria for both inter and intraday measurements. From the foregoing it is apparent that the method is accurate and precise.

3.3.3.4. Matrix effect

The chromatogram showing the matrix effect on Soy GlcCER detection is presented in Fig. 3-2. As it can be seen in the figure there was no signal enhancement or suppression due to the matrix which indicates that the method was free from matrix effect. Matrix effect causes ion suppression or enhancement which could compromises sensitivity and selectivity of a method [139,278]. LC-MS techniques are susceptible to matrix effect due to presence of endogenous compounds such as amino acids, phospholipids, ions and exogenous materials in the mobile phase. The matrix effect is analyte and ionization technique dependent. Though electrospray ionization (ESI) is more susceptible, atmospheric pressure chemical ionization (APCI) technique is not free from matrix effect, presumably due to electron affinity difference between compounds in the gas phase [278,279]. There are two approaches to identify matrix effect in the analyte, post-extraction addition and post-extraction infusion. The second method, used in this study, is commonly employed during

method development as it clearly identifies the chromatographic region where the sample would be susceptible to ion suppression or enhancement [279,280].

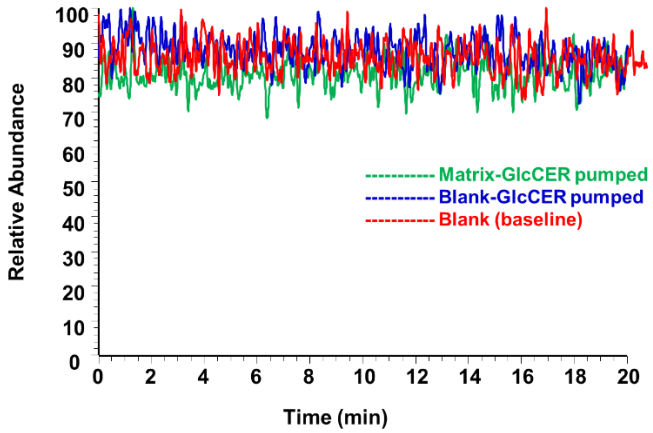

Figure 3-2: Extracted ion chromatograms of blank base line (red), blank pumped through LC-column while Soy GlcCER is injected by syringe (blue) and matrix pumped through LC column-while Soy GlcCER was injected by syringe (green) using UHPLC-LTQ-Orbitrap-MS/MS.

3.3.3.5. Carryover effect

The base peak and extracted ion chromatograms of the mobile phase injected after high concentration of Soy GlcCERs are presented in Fig. 3-3A and B, respectively. EMA guideline specifies the limit of acceptance for carryover effect as not greater than 20% of the LLOQ. In this study, nothing was detected in the blank injected after 4000 ng/ml Soy GlcCER which makes the method free from carryover effect.

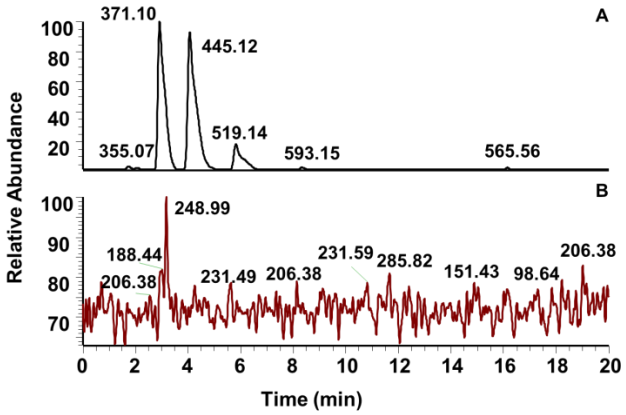

Figure 3-3: Base peak chromatogram (full scan: *m/z* 220-1000) (A) and extracted ion chromatogram (B) of mobile phase injected after high concentration of analyte (4000 ng/ml Soy GlcCER) obtained after MS-Ql and MS/MS scans, respectively using UHPLC-LTQ-Orbitrap-MS/MS.

3.3.3.6. Selectivity

Appearance of isobaric or isomeric compounds was not detected in both Q1 (full) and MS3 scans of standard spiked matrix at the retention time of the analyte (t_R=7.89 min) indicates that the method was selective to GlcCERs. The base peak and extracted ion chromatograms of standard spiked matrix and base peak chromatogram of pure matrix are shown in Fig. 3-4 A, B and C, respectively. Analytical method of quantification should be able to differentiate the analyte (s) of interest from endogenous components in a matrix or other components in a sample. A minimum of six independent sources of the same matrix is recommended for selectivity study. However, LC-MS/MS is among the best alternative analytical method to enhance selectivity and use of a single matrix is sufficient for hyphenated MS (LC-MS and LC-MS/MS) based methods so long as, matrix effects is investigated to ensure precision, selectivity and sensitivity [275].

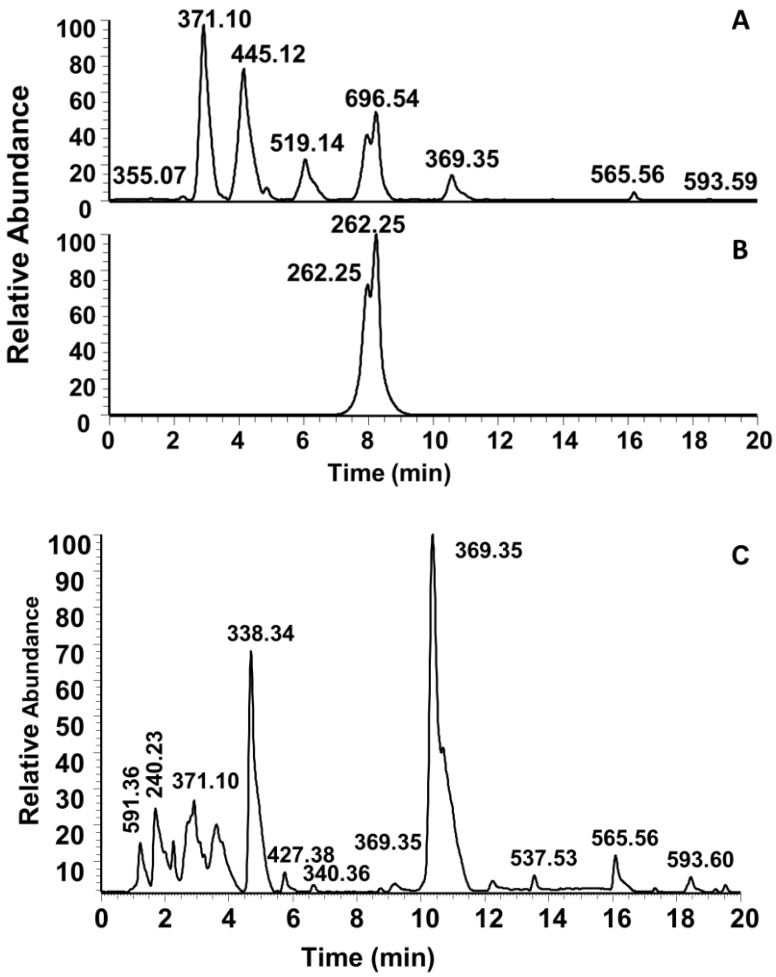

Figure 3-4: Base peak (full scan: *m/z* 220-1000) (A) and extracted ion chromatograms (B) of GlcCER extracted from skin homogenate and base peak chromatogram (full scan: *m/z* 220-1000) (C) of the matrix using UHPLC-LTQ-Orbitrap-MS/MS.

3.3.4. UHPLC-LTQ-Orbitrap-MS/MS based GlcCERs quantification

The percentage recovery of Soy and lupin GlcCERs were found to be 94.68 ± 0.19 and 88.92 ± 0.54, respectively. The recovery from lupin GlcCER was lower as compared with Soy GlcCER which might be due to less purity of lupin GlcCER extract. GlcCERs from Soy and lupin were incubated with epidermal homogenate targeting its hydrolysis by glucosidase enzyme into CER and the unhydrolysed form was quantified. The base peak chromatogram of the total lipid extract containing Soy GlcCER (*m/z* 714.55) and extracted ion chromatogram of its product ion (*m/z* 262.25) are shown in Fig. 3-5 A and B, respectively. The characteristic signals of GlcCER fragments (*m/z* 696.54, 552.49 and

534.48) due to in-source fragmentation were detected in the MS (Q1 scan) spectrum (Fig. 3-5 C). The MS2 fragmentations of the dominant fragment (*m/z* 696.54) ion provided the target product ion (*m/z* 262.25) which was integrated to quantify GlcCER. Following similar fashion the dominant GlcCER species of lupin was also identified.

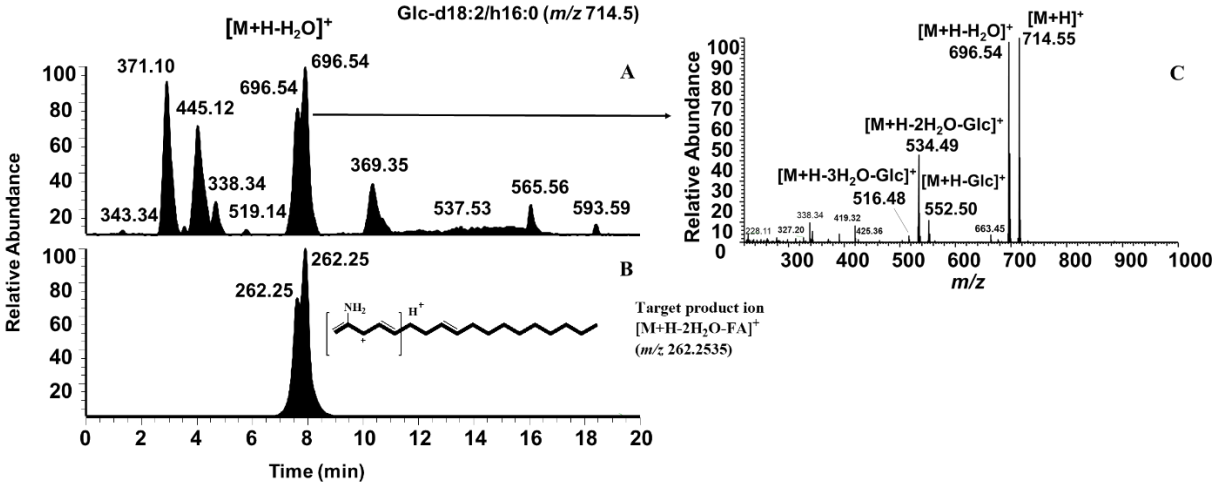

Figure 3-5: Base peak chromatogram (full scan: *m/z* range 220-1000) of epidermal total lipid extract (A), extracted ion chromatogram of product ion (*m/z* 262.25) (B) and mass spectrum (Q1 scan) of GlcCER (*m/z* 714.55) in the lipid extract using UHPLC-LTQ-Orbitrap-MS/MS.

The graph showing unhydrolyzed Soy and lupin GlcCERs versus time is depicted in Fig. 3-6. The unhydrolyzed GlcCERs of both Soy and lupin decreased with time which might suggest degradation of the respective GlcCERs by epidermal beta glucosidase or glucocerebrocidase enzymes. However, we were unable to detect the hydrolysis product i.e. CER from the total lipid extract. The probable reasons might be further CER degradation by skin enzymes into other products which makes CER detection and quantification difficult. The difficulty of direct enzymatic hydrolysis product quantification in a tissue has been mentioned in the literature and most of the authors measure the fluorescence of synthetic substrates such as 4 methylumbelliferul-β-D-glucopyranoside to determine enzymatic activity [252,254,260,281]. Considering the objective of this study synthetic substrates were not considered.

Topical formulations containing specific CERs are available in the market claiming skin barrier function enhancement by maintaining moisturized skin and reducing total epidermal water loss [110,120,122]. It has also been indicated that topically applied synthetic CER interacted with SC lipids in a way that increased the fraction of lipids forming denser lateral packing (orthorhombic) and increased stability [122,123]. However, reliable sources of CERs are still lacking in relation with ethical/safety issues of animal sources and expensive synthetic procedure [89,233,235]. Plants represent reliable, safe and low cost alternative sphingolipids source compared to the other sources. However, CERs are present in trace quantities in plants rather they exist in the form of GlcCERs which require hydrolysis. So far, there is no effective and efficient methods of GlcCERs hydrolysis as enzymatic and chemical hydrolysis are very expensive and specific towards certain GlcCER species, respectively. Plant GlcCERs enzyme hydrolysis in a skin homogenate has never been done before. All the foregoing findings indicate that GlcCERs are hydrolyzed in the skin homogenate paving the way for new mode of skin barrier function enhancement.

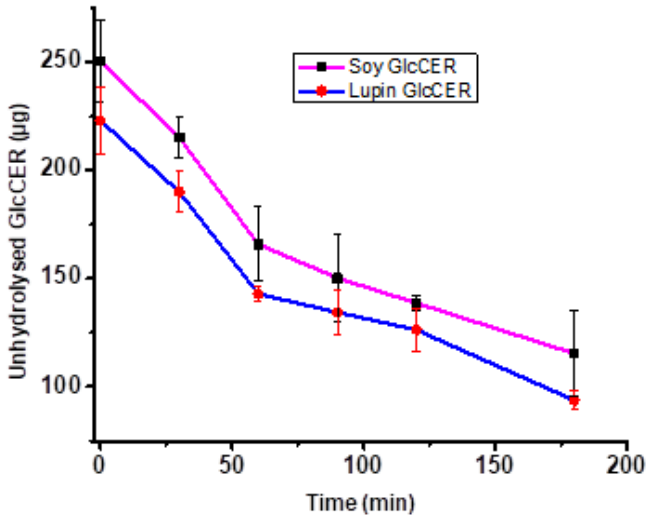

Figure 3-6: Amount of unhydrolyzed Soy and lupin GlcCERs (µg) against time quantified with UHPLC-LTQ-Orbitrap-MS/MS after incubating their respective GlcCERs with homogenized skin epidermis.

3.4. Conclusion

Enzymatic hydrolysis of plant GlcCERs within epidermis homogenate has been investigated for the first time. To quantify the unhydrolyzed Soy and lupin GlcCERs in the total skin lipid extract an effective extraction method was used. The UHPLC/APCI-LTQ-Orbitrap-MS/MS method for quantification of recovered GlcCERs in total lipid extract was free from matrix and carryover effects. The method was precise, accurate and selective. The amount of unhydrolyzed GlcCER was depleted with time due to enzymatic hydrolysis. Considering the drawbacks of animal and synthetic CERs on top of enzymatic and chemical methods of plant GlcCER hydrolysis limitations, topical administration of plant GlcCERs to enhance skin barrier nature would be the best alternative. Yet, reaction kinetics and plant CERs interaction with native skin CERs and other lipid components require further investigation.

4 Nanoemulgel formulation for topical Delivery of plant glucosylceramide: characterization and optimization

4.1 Introduction

Sphingolipids (SPLs) are an important structural membrane constituents of plants [34]. Glycosylceramides are a glycosphingolipid when a glycosyl group is attached with CERs. It is a major SPL in plants such as rice, soya bean, corn and wheat [45,114]. The CER backbones are composed of six different C18 sphingoid bases (SBs) and more than ten different α-hydroxy fatty acids. The SBs are derivatives of D-erythro-sphinganine while the sugar moiety is usually D-glucopyranose in β linkage to the C-1 hydroxy group of the SB [47,48].

Proper composition and organization of SC lipids especially CERs are crucial to maintain normal skin barrier function. Plant SPLs are available as oral or topical skin care products in order to restore skin protective nature due to their chemical similarity with human skin CERs [108,114,117]. Edible plants have emerged as safe and preferred alternative to animal CERs for cosmetic applications [113].

Oral intake of purified or crude plant GlcCERs from wheat, konjac, maize and beets has been shown to enhance skin barrier function affected by ageing or some skin disorders in mice [109] and human [108,114,117]. However, the mechanism is not entirely clear. A report indicated that SBs, as *in-vivo* metabolites of GlcCERs, activated CER synthesis; and also, orally administered radiolabeled SPLs were identified in the skin lipids [117]. Conversely, it has been shown that intestinal absorption of dietary GlcCER from maize was very poor and unique SB of plants were not identified in the SC lipids [108] which might limit the use of plant SPLs as oral skin care products.

Topical application of plant GlcCERs has been reported to enhance epidermal CER content [132] and prevent photo aging of the skin [282]. Yet, successful delivery of GlcCERs to the viable epidermis has been challenging [116] due to the protective nature of the skin [283,284]. To overcome skin permeability challenges, different methods have been proposed such as the use of penetration enhancers [144]. Recently, nanotechnology has been explored to make novel drug carriers with high drug loading capacity and skin permeation profiles for both transdermal and topical drug delivery systems. The nano

carriers include liposomes, ethosomes, polymeric nanoparticles, nanoemulsions (NEs) and nanoemulgels (NEGs) [166]. Among them, the emulsion based formulations are preferred due to their industrial feasibility [140].

NEs are clear, kinetically stable, isotropic colloidal systems composed of oil, water and surfactant/co-surfactant combination [142]. The appearance and stability of NEs depend on their globule size [143,145]. NEs generally appear to be clear or transparent with a mean droplet diameter of less than 200 nm while some appear milky with the droplet size up to 500 nm [144]. Currently, NEs are the area of focus for cosmetics and drug delivery applications attributable to their small size and large surface area [148]. Nevertheless, their application for topical drug delivery is limited due to their low viscosity that leads to poor retention on the skin [146]. Incorporation of NEs to a gelling system has been evolved as a strategy to overcome these problems thereby enhancing their viscosity and related clinical applications [151,166].

NEG is a combined preparation of stable NEs and a hydrogel matrix for therapeutic and application related improvements [140]. NEGs possess gel characteristic with improved NE properties for drug delivery [144,151,285]. The hydrogel in the formulation will enable close proximity of the formulation with the skin facilitating cutaneous absorption of the active moiety. This will lead to accumulation of the active moiety in the skin and prevent leaching into systemic circulation [183].

A Formulation with the required quality attributes can be prepared following careful designing. Experimental designs help to investigate the influence of formulation and process variables on the response variables and the effects of factor interactions [169]. Mixture design, a specialized form of response surface methodology, is a tool employed when the factors are proportions of a mixture and helps to identify the best proportion of more than two components so as to minimize/maximize the response [286]. In such scenario, other experimental designs cannot be applied, since the sum of the components proportion must be 1 and the factors are dependent on each other. Among the different classes of mixture deign, extreme vertices design is employed when the independent variables have both lower and upper values. In order to cover the largest possible area in

the region with a smaller number of experimental runs, D-optimal design is employed [287,288].

Our investigation conducted on hydrolysis of lupin GlcCER in epidermal skin layer provided promising results. Thus, the current study was aimed to develop and characterize an optimized NE and NEG formulations for topical delivery of lupin GlcCER.

4.2 Materials and methods

4.2.1. Materials

Soy GlcCER (Avanti Polar Lipids, AL, USA) was used as a reference standard. Lupin GlcCER was extracted and purified following the procedure described in our previous article [257]. Methanol (Fontenay-sous-bios, France) was purchased from VWR International. Glycerol, chloroform, acetic acid (HAc), acetone (AC), isopropyl alcohol, n-hexane, triethanolamine (TRIS), NaOH, HCl and NaCl were supplied by Carl Roth (Karlsruhe, Germany). HPTLC (silica gel 60 F254, 20 cm × 10 cm) plates were purchased from Merck KGaA (Darmstadt, Germany). Tween 80 and Span 80 were obtained from Sigma Aldrich GmbH (Taufkirchen, Germany). Transcutol P was purchased from Gattefossé (Lyon, France). Basic cream (BC), Miglyol® PPG 810, isopropyl myristate (IPM), propylene glycol (PG) and collodion 4% were purchased from Caesar & Loretz GmbH (Hilden, Germany). Dimethyl sulfoxide (DMSO) was obtained from Fluka Chemie GmbH (Buchs, Switzerland). Euxyl®PE 9010 was supplied by Schülke & Mayr GmbH (Norderstedt, Germany). Carbopol®980 Polymer was obtained from Lubrizol Advanced Materials Europe BVBA (Brussels, Belgium). Dodecanol and n-octanol and were obtained from Sasol Germany GmbH (Brunsbüttel, Germany).

4.2.2. Methods

4.2.2.1. Miscibility test

IPM and Miglyol as the oil phase; Tween 80 and Span 80 as surfactants (SAA-surface active agents); and Transcutol and propylene glycol (PG) as co-surfactant (co-SAA) were screened for physical compatibility in terms of miscibility with each other. Briefly, 500 mg of SAA or co-SAA was added to equal amount of oil in a screw capped glass vial and mixed vigorously by vortex mixer (Vortex Genie, Scientific Industries, New York, USA) for 1 min. Clear, transparent and homogenous mixtures were considered miscible and

physically compatible. Whereas, the appearance of turbidity was considered as a physical incompatibility and the phase separation was regarded as an immiscible system [196].

4.2.2.2. Lupin glucosylceramide solubility

The solubility of lupin GlcCER was determined in the oils, SAAs and co-SAAs selected from the miscibility test using the shake flask method as suggested by Date and Nagarsenker [289]. An excess amount of lupin GlcCER was introduced into 0.5 ml of each components in a 1 ml size Eppendorf tube. Then, it was vortexed and shook on a mechanical shaker for 48 h at room temperature. Each vial was centrifuged at 5,000 rpm for 10 min followed by filtration with a 0.45 μm membrane filter to remove the undissolved GlcCER. Samples were suitably diluted with $CHCl_3$: MeOH (1:1, *v/v*) and the concentration of lupin GlcCER was measured using Automatic Multiple Development High Performance Thin Layer Chromatography (AMD-HPTLC) (see section 4.2.2.10). The experiment was performed in triplicate.

4.2.2.3. Pseudo-ternary phase diagram

Pseudo-ternary phase diagrams were developed at room temperature using aqueous titration method. SAA and co-SAA (S_{mix}) were mixed in different volume ratios to select a suitable hydrophilic lipophilic balance (HLB) value for each oil phase and their mixture. A range of HLB values were investigated for each oil (11, 11.5 and 12 for IPM, and 13, 13.5 and 14 for Miglyol) and their mixture (13.5, IPM: Miglyol, 1:1, *v/v*). To construct the phase diagrams, oil and S_{mix} were mixed ranging from 1:9 to 9:1 (*v/v*) ratios. Sixteen different combinations of oil and S_{mix} (1:9, 1:8, 1:7, 1:6, 1:5, 1:4, 1:3.5, 1:3, 1:2.5, 1:2, 1:1.5, 1:1, 1:0.6, 1:0.5, 1:0.4 and 1: 0.1) were prepared. Then, distilled water with 20% (*v/v*) glycerol was slowly added in 5-10% increment up to 90% with stirring using magnetic stirrer (IKA, C-MAG-HS 7, Staufen, Germany). Clear transparent liquid mixture was considered as NE and marked on the phase diagram [193,290]. Only NE region was plotted and no attempt was made to detect W/O to O/W emulsion transition.

4.2.2.4. Experimental design

Extreme vertices mixture design was developed to investigate the impact of percentage compositions of the independent variables on the globule size of the NEs. Three factors; oil mixture, S_{mix} and aqueous component were studied. Globule size was selected as

dependent variable due to its importance in determining the overall physicochemical characteristics of the formulation and also to determine whether an emulsion is a NE or not. D-optimal design was employed to reduce the number of formulations. The design matrix was developed using Minitab software version 7.1.0 (Pennsylvania, USA). The upper and lower constraint of the factors which were selected from the NE region of the phase diagram, are mentioned in Table 4-1. Based on the design, the input variables were non-negative percentage values of the mixture where the sum had to be equal to 100%. Furthermore, the response had to depend only on the relative proportions of the composition in the mixture and not the volume of the mixture. A total of 10 experiment were run and the results were statistically evaluated. Randomized order of composition of each run was implemented to minimize the unexplained variability in the actual response.

Table 4-1: Independent formulation variables with their upper and lower constraints.

Independent variables	Lower constraint (%, *v/v*)	Upper constraint (%, *v/v*)
IPM: Miglyol	2	3
Tween 80:Transcutol P	15	18
Aqueous phase	79	83

4.2.2.5. Statistical analysis

Optimum composition of the NE was selected upon the condition resulting in a minimum droplet size. The best final model was achieved based on statistical significance ($P < 0.05$) and lack of fit value of the model. Analysis of variance (ANOVA) and coefficient of determination (R^2) were determined to evaluate the goodness of fit of the model and significant differences among the independent variables. Cox response trace, 3D surfaces and contour plots of the fitted polynomial-regression equations were generated to visualize the interaction effect of the independent variables on the response variable. The statistical analysis was performed with Minitab software version 7.1.0 (Pennsylvania, USA).

4.2.2.6. Preparation of lupin glucosylceramide loaded formulations

4.2.2.6.1. Preparation of nanoemulsion

IPM: Miglyol (1:1, *v/v*) mixture, Tween 80, Transcutol P and distilled water with 20% glycerol (*v/v*) were used as oil, SAA, co-SAA and aqueous phase, respectively. Lupin GlcCER (0.25%, *w/w*) was added to the oils mixture, sonicated for 20 min and mixed with the S_{mix} followed by 1 min vortexing. The required amount of aqueous phase was added (1 ml/min) while stirring at 750 rpm using magnetic stirrer. The NE was stirred for 90 min with the same speed after complete addition of the aqueous phase. The globule size and size distribution were measured in triplicate after 24 h of formulation.

4.2.2.6.2. Preparation of nanoemulgel

Hydrogel was prepared using Carbopol 980 (3%, *w/w*) as a thickening agent by dispersing the polymer in a purified water and left overnight for complete swelling. The pH of the gel was adjusted to 6.4 with TRIS (7.5%, *w/v*). Then, it was mixed with lupin GlcCER loaded NE at 2:1 (NE: gel, *w/w*) ratio and Euxyl®PE 9010 (1%, *w/w*) was added as a preservative to the mixture followed by magnetic stirring at 100 rpm until uniform NEG was obtained.

4.2.2.6.3. Preparation of basic cream

Lupin GlcCER loaded basic cream (BC) was prepared after solubilizing the GlcCER in propylene glycol. Then, it was levigated with sufficient amount of BC to make the final concentration of lupin GlcCER 0.25% (*w/w*).

4.2.2.7. Formulation characterization

4.2.2.7.1. Thermodynamic stability

The thermodynamic stability of both lupin GlcCER loaded NEs or NEGs was tested by subjecting them to various stress conditions. Centrifugation, heating and cooling cycle, and freeze–thaw cycle were carried out [199,291].

Centrifugation study: The formulations were centrifuged at 5000 rpm for 30 min and observed for phase separation, creaming or cracking. The formulations that didn't show instability were selected and subjected to heating-cooling cycle.

Heating-cooling test: The preparations were stored at 4 and 40 ˚C at each temperature for 24 h for six cycles. The formulations that were found to be stable at these temperatures were subjected to freeze–thaw stress test.

Freeze-thaw cycle: Formulations were subjected to three freeze-thaw cycles at temperatures between -21 and +25 ˚C (room temperature) with storage at each temperature for 24 h [193].

4.2.2.7.2. Particle size and size distribution

NE particle sizes were measured using Dynamic Light Scattering (DLS) (Nano ZS, Malvern, Worcestershire, United Kingdom), at a scattering angle of 173°, each measurement being the average of 15 runs, each run for a duration of 20 s. To measure the droplets size and size distribution, 100 µl of the formulation was mixed with 900 µl of the aqueous phase in a 1 ml cuvette. Samples were measured after 2 min equilibration at 25 °C and Z-average was taken as an average globule size. The measurements were performed in triplicates. All experiments were carried out at room temperature and the data were analyzed using Zetasizer software version 7.13 (Malvern, United Kingdom).

4.2.2.7.3. Zeta potential and conductivity

The zeta potential and conductivity of the NEs were analyzed using DLS at room temperature. For this purpose, 400 µl of the sample was diluted with 600 µl of aqueous phase in 1 ml cuvette. For a single measurement 30 runs were carried out. The measurement was done in triplicate.

4.2.2.7.4. Refractive index

Refractive index of the NEs was measured using Refractrometer (Mettler Toledo, RM40, Zurich, Switzerland). The average and standard deviation of the readings in triplicate at 25 ºC were calculated.

4.2.2.7.5. pH

The pH of the NEs and NEGs was measured using pH meter (Mettler Toledo, Zurich, Switzerland). The average and standard deviation of the readings in triplicate at 25 ºC were calculated.

4.2.2.7.6. Viscosity

The viscosity of the NEs was measured at 25 °C by using a Rotational Viscometer (Anton Paar GmbH, Graz, Austria). The viscosity of each of the formulation was measured at 16

different shear rates (0.1-100 s^{-1}). The formulation exhibited Newtonian flow and thus the average of the viscosity readings and relative standard deviations (RSD) were calculated.

The viscoelastic characteristics of the NEGs and pure gel were studied using rotational viscometer with cone and plate geometry at 25 °C. Frequency sweep tests were carried out in order to determine the storage (G′) and loss (G″) modulus for a linear viscoelastic region (LVR). The frequency sweep test was done at fixed strain amplitude and varying angular frequency (100-0.1 rad/s).

4.2.2.7.7. Transmission electron microscope imaging

The morphology of the NEs was visualized using a Transmission Electron Microscope (TEM). The sample was homogenized with deionized water and dropped into a 300-mesh formvar coated copper grid (left at 25 °C for 3 min) and negatively stained using 2% uranyl acetate (left at 25 °C for 5 min). Meanwhile, the excess liquid was removed with a piece of Whatman filter paper and dried at room temperature. The dried samples were examined with an EM 900 Transmission Electron Microscope (Carl Zeiss Microscopy, Jena, Germany) at an acceleration voltage of 80 kV. Electron micrographs were taken with a various speed SSCCD camera SM-1k-120 (TRS, Moorenweis, Germany).

4.2.2.7.8. Physical appearance

NEG formulations were inspected visually for their color, homogeneity and consistency [185].

4.2.2.7.9. FTIR-ATR spectroscopic study

The compatibility of lupin GlcCER with NE and NEG formulations was studied with Fourier Transform Infrared (FTIR) spectrometry (Hartmann, 2004). The IR spectra of lupin GlcCER, formulations and their respective ingredients were acquired using a Bruker spectrometer IFS 28 (Bruker Optics, Ettlingen, Germany) equipped with a Thermo Spectra-Tech HATR attachment (Shelton, CT, USA). The sampling compartment is a Fresnel attenuated total reflection (ATR) accessory that uses a zinc selenide (ZnSe) crystal with an angle of incidence of 45° in a horizontal orientation. The diameter of the top of the crystal is 20 mm. Each IR spectrum was collected at about 22 °C with 32 scans and a resolution of 2 cm^{-1} using the Norton-Beer medium apodization.

4.2.2.8. Model membrane preparation

A model membrane was prepared from 100 g membrane solution containing 50 g 8% (*w/w*) dodecanol mixture (dodecanol-octanol-dimethyl sulfoxide (DMSO), 80:10:10, *v/v/v*) in ethanol-diethyl ether (15: 85, *v/v*) and 50 g 4% (*w/w*) collodion solution. The membrane solution was evenly spread over 500 mm x 300 mm size glass surface mounted on a film applicator with adjustable clearance (Workshop, Institute of Pharmacy, Martin-Luther University, Halle-Wittenberg). Then, it was kept under fume hood for about 12 h. The film was removed from the glass surface and cut into 40 mm diameter membrane disc [197,292].

4.2.2.9. *In-vitro* release study

The release and penetration of lupin GlcCER from different formulations was investigated using an *in-vitro* multi-layer membrane model described by Neubert et al [197]. The model contains penetration cells arranged one over the other in a penetration cell stand. Each cell contains four layers of circular 40 mm membrane films arranged one over the other in between the lower circular base plate and upper cover plate. A stencil, with a square opening (4 cm^2) at the center, was put above the membranes. The lower base plate was covered with aluminum foil. The schematic diagram of *in vitro* multi-layer membrane assembly is depicted in Fig. A5 (Appendix). An equivalent mass of the formulation containing 50 µg lupin GlcCER was evenly spread through the stencil over the upper membrane and the cells were kept at 32 ºC in a thermostatic chamber for predetermined time intervals (15, 30, 60,120 and 180 min) allowing release and penetration of lupin GlcCER. Then, the cells were taken out, the formulation remained unabsorbed over the surface of the first layer was removed using a cotton swab and the membranes were separated. The GlcCER was extracted with *n*-hexane-ethanol (2:1, *v/v*) after sonication for 30 min at 50 ºC and dried with N_2-gas stream. AMD-HPTLC was used to quantify lupin GlcCER in five replicates.

4.2.2.10. Plant GlcCER quantification with AMD-HPTLC method

Quantification of lupin GlcCER was carried out using an AMD-HPTLC system with a software CAMAG winCATS Planar Chromatography Manager (Camag, Muttenz, Switzerland). The standard Soy GlcCER solution (100 µg/ml) was prepared in

$CHCl_3$/MeOH (1:1, *v/v*) mixture. The dried lupin GlcCER extracts were diluted with appropriate volume of $CHCl_3$/MeOH (1:1, *v/v*) mixture. Chromatography was performed on precoated silica gel 60 F254 HPTLC plates (20 × 10 cm). Prior to sample application, the HPTLC plate was prewashed (immersed in isopropanol for at least 2 h) and dried in an oven at 100 °C for 30 min. The plate was then cooled to room temperature and different volumes of Soy GlcCER standard solution (0.5, 1, 2, 4, 6, 8, and 10 µL) and appropriate volume of lupin GlcCER solutions were applied on the plate (positioned 8 mm from the bottom and 15 mm from the side edge) as 6 mm bands using a CAMAG Automatic TLC sampler 4 equipped with 25 µL syringe. Chromatographic developments were conducted three times using CAMAG AMD 2. $CHCl_3$/MeOH/HAc (95:4.5:0.5, *v/v/v*) was used as a mobile phase for the first two steps with 70 mm migration distance and $CHCl_3$/MeOH/AC (76:20:4, *v/v/v*) for the last run of 30 mm migration distance. Before each step was run, the plate was automatically vacuum dried for 1.5 min and then conditioned in 4M acetic acid atmosphere. Lupin GlcCER was detected by immersing the HPTLC plate in aqueous $CuSO_4/H_3PO_4$ solution for 20 s using automatic dipping device and charring in an oven at 150 ºC for 20 min. Then the plate was scanned by a CAMAG TLC Scanner 3 in absorbance mode (λ =546 nm) [257].

4.3. Results and discussion

4.3.1. Screening of ingredients

Important criteria for screening of stable drug loaded O/W NE components are the solubility of an active ingredient in the SAA, co-SAA and oil phase and miscibility of the ingredients with each other. Pharmaceutical acceptability related with irritant nature and skin sensitivity, and falling under the generally-regarded-as-safe category are also considered in selecting excipients for topical formulation [293,294].

The miscibility study showed that, IPM, Miglyol, Tween 80 and Transcutol were miscible with each other and considered in the preparation of NEs. PG was immiscible with IPM, Miglyol and Span 80. IPM and Span 80 were immiscible. The solubility of lupin GlcCER was studied in the selected ingredients and found to be 0.48 ± 0.015, 0.54 ± 0.0013 and 0.37 ± 0.0058 mg/ml in IPM, Transcutol and Tween 80, respectively. Its solubility in Miglyol was below the detection limit of the instrument and the aqueous phase was not

included in the solubility study as the GlcCERs was intended to be incorporated in the oil phase and practically insoluble in water. In addition to miscibility and solubility studies, other quality attributes of each formulation ingredient towards stability and pharmaceutical acceptability of the formulations were taken into consideration. IPM is a liquid wax common in topical formulations as skin permeation enhancer [295] and Miglyol (medium chain triglyceride) enhances stability of NEs by increasing the lipophilicity of the oil phase and reducing Ostwald ripening (OR). Tween 80 (non-ionic SAA) is safe for all biological tissues including skin which is compatible with various ingredients used in the preparation of emulsions and not affected by pH [171]. Transcutol (diethylene glycol monoethyl ether) falling in the category of hydroalcoholic co-SAA which enhances NEs stability by reducing the interfacial tension and increasing the fluidity of the interface [158]. Transcutol has a well-established safety profile and penetration enhancer property without compromising the integrity of skin structure. The skin permeation of Transcutol leads to increased drug solubility in the SC, decreasing the skin barrier for actives that readily partition into the viable epidermis [296]. Glycerol can be regarded as a skin barrier stabilizing and moisturizing compound. It moisturizes skin by absorbing water that enhances a water flux which is considered to be a stimulus for barrier repair [297].

4.3.2. Phase diagram development

Phase diagram serves as an important tool for screening of formulation components. It is used to describe a specific system with respect to concentration of different components that exists in a single or multiple phases [290]. The phase diagrams of Miglyol, IPM and their mixture are represented in Figure 4-1A-F and 4-2, respectively. Among the S_{mix} ratios investigated, HLB values of 13.5 and 12 provided broader NEs regions for Miglyol (Fig. 4-1B) and IPM (Fig. 4-1F), respectively. It is important to find the chemical type of SAA which best matches that of the oil, as the chain length compatibility of a SAA and an oil phase is critical in the formation of NE systems. The HLB of the SAA that matches the required HLB of the selected oil provides the lowest interfacial tension between the oil and water phases [171] which shows greater nano emulsification efficiency and provides larger NE region [184].

In both Miglyol and IPM phase diagrams, the NEs region at low S_{mix} concentration (< 20%, *v/v*) using distilled water as an aqueous phase were narrow. With the intention of increasing the NEs region at low S_{mix} concentration and enhancing formulation stability, a phase diagram was constructed with IPM: Miglyol (1:1, *v/v*) mixture, S_{mix} and an aqueous phase containing glycerol as a co-solvent. As it can be seen in the figure (Fig. 4-2), the area was increased and it was possible to formulate NEs at 1:1, oil to S_{mix} ratio unlike the pure oils. The possible reason might be the incorporation of glycerol into the surfactant film and the decreased polarity of water which in turn sufficiently reduce the interfacial tension ([184]. Additionally, the continuous phase viscosity enhancement due to glycerol and the presence of Miglyol in the formulation might contribute to the stability by limiting the internal phase mobility and Ostwald ripening [142], respectively.

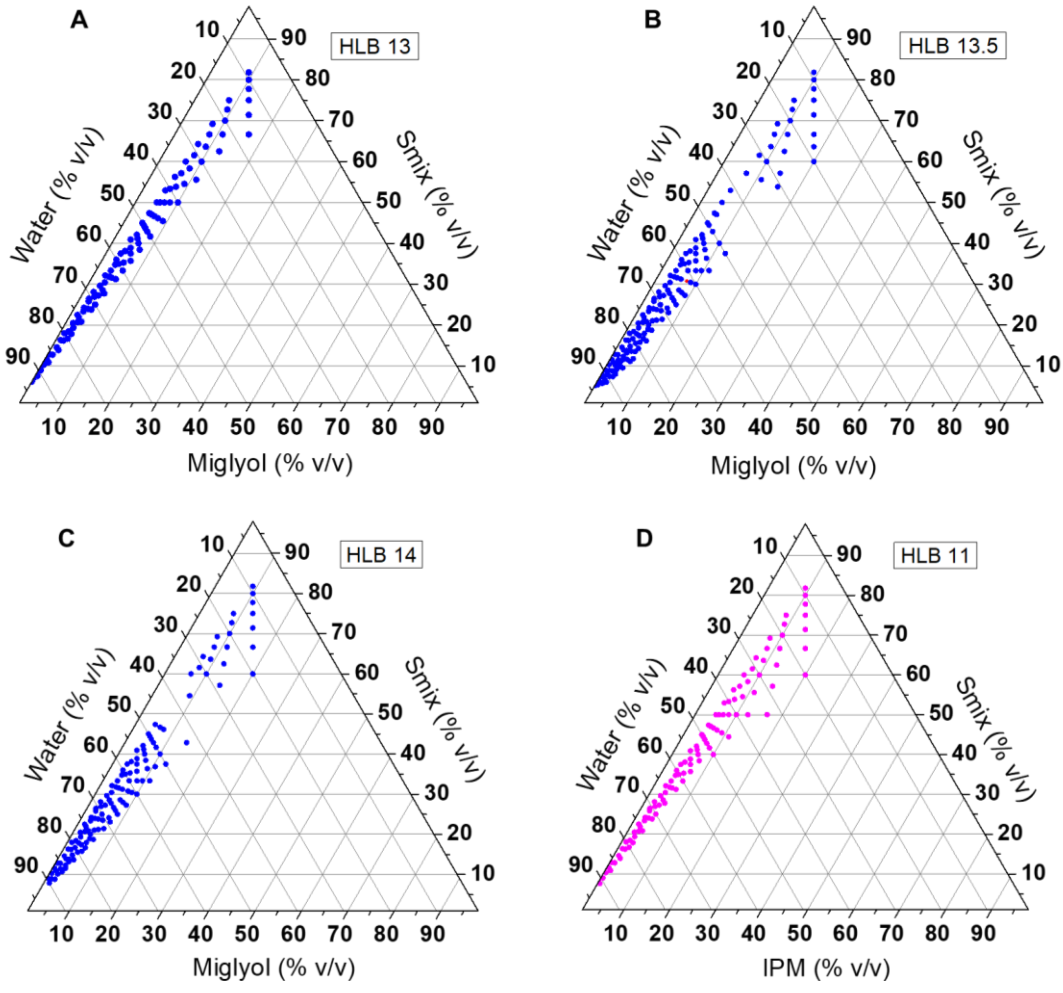

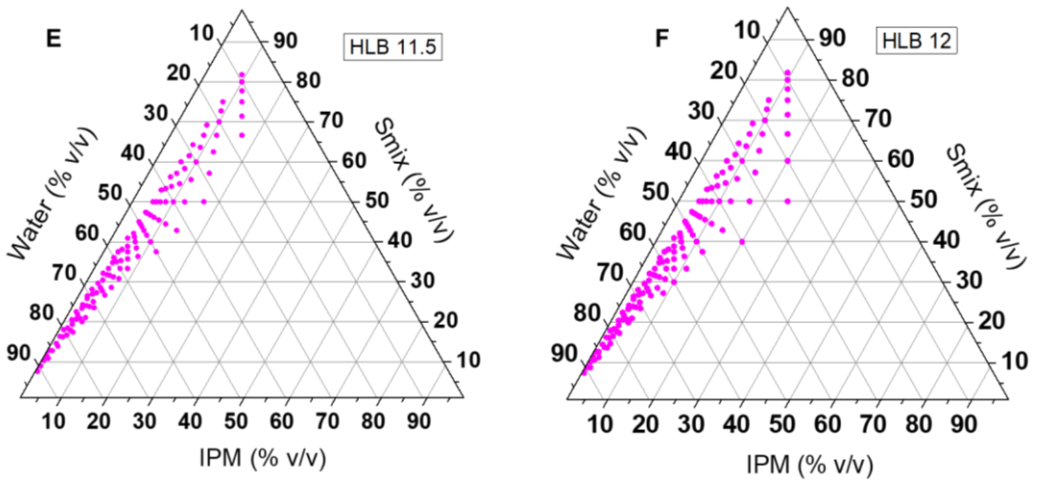

Figure 4-1: Pseudo ternary phase diagrams showing the NE region of Miglyol at HLB value of 13 (A), 13.5 (B) and 14 (C) and IPM at HLB value of 11 (D), 11.5 (E) and 12 (F) using distilled water as an aqueous phase.

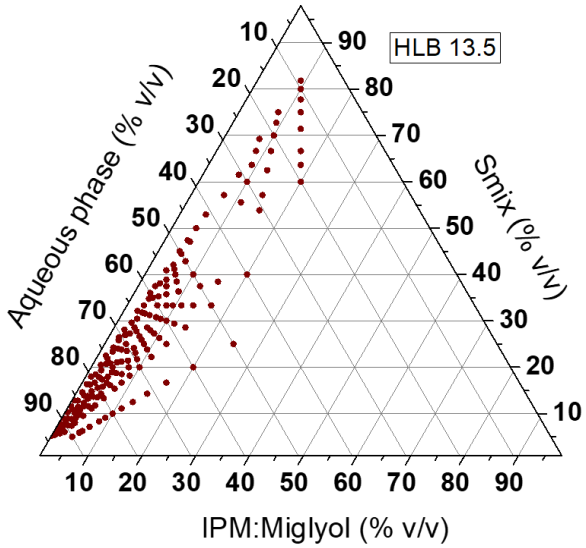

Figure 4-2: Pseudo ternary phase diagram showing the NE region of IPM: Miglyol (1:1, *v/v*) mixture at HLB value of 13.5 using distilled water containing 20% glycerol (*v/v*) as an aqueous phase.

4.3.3. Lupin GlcCER nanoemulsion formulation

Lupin GlcCER loaded NEs were formulated using emulsion inversion point technique which is one of the low energy emulsion preparation technique. Most of commercial topical CER formulations contain 0.2% CERs [298] and in our study we decided to incorporate

0.25% lupin GlcCER into the optimized NEs. Low energy techniques are preferred because of more energy efficiency and the requirement of less sophisticated instruments [174]. Formulation of NEs possessing a uniform droplet size with properly selected preparation method is crucial in the pharmaceutical industry. This is because pharmacokinetic and physicochemical properties of NE such as stability, color, appearance, rheology and penetration are greatly affected by its droplet size and size distribution [147,299]. The size of the droplets formed depends on both formulation and process variables, such as stirring speed, time and rate of water addition [176]. Therefore, these process variables were studied during Miglyol phase diagram development. Miglyol NEs prepared at 1:5 to 1:9, oil to S_{mix} ratios using distilled water with 5, 30 and 60 min stirring time at 500 rpm were transparent immediately after preparation. However, except 1:9 oil to S_{mix} ratio all the rest turned to white color after overnight standing (1:5 and 1:6, oil to S_{mix} ratio) and 3 days of storage (1:7 and 1:8 oil to S_{mix} ratio) which was indicative of instability due to droplet size increment. Similar stability problem was observed after increasing the stirring speed to 750 rpm. Then, the formulations physical appearance was investigated by increasing the stirring time (90 and 120 min) at 750 rpm. The formulations were transparent for a week and NEs globule size did not appear different at stirring time of 90 and 120 min. Thus, 750 rpm and 90 min were selected as stirring speed and time. The aqueous phase addition rate was maintained constant (1 ml/min) during the whole process. The aforementioned process variables were employed in the optimization process.

Thermodynamic stability of NEs from the lower part of NE region of IPM: Miglyol mixture phase diagram (Fig. 4-2) was investigated for the purpose of differentiating metastable and stable NEs. Lower NEs region was preferred to minimize S_{mix} concentration in the formulation. The result showed that 1:1 to 1:4 oil to S_{mix} ratios were unstable with white color or creaming and hence not considered for further optimization. NEs with 1:5 oil to S_{mix} ratio and above were included in a mixture design for optimization. In order to remove metastable NEs, which are not stable and take long time to separate, thermodynamic stability tests are recommended [163,194].

4.3.4. Model fitting

D-optimal extreme vertices mixture design was developed to investigate the effect of percentage composition of oil phase, S_{mix} and aqueous phase on globule size of O/W NEs. The actual and predicted globule size of the NEs obtained from D-optimal design fitted into a quadratic model are shown in Table 4-2. The globule sizes obtained from actual measurement were in excellent agreement with the predicted value of the model. The globule sizes were between 24 and 44 nm. The design is represented by a quadratic regression model and the equation to predict the globule size is given below (Eq.1):

$$Y = 191482A + 7321B + 249C - 237142AB - 194040AC - 9449BC \quad (1)$$

Where, Y, A, B and C stand for globule size, oil phase, S_{mix} and aqueous phase proportions, respectively.

Table 4-2: Measured and predicted globule size of NEs obtained from D-optimal extreme vertices mixture design using Minitab software (version 7.1.0).

Oil phase (% *v/v*)	S_{mix} (% *v/v*)	Aqueous phase (% *v/v*)	Globule size (nm)	
			Measured	Predicted
2	15	83	25.34	25.53
3	15	82	44.29	44.00
2	18	80	27.32	27.57
2	16.5	81.5	24.88	24.43
2.5	16.5	81	26.52	26.29
2.5	15	82.5	29.74	29.92
2.5	18	79.5	26.86	26.91
3	16.5	80.5	37.17	37.85
3	15	82	44.09	44.00
3	18	79	36.26	35.95

The suitability and significance of the final model were assessed with ANOVA analysis. The ANOVA table is presented in Table A4 (Appendix). The model was significant (F value =397 and $P < 0.0001$) and acceptable to show the actual relationship between the response and the independent variables. The coefficient of determination (R^2) and adjusted R^2 values were 99.80% and 99.55%, respectively. The lack of fit was not significant (F

value = 17.06 and P = 0.176) indicating its appropriateness to predict the response based on the independent variables. Insignificant lack of fit, together with the high R^2 and adj-R^2 values, indicate that the quadratic model was capable of representing the system under the given experimental domain [184].

The mixture surface response and contour plots of NEs globule size vs the independent variables are displayed in Fig. 4-3 A and B, respectively. From the plots it is evident that the NEs with the smallest globule size can be obtained at low proportion of the oil phase. However, in mixture design the impact of each formulation component on the response variable cannot be directly interpreted by the coefficient of the model unlike the other experimental designs. Because the effect of a component corresponds to the variation of the response generated by the introduction or removal of a certain amount of the component itself while the fractions of all the remaining components correspondingly decrease or increase, respectively with their ratios unchanged. Thus, trace plot helps to show how each component affects the response relative to a reference blend. A reference blend is the centroid of the design vertices. Components with the greatest effect on the response will have the steepest response traces. The response trace plot showing the influence of each formulation component on NEs globule size is depicted in Fig. A6 (Appendix). The oil phase showed the highest impact on the globule size of the formulation. As the proportion of the oil increased while the other components decreased, the globule size increased. This might be attributed to the difficulty of oil droplet disruption process due to increased resistance of flow and increased rates of emulsion droplets collision frequency [169]. On the other hand, globule size was slightly reduced when the proportions of S_{mix} and aqueous phase increased. However, further increase of these components resulted in globule size growth. The S_{mix} impact might be due to an enhanced aqueous phase penetration into the oil droplets mediated by excess SAA concentration causing disruption of interfacial surface and led to the ejection of oil droplets into the aqueous phase, which in turn forms a coarse emulsion having larger droplet size [300]. The aqueous phase influence on globule size might be due to the elimination of the film around the globules which leads to the coalescence of the droplets and increase in particle size [301].

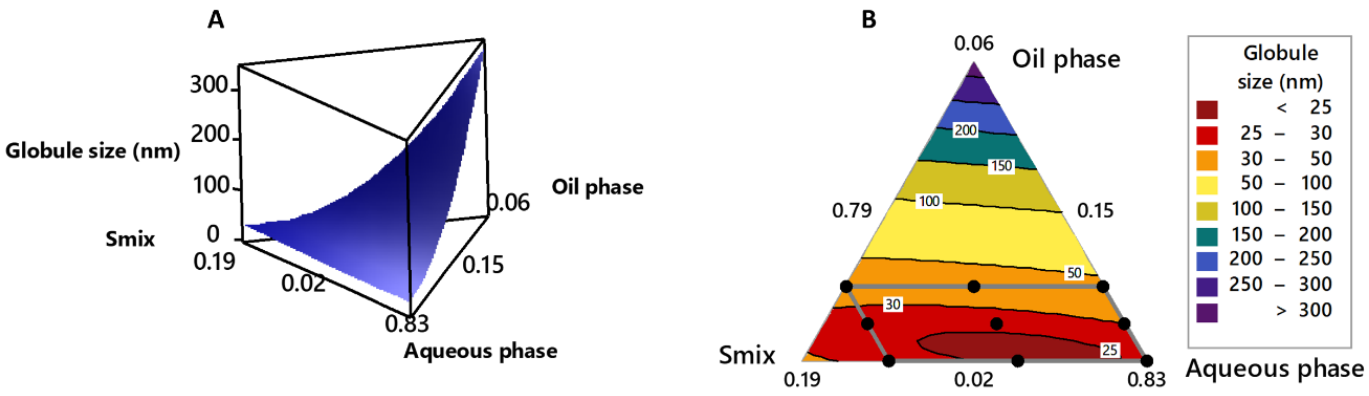

Figure 4-3: Mixture surface (A) and contour (B) plots of IPM: Miglyol (1:1, *v/v*) NEs showing the influence of the formulation components on globule size.

4.3.5. Optimization

NEs are usually characterized by globule size of 20 -200 nm. The smallest size is known to enhance skin penetration of the internal phase thereby the loaded active ingredient into the skin [180]. The formulation of NE would be considered optimum if the applied optimization criteria resulted in smallest average droplet size and narrow PDI-value range within the extreme vertices design region. Thus, numerical and graphical optimization procedures were carried out for predicting the optimum level of oil phase, S_{mix} and aqueous phase to obtain minimum globule size. The optimization plot is depicted in Fig. A7 (Appendix). The minimum point of the graphic optimization could be determined by numerical optimization of the obtained valid quadratic model. By setting the independent variable goals "within the range" and the response to "minimize", the numerical optimization can provide the minimum level of a response (globule size). The numerical optimization suggested 2.15% oil phase, 16.39% S_{mix} and 81.46% aqueous phase would provide a globule size of 23.96 nm with the formulation desirability of 1. Accordingly, the NE prepared from the suggested percentage of each formulation component provided 23.92 ± 0.24 nm which is in excellent agreement with the predicted globule size. A desirability value less than 0.63 is considered as insufficient [180] which shows the best quality of the formulation. The particle size and PDI of optimized lupin GlcCER nanoemulsion is presented in Fig. A8 (Appendix).

4.3.6. Model verification

Model verification is performed by preparing several random formulations or optimized formulations and then comparing the experimental and predicted values. The relative standard error (RSE) of the two values helped to verify the validity of the model. The selected model was verified by preparing the optimized NE in triplicate (F1-F3). The formulation components and verification parameters are presented in Table 4-3. The experimental and predicted values of NE globule size were very close and all the RSE were less than 5% which indicate the appropriateness of the model to predict the response based on the percentage composition of the independent variables. RSE was calculated as; RSE= (experimental value- predicted value)/predicted value*100 [167,302].

Table 4-3: Formulation components of optimized NEs with their respective globule size, RSE and PDI.

S.no	Oil (%, *v/v*)	S_{mix} (% *v/v*)	Aqueous phase (%, *v/v*)	Globule size (nm)		RSE (%)	PDI
				Experimental	Predicted		
F-1	2.15	16.39	81.46	23.93 ± 0.25	23.96	0.12	0.01 ± 0.01
F-2	2.15	16.39	81.46	24.78 ± 0.11	23.96	3.42	0.05 ± 0.02
F-3	2.15	16.39	81.46	23.72 ± 0.06	23.96	1.00	0.07 ± 0.01

PDI: poly dispersity index, RSE: relative standard error

4.3.7. Characterization of optimized nanoemulsion

4.3.7.1. Droplet size, PDI and zeta potential

The physicochemical characteristics of lupin GlcCER loaded and unloaded optimized NEs are summarized in Table 4-4. The average globule sizes of lupin GlcCER loaded and unloaded optimized NEs were 24.75 ± 0.28 and 23.93 ± 0.25 nm, respectively. The globule size didn't show significant difference ($P < 0.005$) with and without lupin GlcCER. NEs with smaller droplet size (< 100 nm) are highly desirable in pharmaceutical and cosmetic industries as it provides extremely low surface tension for the whole system and interfacial tension of O/W droplets. Moreover, NEs possess a large interfacial area, which helps to overcome the epidermal barrier that might favor skin permeation of active substances [184]. The PDI of both loaded and unloaded NEs were 0.07 ± 0.02 and 0.02 ± 0.01,

respectively. PDI is the ratio of standard deviation to mean globule size which indicate the uniformity of globule sizes [158]. A value less than 0.25 indicates a narrow size distribution which in turn shows enhanced physical stability against Ostwald ripening [179,303].

As seen in Table 4-4, both formulations possessed almost similar zeta potential ($P < 0.05$). Emulsifiers stabilize NEs through repulsive electrostatic interaction (zeta potential) and steric hindrance. The values of zeta potential to provide a significant repulsive force between particles are either > +30 mV or < -30 mV [201]. However, stable NEs were reported irrespective of their zeta potential values due to steric stabilizing effect of non-ionic emulsifier [166,169,200]. Steric hindrance is known to be dominant in stabilizing smaller NEs (<50 nm) as the ratio of the SAAs thickness surrounding the internal phase to their size would be higher [149,304]. The stability of NEs obtained in this study might majorly be contributed from steric hindrance effect of Tween 80 and Transcutol.

Table 4-4: Physicochemical characteristics of lupin GlcCER loaded and unloaded optimized NEs.

	Reflectance	pH	Viscosity (mPa.s)	Globule size (nm)	Zeta potential (mV)	PDI	Conductivity (mS/cm)
NE_L	1.38 ± 0.00	4.27 ± 0.01	6.75 ± 0.33	24.75 ± 0.28	-23.30 ± 1.98	0.07 ± 0.02	0.03 ± 0.00
NE	1.38 ± 0.00	4.32 ± 0.01	6.21 ± 0.42	23.93 ± 0.25	-23.95 ± 1.20	0.02 ± 0.01	0.02 ± 0.00

NE_L: NE loaded with 0.25% lupin GlcCER

4.3.7.2. Reflectance, pH and conductivity

As shown in Table 4-4 the reflectance, pH and conductivity of both loaded and unloaded optimized NEs did not show significant difference ($P< 0.05$). Refractive index of a formulation indicates isotropic nature of a formulation. Similarity of reflectance in both GlcCER loaded and pure NEs signifies the formulation remain isotropic after GlcCER loading without chemical interaction with NE components [151,158]. The pH of the formulations were within the range (4-7) for topical application [180,305]. Conductivity helps to investigate the ability of the NEs to conduct electricity which indicate the free amount of water and ions in the system. It also helps to identify the type of NEs as high values signify O/W NEs [180] like values obtained in this study.

4.3.7.3. TEM imaging

The TEM images of unloaded and lupin GlcCER loaded NEs are presented in Fig. 4-4A and B, respectively. The droplets were spherical and distributed uniformly without aggregation. Interestingly, the particle size obtained from DLS measurement were in agreement with TEM globule size imaging analysis for both loaded and unloaded NEs.

4.3.7.4. Lupin GlcCER loaded NEG physical appearance and pH

Clear NEG with a smooth and homogeneous appearance was obtained. The pH of the formulation was 6.2 ± 0.01 which is considered acceptable to avoid the risk of irritation upon application to the skin.

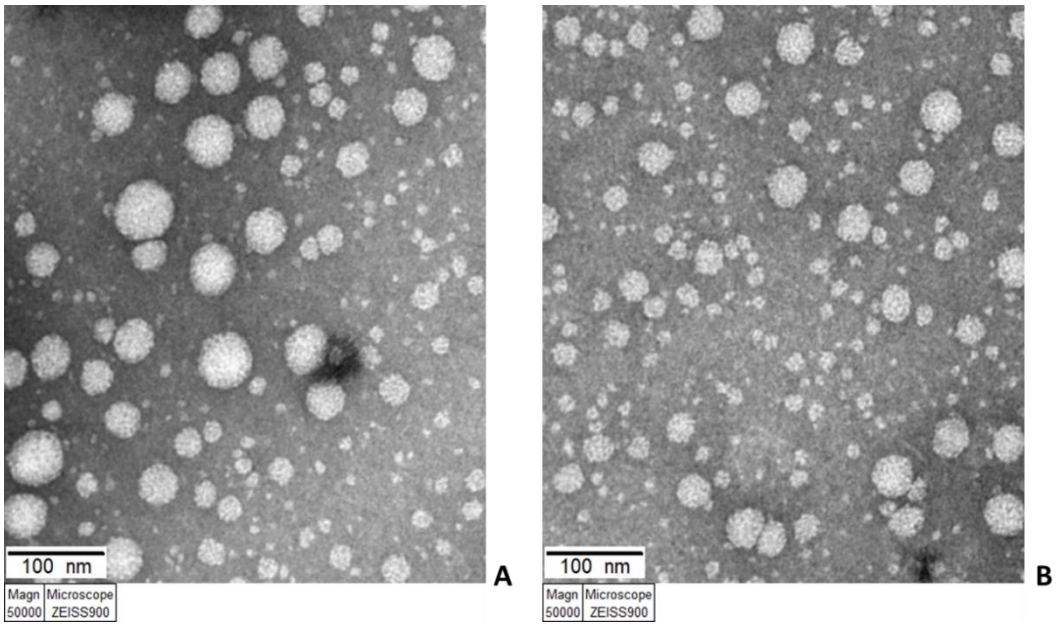

Figure 4-4: Transmission electron micrographs of unloaded (A) and lupin GlcCER optimized NEs (B), negatively stained with Uranyl acetate, respectively, at 50000 magnification.

4.3.7.5. Stability and compatibility

Both lupin GlcCER optimized NE and NEG formulations were stable after thermodynamic stability testing. Neither creaming nor phase separation were observed after all the three tests showing the stability of the formulations under the testing conditions. Thermodynamic stability testing is recommended with the intention of identifying stable NEs from the metastable forms which takes long time to exhibit instability problems such

as phase separation. Those NE formulations that survive the stress testing conditions, are considered stable and do not require frequent testing during storage [163].

Real time stability of both lupin GlcCER NE and NEG formulations at room temperature for 12 months was studied. The droplet size, PDI, refractive index and pH of lupin GlcCER NEs were 24.87 ± 0.11 nm, 0.033 ± 0.00, 1.38 ± 0.00 and 4.1, respectively. However, the unloaded NEs globule size was increased to 67 nm. The globule size increment over 12 months was significant as compared to its size immediately after preparation. Ultra-sonication of loaded NEs to enhance GlcCER solubility might contribute to the stability of the formulation. The pH of the NEG was 5.9 which is still within the acceptable range for topical preparations. The stability of lupin GlcCER NEs would contribute further for the stability of lupin GlcCER NEGs on top of Carbopol 980 gel stability enhancement effect which is in line with other study finding [185].

The FTIR spectra of lupin GlcCER NEG, pure NEG and lupin GlcCER are summarized in Fig. A9 (Appendix). Lupin GlcCER spectrum showed strong absorption bands at 3271.73, 2917.18, 2848.88, 1647.38 and 1535.45 cm^{-1} which correspond to hydroxyl, methylene symmetric, methylene asymmetric, amide I and amide II groups stretching vibrations, respectively. Weak absorption bands were also detected from 1000-1100 cm^{-1} due to head group sugar C-O bond, at 963.16 cm^{-1} due to trans double bond and at 900 cm^{-1} due to β-glycosidic bond. These absorption peaks were in line with other FTIR spectra detected from different plant cerebrosides [242,306–308]. Both lupin GlcCER loaded and unloaded NEGs possessed similar FTIR spectra which were different from lupin GlcCER spectrum. The absorption bands of lupin GlcCER were not detected in the formulation probably due to its restriction inside the formulation matrix and less concentration. Conversely, new absorptions peaks were not also detected in the spectra of lupin GlcCER NEGs which indicate the chemical stability of lupin GlcCER in the formulation [158,309].

4.3.7.6. Rheology

The NEs were less viscous liquid preparations which exhibited Newtonian flow while the NEG exhibited non-Newtonian flow with shear thinning behavior. The viscosity curve of NEG is shown in Fig. A10 (Appendix). The viscosity values with RSD were 6.21 (0.42) and 6.75 (0.33) mPa.s for pure and lupin GlcCER NEs, respectively. The viscosity of the

two formulations were significantly different (P< 0.05) which is supported by Tukey Post hoc test. Liquids are not suitable for topical application due to their less viscous nature. Maximizing the contact duration of a topical formulation with the skin is crucial to enhance drug permeation into the skin. Consequently, the NEs were formulated in the form of NEG to enable the GlcCER remain on the skin for an adequate time. Elastic modules (G'), loss modules (G'') and tan δ of the gel formulations were also investigated in order to determine their viscoelastic characters. The frequency sweep of lupin GlcCER NEG and Carbopol 980 gel are illustrated in Fig. 4-5A and B, respectively. As it can be seen from the graph G' and G" were parallel and tan δ was constant with a value less than 45º. A gel like material exhibit parallel G' and G" which are hardly affected by the frequency and constant phase angle (δ) with a value between 0 and 45º [310] which is in line with our study findings. Besides, G' override G'' in both gel preparations showing the elasticity of the formulation was higher than their viscous behavior producing a well viscoelastic and stable gel [311]. Similarly, tan δ was found to be < 1 indicating the predominant nature of the gel elastic behavior [312]. The NEG and Carbopol 980 gel did not show significant difference in their G', G'' and tan δ values (P > 0.05) which is an indicative of NEs compatibility with the gel.

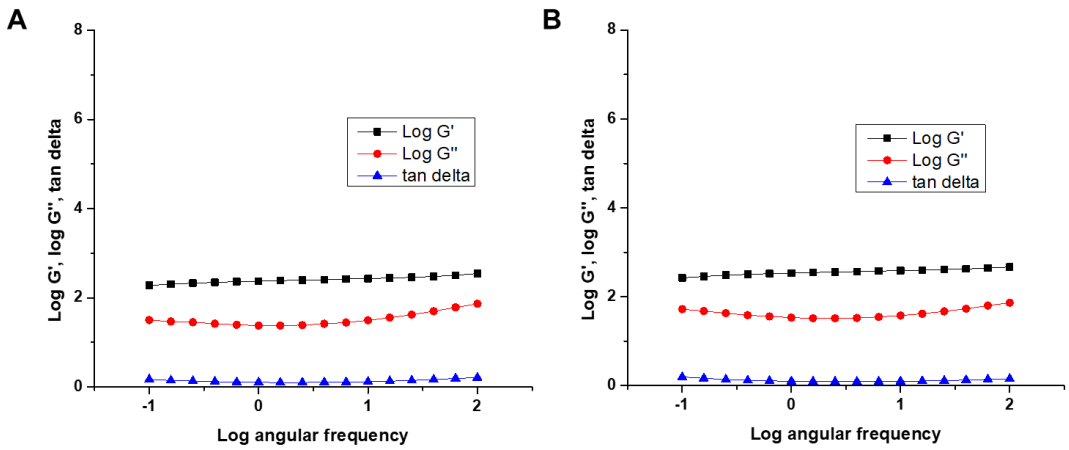

Figure 4-5: Frequency sweep of lupin GlcCER NEG (A) and Carbopol 980 gel (B) measured at 25 ºC

4.3.7.7. *In-vitro* release and penetration of lupin GlcCER

Topical administration of GlcCER is intended to be delivered into the *Stratum corneum* - *Stratum granulosum* junction in order to be hydrolyzed by epidermal enzyme into CER and strengthen the lipoidal structure of SC in aged and/or diseased skin [313]. The release of active substance from the formulation and its penetration deep into different skin layers have to be investigated using best suiting *in-vitro* model such as multilayer membrane. The membrane is composed of collodion as a matrix former and dodecanol mixture (dodecanol-octanol-DMSO (8:1:1, *v/v/v*)) as lipid [197]. Octanol and DMSO were included for the purpose of enhancing membrane stability and increasing GlcCER solubility in the membrane to reduce the number of membrane required to maintain sink condition [292,314]. The *in-vitro* lupin GlcCER release and penetration profiles from NEs, NEGs and BC are summarized in Fig. 4-6A, B and C, respectively. During the experiment four membrane layers were employed which were sufficient to attain sink condition based on the solubility of lupin GlcCER in dodecanol mixture. Sink condition was assumed when the maximum amount of GlcCER dissolved in the membrane was <15% of its saturation solubility in the lipid mixture. BC loaded with 0.25% lupin GlcCER was employed as a reference formulation.

The amount of lupin GlcCER released and penetrated into each membrane layer at different time point was in the order of NEs > BC> NEGs. NEs showed enhanced release and penetration as compared to BC and NEG. On the other hand, the release was highly retarded and showed sustained release character from the NEG which might be attributed to the viscous nature of the formulation. The overall release and penetration profile of lupin GlcCER from the three formulations is shown in Figure 4-7. After 180 min, 51%, 84% and 96% of lupin GlcCER was released and penetrated into the membrane layers from NEG, BC and NEs, respectively. As shown in the figure, the release and penetration of GlcCER from NEs declined after it was incorporated into Carbopol 980 gel (NEG). The GlcCER release and penetration were higher from the NEs than the other two formulations which is in line with other studies. It has been reported in literature that drug release can be improved with nano-sized formulations which provided large surface area for the release of drug and thus permitting faster rate of drug release [162]. The slow release of GlcCER from NEGs is crucial to limit its penetration into the SC of epidermal skin layer and thereby

reduces absorption by the systemic circulation *in-vivo* [166]. It has been reported that NEG slowed the release of active ingredients by 9.12 fold than the conventional formulation [284].

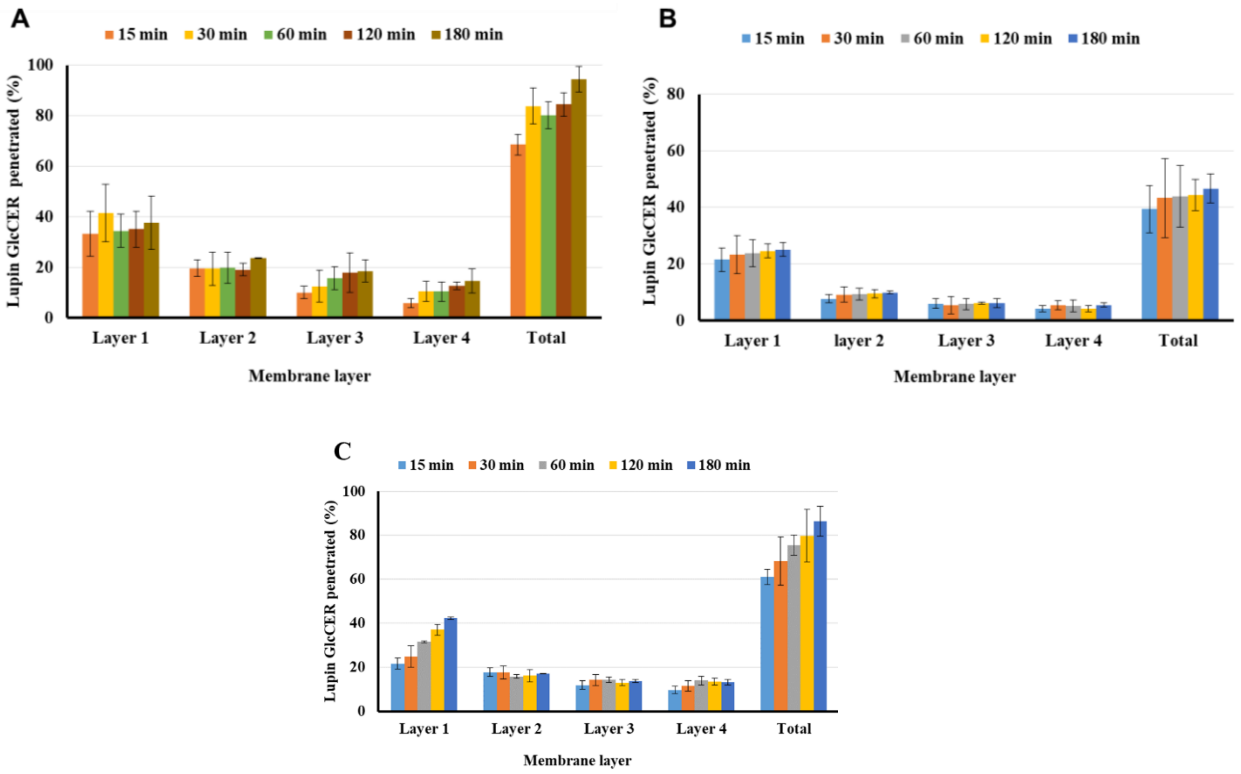

Figure 4-6: Lupin GlcCER release and penetration into multilayer model membranes from NE (A), NEG (B) and BC (C).

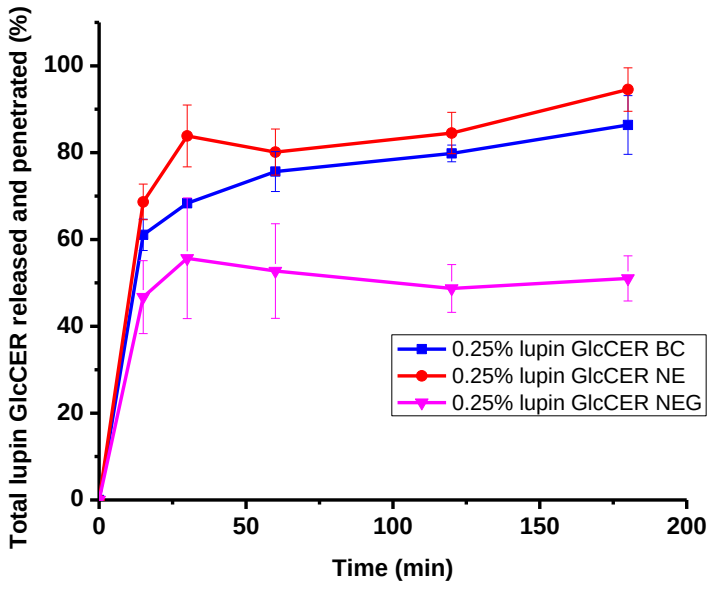

Figure 4-7: Cumulative release and penetration profile of lupin GlcCER from various formulations into multilayer model membranes.

4.4. Conclusions

With the aim of formulating lupin GlcCER for topical delivery optimized NEs and NEGs were prepared and characterized for the first time. Proper selection of S_{mix} HLB value using pseudo ternary phase diagram and use of glycerol as a co-solvent enhanced the nano emulsification process and stability of the formulations. The D-optimal extreme vertices mixture design fitted into quadratic model was accurate in predicting the impact of the independent variables on NEs globule size. Among the independent variables the oil phase showed pronounced negative influence on the globule size of NEs. Both NE and NEG formulations were stable at room temperature for more than 12 months. The release and penetration of lupin GlcCER into the multilayer membrane model were slow and retarded from the NEGs in comparison to BC and NEs. Thus, the nano sized oil phase from the optimized NE and enhanced viscosity from the gel enabled the NEG to be retained topically for longer time and slowly release the GlcCER into the membrane layers. From the foregoing, it can be concluded that NEG could be an alternative for topical delivery of GlcCER into the skin after further *ex-vivo* release and penetration study.

5 Formulation and evaluation of nanoemulgel loaded with essential oils with potential mosquito repellent activities

5.1. Introduction

Over the centuries, vector-borne diseases have imposed a serious public health threat to mankind in terms of illness and deaths globally. Malaria is one of vector-borne diseases caused by *Plasmodium* species and transmitted by female anopheles mosquitoes [212,315]. *Anopheles arabiensis* species is the major vector of both *Plasmodium falciparum* and *Plasmodium vivax,* which is responsible for most malaria transmission [316,317]. Malaria is endemic in 87 countries and poses a risk of malarial infection for almost half of the world's population. In 2019, an estimated 229 million cases of malaria occurred worldwide of which 215 million cases were African [202,203].

Malaria control requires integrated approaches including, prevention and treatment. A global technical strategy for malaria was developed in 2015 to reduce malaria incidence and mortality rates by 90% and eliminate malaria from at least 35 countries by 2030. Huge capital is being invested to achieve the aforementioned goals however, the focus on malarial vector control is relatively lower [202,318]. Larva source management, genetic control, biological control, housing improvement, indoor residual spray (IRS), insecticide treated net (ITN) and long-lasting insecticide treated net (LLIN) are the commonly used malaria vector control strategies. Mosquito repellents are also practiced to prevent mosquito bites outdoors where the individual is not benefiting from the above mentioned strategies. It is also relatively cheap and easy to distribute mosquito repellents during acute emergency situations [210,318]. The mode of action of repellents is very complex and poorly understood. However, the repellents are presumed to work by blocking the odor receptor neurons of the mosquito from detecting the odor of the host [316,317,319].

Despite the efforts being made, many people are still suffering from malaria due to the development of multi-drug resistant *Plasmodium* species and the resistance of malaria vectors [210]. Malaria vectors are also shifting their biting time to day light and preferring to rest outdoors after feeding which limit LLINs and IRS effectiveness and necessitated the use of mosquito repellent [316,320]. Natural and synthetic mosquito repellents are available. N, N-diethyl-3-methylbenzamide (DEET) is the oldest and most widely used

synthetic repellent. However, severe adverse reactions have been reported arising from its cutaneous absorption [213,215,321].

The repellency of plant materials has been exploited for centuries by applying essential oils on the skin and clothes [189,322]. A number of essential oils are known to have repellent activity, including citronella, palmarosa, lemon grass, garlic, eucalyptus, turmeric and basil [224,323]. The essential oils are mainly composed of monoterpenes, monoterpenoids, sesquiterpenes, sesquiterpenoids and alcohols [324–326].

Nevertheless, plant essential oils effectiveness is short-lived derived from their volatile nature. Ideal repellents are expected to be effective against multiple mosquito species for at least 8 h with no skin irritation and systemic toxicity [214]. Despite the difficulty of getting a single repellent possessing all the required qualities, the repellency of volatile oils could be significantly improved if they are formulated as modified release dosage forms [156,327,328]. Citronella oil (CO) has been tested as a mosquito repellent in the form of an oil blend [226], patch [215], cream [186], microcapsules [227] and nanoemulsion [178]. However, except for the microcapsulated CO, which did not report protection time against mosquitoes, the other reports showed very short protection time, albeit the concentration of CO varied from 5 to 20%. On the other hand, 6 to 8 h protection time has been reported for palmarosa oil (PO) [221]. It has been indicated in the literature that the more the essential oil release is sustained, the longer will be the protection time [181,329,330]. Therefore, the aim of the current study was to formulate essential oils (*Cymbopogon nardus* and *C. martini,* family Poaceae) with mosquito repellent activities in the form of nanoemulgels (NEGs) in order to prolong the *in vitro* release at least for 12 h.

5.2. Materials and methods

5.2.1. Materials

Glycerol, n-hexane, NaOH, HCl and NaCl (Carl Roth, Karlsruhe, Germany), ethanol (Brüggemann GmbH & Co. KG, Heilbronn, Germany), Tween 80 and Span 20 (Sigma Aldrich GmbH, Taufkirchen, Germany). Transcutol P (Diethylene Glycol Monoethyl Ether) (Gattefoss´e, Lyon, France), Carbopol®934 polymer (Lubrizol Advanced Materials Europe BVBA, Brussels, Belgium), Tween 80, Span 20, citronellal and geranium reference standards (Sigma-Aldrich GmbH, Steinheim, Germany) were used as received. Citronella

oil (CO) and palmarosa oil (PO) were obtained from Agri-saft MIDROC Group (Addis Ababa, Ethiopia).

5.2.2. Methods

5.2.2.1. GC-MS analysis

The constituents of CO and PO were analyzed after dilution (100 fold) with *n*-hexane with GC-MS (GC/MS/MS Agilent 7890A/5975C/Chromtech Evolution 3, Agilent, Santa Clara, USA). One µl of the sample was injected at 250 °C in a split mode (25:1) with a helium gas flow set to 1 ml/ min. Chromatography was performed with a 30-m Zebron capillary GC-Column (ZB-5MS plus-Phenomenex, 30 m, 0.25 mm, 0.25 µm). The helium gas flow was constant at 1 ml/min. The temperature program was set to 40 °C with a holding time of 3 min followed by a linear ramp of 7 °C/min up to 200 °C. This was followed by another linear ramp of 100 °C/min up to 300 °C and withholding time of 3 min. Throughout the run, the transfer line, source and quadrupole were set to 280 °C, 230 °C and 150 °C respectively. The raw data was processed by Mass Hunter Qualitative Analysis software (Agilent, B.07.00) and the identification of the chromatographic peaks was confirmed using the essential oil GC/MS library (Adams Library-Version 4).

5.2.2.2. Miscibility test

Surface active agent (SAA), co-SAA and essential oils (CO and PO) were screened for physical compatibility in terms of miscibility with each other. Briefly, 500 mg of SAA/co-SAA was added to 500 mg of either CO or PO in a screw capped glass tube and mixed vigorously by a vortex mixer (Vortex Genie, Scientific Industries, New York, USA) for 1 min. The mixture was observed visually for its clarity and miscibility. Clear, transparent and homogenous mixtures were considered miscible and physically compatible. Whereas the appearance of turbidity was considered a physical incompatibility and the phase separation into layers was regarded as an immiscible system [196].

5.2.2.3. Phase diagram development

Pseudo-ternary phase diagrams were developed at room temperature using the aqueous titration method at selected hydrophilic-lipophilic balance (HLB) values. Suitable HLB values of surfactant mixture (S_{mix}) for both CO and PO were selected after preparing a formulation at different HLB values ranging from 11 to 14. The oil: S_{mix} ratio (1:1, *v/v*), oil

concentration (5% *v/v*) and sonication time (10 min) remained the same. S_{mix} HLB value, which resulted in NE with the smallest droplet size was selected. The phase diagrams were then constructed by mixing oil and S_{mix} at different ratios ranging from 1:9 to 9:1 (*v/v*). Sixteen different combinations of oil and S_{mix} (1:9, 1:8, 1:7, 1:6, 1:5, 1:4, 1:3.5, 1:3, 1:2.5, 1:2, 1:1.5, 1:1, 1:0.6, 1:0.5, 1:0.4 and 1: 0.1) were prepared. Then, distilled water with 40% (*v/v*) glycerol was slowly added in 5-10% increments up to 90% with stirring followed by ultrasonication. A clear transparent liquid mixture was considered as a NE and marked on the phase diagram [193,290]. Only the NE region was plotted and no attempt was made to detect the W/O to O/W emulsion transition.

5.2.2.4. Formulation preparation

5.2.2.4.1. Nanoemulsion formulation

Either CO or PO constitute the oil phase. Tween 80, Transcutol P and distilled water with 40% (*v/v*) glycerol were used as SAA, co-SAA and aqueous phase, respectively. The oil and S_{mix} were thoroughly mixed with a vortex mixer (IKA, VG-3, Scientific Industries, USA) for 1 min. The required amount of the aqueous phase was added slowly while stirring. The primary emulsion was then sonicated for different durations (10 to 60 min) with a probe ultrasonicator (VCX 750, Sonics & Materials INC, USA) using an ice cold water jacketed beaker. The sonication conditions were as follows: 20 kHz energy with 40% amplitude, 5 sec pulse on and 4 sec pulse off.

5.2.2.4.2. Preparation of nanoemulgel

Hydrogel was prepared using Carbopol® 934 (3%, *w/w*) as a thickening agent by dispersing in a distilled water and leaving it overnight for complete swelling. The pH of the gel was adjusted to 6.4 with a 1N NaOH solution. Then, it was mixed with either CO or PO loaded NE at a 2:1 (NE: gel, *w/w*) ratio and methylparaben (1%, *w/w*) was added as a preservative to the mixture, followed by magnetic stirring at 100 rpm until a uniform NEG was obtained.

5.2.2.5. Formulation characterization

5.2.2.5.1. Thermodynamic stability studies

The thermodynamic stability studies of both NEs and NEGs prepared from CO and PO were tested in order to differentiate the stable NEs from the metastable by subjecting them

to various stress conditions. Centrifugation, heating-cooling cycles, and freeze-thaw cycles were carried out [163].

Centrifugation: the prepared formulations were centrifuged at 5000 rpm for 30 min and observed for phase separation, creaming or cracking. The formulations that didn't show any instability (creaming, cracking, phase separation) were selected and subjected to a heating-cooling cycle.

Heating-cooling test: the preparations were stored at 4 and 40 °C for 24 h at each temperature for six cycles alternately. The formulations that were found to be stable at these temperatures were subjected to a freeze-thaw stress test.

Freeze-thaw cycle: formulations were subjected to three freeze-thaw cycles at temperatures between -21 and +25 °C (room temperature), with storage at each temperature for 24 h [160,331].

5.2.2.5.2. Droplet size and size distribution

NE droplet sizes were measured using Photon Correlation Spectroscopy (PCS) (90Plus, Brookhaven Instruments Corporation, New York, USA) at a scattering angle of 90°, with each measurement being the average of 3 runs, each of 90 s duration. To measure the droplets size and size distribution, dilution was performed to make the average count rate between 50 and 300 cps. Samples were measured at 25 °C and the Z-average was taken as an average globule size. The measurements were performed in triplicate. The data were analyzed using 90Plus Particle Sizing software version 3.93 (New York, USA) [299].

5.2.2.5.3. Dilution test

A dilution test was performed in order to observe the phase separation of the NE. For this, 1 ml of optimized NE was diluted with 10 ml of water in a test tube and observed for phase inversion [289]. The experiment was performed in triplicate.

5.2.2.5.4. Viscosity

The viscosity of the NEs was measured at 25 °C by a ViscoStar^{+} L rotational viscometer (Kinematica AG, Luzern, Switzerland) using spindle #L1 at different rotational speeds (20-100 rpm) in triplicate. The formulation exhibited Newtonian flow and thus the average of the viscosity readings and relative standard deviations (RSD) were calculated.

The rheology of the NEGs and pure gel was studied using a rotational viscometer (CAP 2000+L, Brookfield Engineering Laboratories, Inc., Middleboro, USA) with cone and plate geometry at 25 °C in triplicate. For each sample, a continuous variation of shear rate (66-800 s^{-1}) was applied and the resulting shear stress was measured.

5.2.2.5.5. Refractive index

The refractive index of the NEs was measured using a refractrometer (Mettler Toledo, RM40, Zurich, Switzerland). The average and standard deviation of the readings in triplicate at 25 ºC were calculated.

5.2.2.5.6. pH

The pH of the NEs and NEGs was measured using a pH meter (Mettler Toledo, Zurich, Switzerland). The average and standard deviation of the readings in triplicate at 25 ºC were calculated.

5.2.2.5.7. Transmission electron microscope imaging

The morphology of the NEs was visualized using a Transmission Electron Microscope (TEM). The sample was diluted with an equal volume of distilled water and dropped into a 300-mesh formvar coated copper grid (left at 25 °C for 3 min) and negatively stained using 2% uranyl acetate (left at 25 °C for 5 min). Meanwhile, the excess liquid was removed with a piece of Whatman filter paper and dried at room temperature. The dried samples were examined with an EM 900 Transmission Electron Microscope (Carl Zeiss Microscopy, Jena, Germany) at an acceleration voltage of 80 kV. Electron micrographs were taken with a various speed SSCCD camera SM-1k-120 (TRS, Moorenweis, Germany).

5.2.2.5.8. Physical appearance

NEG formulations were inspected visually for their color, homogeneity and consistency [185].

5.2.2.5.9. FTIR-ATR spectroscopic study

The compatibility of CO and PO NEs and NEGs was studied with Fourier Transform Infrared (FTIR) spectroscopy (Hartmann, 2004). The IR spectra of CO and PO formulations and their respective ingredients were acquired using a Bruker spectrometer

IFS 28 (Bruker Optics, Ettlingen, Germany) equipped with a Thermo Spectra-Tech HATR attachment (Shelton, CT, USA). The sampling compartment is a Fresnel attenuated total reflectance (ATR) accessory that uses a zinc selenide (ZnSe) crystal with an angle of incidence of 45° in a horizontal orientation. The diameter of the top of the crystal is 20 mm. Each IR spectrum was collected at about 22 °C with 32 scans and a resolution of 2 cm^{-1} using the Norton-Beer medium apodization.

5.2.2.6. Analytical method validation

The GC-MS method for quantification of both CO and PO was validated with respect to linearity, limit of detection (LOD), limit of quantification (LOQ), accuracy, precision and carry-over effect as per the EMA guideline on validation of bioanalytical methods [244]. Citronellal and geraniol were used as markers for the quantification of CO and PO, respectively. Thus, citronellal and geraniol reference standards were used to validate the method.

5.2.2.6.1. Linearity

Citronellal and geraniol reference standards were diluted using *n*-hexane to prepare 2 µg/mL of stock solution. Then, different concentrations of citronellal (50, 100, 150, 200, 250 and 300 µg/mL) and geraniol (30, 40, 60, 80, 100, 140 and 200 µg/mL) in *n*-hexane were prepared. The linearity of the response over those concentration ranges was investigated using GC-MS. The corresponding extracted ion chromatogram peak area of the ion (*m/z* 154.0) was integrated and calibration curves were drawn.

5.2.2.6.2. Limit of detection and limit of quantification

Limit of detection (LOD) and limit of quantification (LOQ) were calculated from separate calibration curves drawn using five levels of citronellal (50, 100, 150, 200 and 250 µg/mL) and geraniol (30, 40, 60, 80 and 100 µg/mL) (n=3). The concentrations were equally spaced, LOQ being the lowest level. The standard deviation of the response (δ) and slope of the curve (S) were taken to calculate LOD (LOD = 3.3 δ/S) and LOQ (LOQ = 10δ/S).

5.2.2.6.3. Accuracy and precision

The within-run accuracy and precision of the method were assessed by analyzing three concentration levels of citronellal (50, 150 and 300 µg/mL) and geraniol (30, 100 and 200

µg/mL) in triplicate on the same day. Similar concentration and determination levels were used to analyze between-run accuracy and precision on two different days. The percentage recovery and relative standard deviation (RSD) were used to estimate the accuracy and precision of the method, respectively.

5.2.2.6.4. Carryover effect

The carryover effect was tested by injecting blank (*n*-hexane), after high concentrations of citronellal (300 µg/mL) and geraniol (200 µg/mL) and checking the chromatograms for the appearance of the respective component peaks. The experiment was conducted in triplicate.

5.2.2.7. *In vitro* membrane permeation

Permeation studies of the formulations were conducted using vertical diffusion cells (Orchid Scientific, Ambad, India). The samples were placed on a cellulose acetate membrane (0.2 µm pore size, 25 mm diameter, Sartorius, Göttingen, Germany). Prior to vertical cell assembly, the membrane was soaked in isopropyl myristate in order to mimic the lipophilic nature of *stratum corneum*. Then, the membrane was mounted on the vertical cell containing 20 ml of water-ethanol solution (50:50, *v/v*) in a receptor compartment. A formulation containing equivalent to 20 µl of essential oil (CO or PO) was placed in the donor compartment and covered with aluminum foil to create an occlusive environment. The receptor compartment was constantly stirred (700 rpm) and thermostated at 32 °C with a water jacket. The first sample was taken after 30 min of equilibration. Then, an aliquot of a sample (500 µl) from the receptor medium was collected at a predetermined time intervals (0 min, 30 min, 1, 2, 3, 4, 5, 6, 8, 10 and 24 h) and replaced with a similar volume of preheated receptor medium. The collected samples were extracted with *n*-hexane and analyzed by GC-MS in triplicate [227].

5.2.2.8. *In vitro* release study

The *in vitro* release profiles of CO and PO loaded NEGs were investigated using a vertical diffusion cell. The procedure is similar to the *in vitro* membrane permeation study (section 5.2.2.7) except the membrane used for release was dialysis membrane (MWCO 12000 Da, Sigma-Aldrich, USA) [332–334].

5.2.2.9. GC-MS based quantification

The samples obtained from permeation and release studies were analyzed with GC-MS (Agilent 7890B / 5977B Inert Plus, Agilent, Santa Clara, USA). One µl of the sample was injected at 250°C with a helium gas flow set to 1 ml/ min. Chromatography was performed with a 30-m Zebron Capillary GC-Column (ZB-5MS plus-Phenomenex, 30 m, 0.25 mm, 0.25 µm). The helium gas flow was constant at 1 ml/min. The temperature program was set to 40 °C with a holding time of 3 min followed by a linear ramp of 7 °C/min up to 200 °C. This was followed by another linear ramp of 100 °C/min up to 300 °C and a withholding time of 3 min. Throughout the run, the transfer line, source and the quadrupole were set to 280 °C, 230 °C and 150 °C respectively. The raw data was processed by Mass Hunter Qualitative Analysis software (Agilent, B.07.00) and the identification of the chromatographic peaks was confirmed using the essential oils GC-MS library (Adams Library-Version 4). The extracted ion chromatograms (EIC) of citronellal and geraniol were integrated for quantification.

5.3. Results and discussion

5.3.1. GC-MS profiling of the essential oil

The base peak chromatogram of CO and MS spectrum of citronellal are presented in Fig. A11 (Appendix). The GC-MS results showed that citronellal (retention time (t_R) 12.75 min), citronellyl propanoate (t_R 14.34 min) and geraniol (t_R 14.90 min) with relative percentage compositions of 37%, 21% and 14%, respectively were the main components of CO. Isopulegol, terpinen-4-ol and elemol were also identified. Similar components of CO have also been reported in the literature, citronellal being the primary constituent [335–337]. However, the reported percentage of citronellal varied from 22.15% [228] to 37.87% [337].

The base peak chromatogram of PO and MS spectrum of geraniol are depicted in Fig. A12 (Appendix). Geraniol (44%) and geraniol acetate (23%) were the main constituents of PO, the former being the major constituent. Linalool and geranyl formate were also detected in lesser quantities. Similar results indicating geraniol as a major component of PO have been reported [326,338] though its percentage ranges from 65% [339] up to 85% [229,230,325]. Component identification for both CO and PO was performed by comparing the MS spectra of the identified peaks with the reference compound at NIST/NIH library and the total GC-chromatogram peak areas of the identified essential oil components were used to calculate the relative percentage compositions of each constituent.

5.3.2. Ingredient selection for NEs formulation

Miscibility is an important parameter for the stability of a NE. An oil phase, as a main component of the formulation, is required to be miscible with the selected SAA, co-SAA or combination thereof while, immiscibility instigates formulation instability due to phase separation [293,333]. Both essential oils included in the study were miscible with the SAAs (Tween 80, Span 20) and co-SAA (Transcutol P). The SAAs and co-SAA were also miscible in each other. Consequently, Tween 80, Span 20 and Transcutol P were compatible with both CO and PO. In order to identify suitable S_{mix} and HLB values for the essential oils to form O/W NE, a mixture of Tween 80/Span 20 and Tween 80/Transcutol P were employed to prepare NEs. The globule size and PDI of CO and PO NEs prepared at different HLB values of Tween 80/Transcutol P and Tween 80/Span 20 mixture are

given in Table A5 (Appendix). HLB values of 11 and 12 provided the smallest globule size CO and PO NEs, respectively using both Tween 80/Span 20 and Tween 80/Transcutol P mixtures. However, NEs formulated using Tween 80/Transcutol P mixture exhibited significantly lower ($p < 0.05$) globule size than NEs obtained from the Tween 80/Span 20 mixture for both essential oils. Thus, Tween 80 and Transcutol P were selected as a SAA and co-SAA, respectively. Non-irritant nature and good skin tolerance are among the major priorities for topical formulation excipients selection. Non-ionic surfactants, such as Tween 80, are less toxic, biocompatible, less irritant, less affected by pH and ionic strength, and classified as generally regarded as safe (GRAS) by FDA [150,157,171].

Then, phase diagrams were developed for both CO and PO NEs at the selected HLB values in order to optimize the formulations. The phase diagrams of CO and PO NEs are depicted in Fig 5-1.

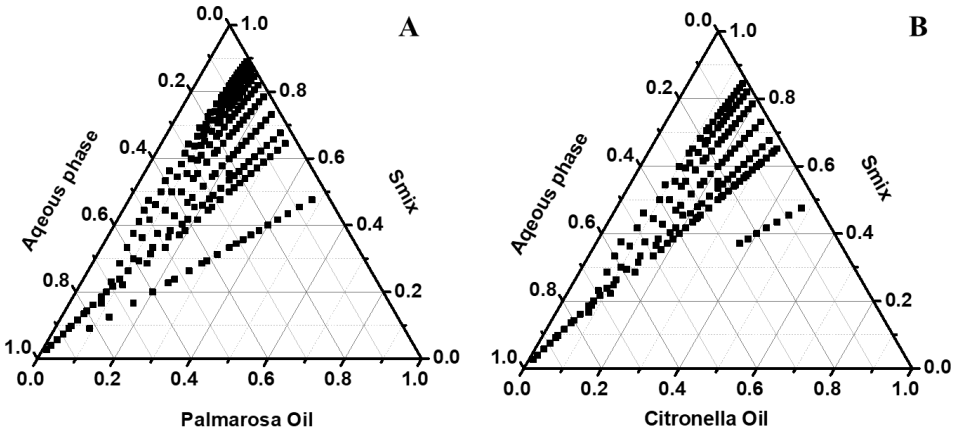

Figure 5-1: PO and CO phase diagrams developed at 12 and 11 HLB values of Tween 80/Transcutol P mixture, respectively using 40% glycerol aqueous phase and sonicated (20 kHz) for 10 min.

Distilled water, with or without a co-solvent is among the commonly employed aqueous phases of NEs. Co-solvents are helpful to enhance the stability of NEs by altering the physicochemical properties of the emulsifier molecules, such as surface-activity, partition coefficient, the ability to form colloidal structure and optimizing dispersed-to-continuous phase viscosity ratio [178,179]. Glycerol was employed as a co-solvent for both CO and PO NEs. The impact of glycerol concentration in the aqueous phase on the stability of NEs

was studied. NEs prepared with aqueous phase containing 10%, 20% and 30% glycerol failed to pass thermodynamic stability tests. However, CO and PO NEs containing 40% (*v/v*) glycerol in distilled water were stable and selected for the final formulation.

Appropriate S_{mix} concentrations to provide stable NEs of CO and PO were selected after thermodynamic stability testing of the formulations within the NE region of the respective phase diagrams. The oil to S_{mix} ratio of 1:1, 1:2, 1:3, 1:3.5 and 1:4 (*v/v*) were included in the stability study. NEs of 1:3 and 1:3.5 oil to S_{mix} ratios were found to be stable for CO and PO, respectively. Accordingly, kinetically stable 10% CO NE was obtained using 30% S_{mix} while 35% S_{mix} was found to be suitable to prepare 10% PO NE. Regarding the selection of essential oil concentration, apart from the phase diagram, toxicity profiles of the essential oils were also considered. It has been indicated that high concentration of CO (20%) in the formulation created difficulty for the clients to use due to its pungent odor [340] and a concentration of 0.05-15% (*w/v*) CO was registered as a safe and effective mosquito repellent [186]. A high concentration of PO was also reported to have cytotoxicity [341].

5.3.3. Effect of sonication time

Ultrasonication is among the high energy methods of NE formulation techniques which employs high frequency (20-100 KHz) sound energy. The energy results in mechanical vibrations that lead to acoustic cavitation phenomena. These cavities collapse with generation of high temperature and pressure whereby such a pressure surge produces a powerful shock waves which break the coarse droplets of micron size into nano-sized globules [342–344].

The impact of sonication time on the globule size of NEs is shown in Fig. 5-2. The globule size of both CO and PO NEs decreased with time. However, the globule size reduction was not significant ($P > 0.05$) after 40 min. It has been reported that increasing sonication time leads to more droplet disruption and size reduction until certain limit is reached [342,345]. Thus, 40 min was selected as the optimum time of sonication for both CO and PO NEs. The temperature rise during ultrasonication was controlled using ice cold water jacketing and manipulating sonication pulse on and off duration. High temperature might be helpful to facilitate emulsification by reducing the viscosity of the medium and enhancing

diffusion, yet cavitation is better attained at lower temperature on top of its impact on heat labile component of the formulation [346,347].

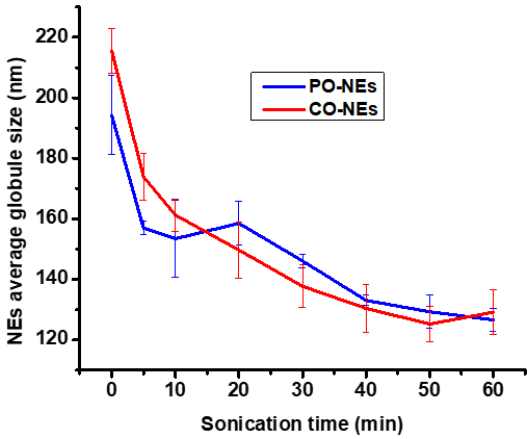

Figure 5-2: Impact of sonication time on the globule size of PO and CO NEs prepared using ultrasonication technique (20 kHz).

5.3.4. Formulation characterization

5.3.4.1. Globule size and PDI

The physicochemical characteristics of CO and PO NEs are presented in Table 5-1. The average globule sizes of optimized CO and PO NEs were 131.34 nm and 120.77 nm, respectively. Moreover, the formulations were less polydisperse with PDI values of 0.240 and 0.220 for CO and PO NEs, respectively. On top of other factors, globule size and size distribution of NE dictate kinetic stability of the formulation against Ostwald ripening. NEs with a low range (< 0.25) of PDI possess homogenously distributed droplets which enhance the stability of the formulation. Ultrasonication is known to produce less polydispersed and more stable NE [342,348,349].

5.3.4.2. Reflectance, pH and conductivity

Clear light yellow NEs were obtained from both CO and PO which might be due to the color of the essential oils and Tween 80. The refractive index of both NEs was found to be similar (Table 5-1). Refractive index shows the isotropic nature of a formulation which is the average value of its constituents. The value also indicates the interaction of a formulation components with each other [151,158]. The pH values of both CO and PO NEs were within the recommended range for topical application [180].

The conductivity of a formulation indicates whether the emulsion is O/W or W/O. O/W emulsions possess high conductivity due to the electric conducting potential of water and ions while W/O emulsions exhibit very low or no conductivity [1,154]. Thus, both CO and PO NEs were considered to be O/W emulsion type.

Table 5-1: The physicochemical characteristics of optimized CO and PO NE formulations (n = 3).

	pH	Globule size (nm)	PDI	Viscosity (cP)	Conductivity (mS/cm)	Refractive index
CO-NE	4.3 ± 0.00	131.34 ± 5.58	0.24 ± 0.02	185.52 ± 11.43	0.035 ± 0.00	1.42 ± 0.00
PO-NE	4.6 ± 0.00	120.77 ± 2.77	0.22 ± 0.03	251.63 ± 5.82	0.042 ± 0.00	1.42 ± 0.00

Mean ± SD

5.3.4.3. TEM images

The Transmission electron micrographs of CO and PO NEs are presented in Figure 5-3 A and B, respectively. The shapes of both NE's oil phase droplets were spherical. The sizes of the droplets were also in the nanometer size range which are in agreement with the results obtained from PCS. Due to the viscous nature of the formulations, diluted NEs with distilled water (1:1, *v/v*) were used for TEM imaging. TEM is a commonly employed instrument for the purpose of investigating the NE's size, shape and morphology [1,300].

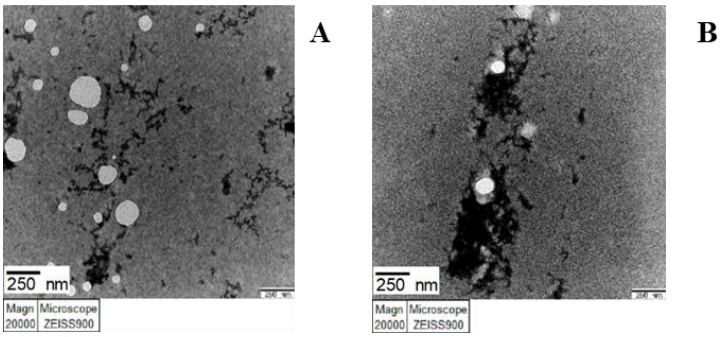

Figure 5-3: Transmission electron micrograph of CO-NE (A) and PO-NE (B) negatively stained with Uranyl acetate at 20,000X magnification.

5.3.4.4. Physical appearance, stability and pH of nanoemulgel

Translucent CO and PO NEGs were obtained. The yellowish color of NEs might be the reason for the translucent appearance of the NEG formulations. Thermodynamic stability study of both NEs and NEGs prepared from either CO or PO showed that all the formulations did not exhibit phase separation, cracking or creaming. Thermodynamic stability study is crucial to differentiate stable from metastable formulations that require some time to manifest instability [151,333]. Formulation pH measurement is crucial to ensure compatibility of the formulation with the skin, as very high and very low formulation pHs result in irritation [151,194]. The pH of CO and PO NEGs was 6 and 6.2, respectively, which is within the recommended range for topical preparations.

5.3.4.5. FTIR analysis

The FTIR spectra of pure essential oils (CO and PO) and their NE and NEG preparations are shown in Fig. A13 (Appendix). Several absorption peaks appeared at different wave numbers corresponding to various functional groups of CO components such as citronellal, geraniol and citronellyl propionate. The absorption peaks at 3413, 2724, 1726, 1645, 1376 and 1021 cm^{-1} represent O-H stretch, aldehydic C-H stretch, C=O stretch, O-H bend, deformation of C-O-H group and C-O stretch, respectively. The IR spectra of CO NE and NEG were overlapping. The major peaks representing CO were detected in the formulations IR spectra though the peak intensities were low which might be due to their low concentration and entrapment in the gel matrix. However, new absorption bands were not detected which is an indication of the absence of interaction between the formulation components [309].

Similarly, major absorption peaks at 3389, 2917, 1721, 1669, 1443, 1376, 1231, and 998 cm^{-1} were identified in the FTIR spectra of PO. The absorption bands detected at 3389, 1669, 1231 and 998 cm^{-1} denote O-H stretch, C=C stretch, C-C stretch and C-O stretch of geraniol, respectively. The peak that appeared at 1721 cm^{-1} was due to the carbonylic stretch of geranyl acetate [350]. All of these absorption peaks were also detected in the FTIR spectra of PO NE and NEG formulations albeit with lower intensity. Moreover, new absorption bands did not appear in the spectra of the formulation, suggesting chemical compatibility of the formulation components.

5.3.4.6. Rheology of NEs and NEGs

Rheological properties of topical formulations are critical evaluation parameters, as rheology influences the flow behavior during manufacturing, pumping, filling and application of the products [172,311]. The NEs prepared from both CO and PO exhibited Newtonian flow and the average of the viscosity measurements was taken. The viscosities of CO and PO NEs were 185.52 cP and 251.63 cP, respectively (Table 5-1). PO NE was more viscous than CO NE which might be due to its higher S_{mix} concentration [344]. The rheograms of CO and PO NEGs are shown in Fig. 5-4. Both NEG formulations showed non-Newtonian, shear thinning property (Fig. 5-4A), with a hysteresis loop (Fig. 5-4B). The area of the loop represents the energy loss required to obtain the sol-gel transition and also indicates the extent of thixotropy in the formulation. Shear thinning characteristics of a topical formulation is advantageous as it facilitates even topical application of the product [164,312].

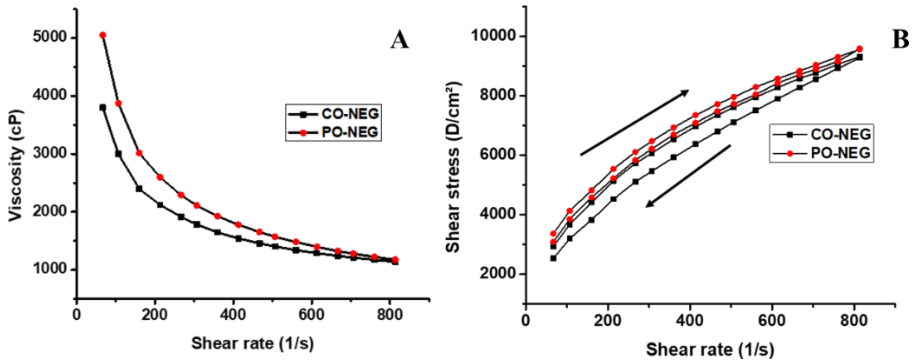

Figure 5-4: Shear thinning characteristics of CO and PO NEGs (A) and hysteresis loop (B).

5.3.4.7. Analytic method validation parameters

A method previously used for monoterpene analysis was validated to ensure its suitability for the quantification of citronellal and geraniol contents of CO and PO in the formulations, respectively. The calibration curves and accuracy and precision data are presented in Fig. A14 and Table A6 (Appendix). The linear ranges of the responses were 50-300 µg/mL and 30- 200 µg/mL for citronellal and geraniol, respectively. The upper limit of the linear range was selected based on the saturation level of the GC-MS signal detector. The R^2 values of the calibration curves for CO and PO were 0.9982 and 0.9997, respectively. The accuracy and precision results were within the standard. The LOD and LOQ values of citronellal

were 16 and 50 µg/mL, respectively. While geraniol possessed 9 µg/mL and 30 µg/mL LOD and LOQ values, respectively. The method was also found to be free from carryover effect.

5.3.4.8. *In vitro* release and membrane permeation of the NEs and NEGs

The *in vitro* release profiles of CO and PO NEGs are shown in Fig. 5-5. A Minimum burst effect was observed from both CO and PO NEGs as only 21% and 23% of their contents were released during the first 2 h, respectively. Moreover, 89% and 90% of the CO and PO contents of the NEGs were released within 24 h of the experiment, respectively. Thus, the mosquito repellent effect of the formulations might be sustained up to 24 h since the slow release of the oil prolongs the protection time against mosquitoes [178]. It has been reported that NEG formulations have the capacity to prolong release of active ingredients due to thier high viscosity and effective retention capacity on the skin [153,192,333].

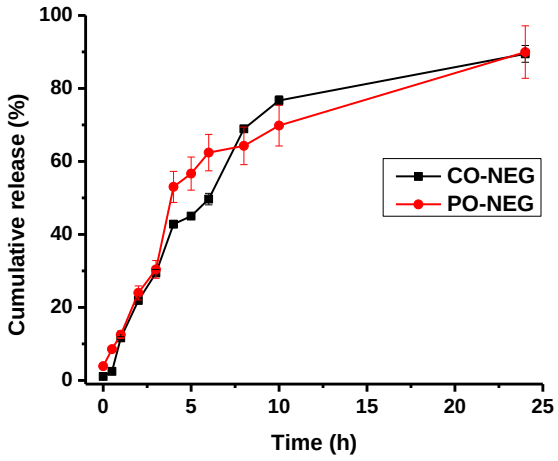

Figure 5-5: *In vitro* release profiles of CO and PO NEGs using dialysis membrane in vertical Franz diffusion cell.

Active substance releases from the formulation and penetration via a cellulose acetate membrane indicate the amount of a substance available for absorption through the skin [172]. The permeation profiles of NEs and NEGs prepared from CO and PO are depicted in Fig.5-6. The amount of essential oils penetrating the membrane from all the formulations increased with time, though the percentage varies with the types of formulation. After 24 h of the experiment, 18% and 30% of CO and PO permeated via the synthetic membrane from the NEG formulations, while 40% and 68% of CO and PO penetrated the membrane

from the NEs, respectively. As can be observed from the figure, both CO and PO NEs showed enhanced permeation as compared to their respective NEG formulations. The NEG formulations reduced the permeation of CO and PO via the synthetic membrane by 2.5 and 2.4 folds at the 24th h, respectively, as compared to their respective NE formulations. The reduced permeation of essential oils from the NEG formulations might be due to the entangled oils within the gelling agent and its higher viscosity, which limit the release of the oils [142]. Moreover, gelling agents are also known to reduce the volatility of essential oils that could possibly reduce the pungent odor of the oil and enhance user compliance [340,351]. Non-irritating nature to the skin and low permeation rate are among the desirable properties of mosquito repellent formulations [327]. On the other hand, PO NE had a higher percentage of permeation than CO NE, which might be related to its higher S_{mix} content and smaller droplet size. SAAs and NE are known to enhance permeation of active ingredients via the skin/synthetic membrane due to their lipid solubilizing capacity and small droplet size, respectively [142,172,178]. Most of the permeation studies are conducted using animal skin [185,321] though synthetic membranes [178,227] are also employed. It has been reported that permeation of insect repellent from advanced formulation such as polymeric micelle and microcapsule were very low compared to their respective conventional topical formulations [227,321].

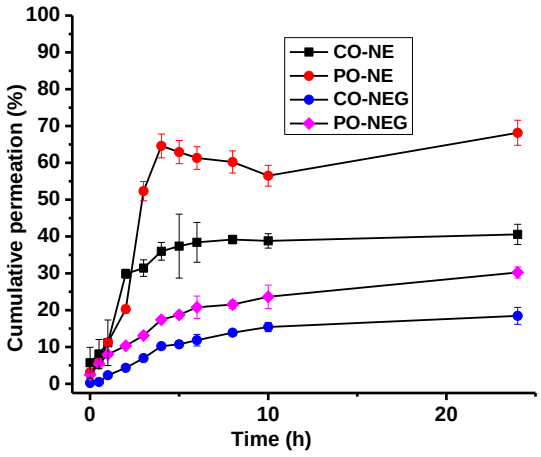

Figure 5-6: Permeation profiles of NE and NEG formulated from CO and PO investigated using cellulose acetate membrane in 50% ethanol.

5.4. Conclusion

Kinetically stable CO and PO NEs were prepared using ultrasonication, a high energy emulsification technique. The droplet size of the NEs decreased with ultrasonication time until 40 min. The incorporation of glycerol in the aqueous phase contributed to the stability of NEs. CO and PO NEGs possessing suitable physicochemical characteristics for topical application were obtained. The GC-MS method employed for quantification of citronellal and geraniol was accurate, precise and free from carryover effects. The NEG formulations effectively reduced the percentage of essential oils permeated via the synthetic membrane by more than 2 folds and prolonged the release up to 24 h. From the foregoing, NEG formulation could be used as an alternative formulation to prolong the protection time of CO and PO against mosquito bites though further confirmatory laboratory and field human bait studies are required.

Suggestions for further work

Based on the findings of the investigation carried out in this study, the following points are forwarded for further research.

- Investigating the kinetics of enzymatic GlcCER hydrolysis and the interaction of the hydrolysis products (CERs) with native skin CERs.
- Performing cytotoxicity studies for the GlcCERs loaded formulations.
- Conducting *in-vivo* skin penetration study of GlcCERs on animal and human volunteers.
- Determining the complete protection time of CO and PO NEGs using WHO approved human bait procedure.

List of publications

1. Adem A.A, Belete A, Soboleva A., Frolov A., Tessema E. N, Gebre-Mariam T., Neubert R.H.H. 2020, Structural characterization of plant glucosylceramides and the corresponding ceramides by UHPLC-LTQ-Orbitrap mass spectrometryFormulation. Journal of Pharmaceutical and Biomedical Analysis 192: 1-12.
   https://doi.org/10.1016/j.jpba.2020.113677
2. Adem A.A, Belete A, Lai K. K., Hage C., Neubert R.H.H., Gebre-Mariam T., 2021. Nanoemulgel formulation for topical delivery of plant glucosylceramide: Characterization and optimization. Journal of Drug Delivery Science and Technology 79: 104056 https://doi.org/10.1016/j.jddst.2022.104056

Lists of publishable manuscripts

1. Adem A.A., Belete A., Raorane L.R., Neubert R.H.H, Gebre-Mariam T. Formulation and Evaluation of Nanoemulgel Loaded with Essential Oils with Mosquito Repellent Activity**. *Submitted to International Journal of Pharmaceutics***
2. Adem A. A., Belete A, Soboleva A., Frolov A., Hage C., Wohlrab J., Gebre-Mariam T., Neubert R.H.H. Investigation of Plant Glucosylceramides Hydrolysis within the Skin Epidermis using a Validated Quantitative LC-HRMS/MS Method. ***Ready for submission***

References

[1] C.M.R.R. Nastiti, T. Ponto, E. Abd, J.E. Grice, H.A.E. Benson, M.S. Roberts, Topical nano and microemulsions for skin delivery, Pharmaceutics. 9 (2017) 1–25. https://doi.org/10.3390/pharmaceutics9040037.

[2] M. Suzuki, Y. Ohno, A. Kihara, Whole picture of human stratum corneum ceramides, including the chain-length diversity of long-chain bases, J. Lipid Res. 63 (2022) 100235. https://doi.org/10.1016/j.jlr.2022.100235.

[3] A.C. Kendall, M. Kiezel-Tsugunova, L.C. Brownbridge, J.L. Harwood, A. Nicolaou, Lipid functions in skin: Differential effects of n-3 polyunsaturated fatty acids on cutaneous ceramides, in a human skin organ culture model, Biochim. Biophys. Acta - Biomembr. 1859 (2017) 1679–1689. https://doi.org/10.1016/j.bbamem.2017.03.016.

[4] H.J. Cho, B.Y. Chung, H.B. Lee, H.O. Kim, C.W. Park, C.H. Lee, Quantitative study of stratum corneum ceramides contents in patients with sensitive skin, J. Dermatol. 39 (2012) 295–300. https://doi.org/10.1111/j.1346-8138.2011.01406.x.

[5] M. Moskot, K. Bocheńska, J. Jakóbkiewicz-Banecka, B. Banecki, M. Gabig-Cimińska, Abnormal sphingolipid world in inflammation specific for lysosomal storage diseases and skin disorders, Int. J. Mol. Sci. 19 (2018). https://doi.org/10.3390/ijms19010247.

[6] D.C. Swartzendruber, P.W. Wertz, K.C. Madison, D.T. Downing, -corneocyte bound with lipid envelop.pdf, J. Invest. Dermatol. 88 (1987) 709–713.

[7] H. Imai, H. Hattori, M. Watanabe, An improved method for analysis of glucosylceramide species having cis-8 and trans-8 isomers of sphingoid bases by LC-MS/MS, Lipids. 47 (2012) 1221–1229. https://doi.org/10.1007/s11745-012-3725-7.

[8] K. Vavrova, A. Kovačik, L. Opalka, Ceramides in the skin barrier, Eur. Pharm. J. 64 (2017) 28–35. https://doi.org/10.1515/afpuc-2017-0004.

[9] L. Coderch, O. López, A. De La Maza, J.L. Parra, Ceramides and skin function, Am. J. Clin. Dermatol. 4 (2003) 107–129. https://doi.org/10.2165/00128071-200304020-00004.

[10] L. Coderch, O. López, A. De La Maza, J.L. Parra, Ceramides and skin function, Am. J. Clin. Dermatol. 4 (2003) 107–129. https://doi.org/10.2165/00128071-200304020-00004.

[11] Y. Masukawa, H. Narita, E. Shimizu, N. Kondo, Y. Sugai, T. Oba, R. Homma, J.

Ishikawa, Y. Takagi, T. Kitahara, Y. Takema, K. Kita, Characterization of overall ceramide species in human stratum corneum, J. Lipid Res. 49 (2008) 1466–1476. https://doi.org/10.1194/jlr.M800014-JLR200.

[12] J. Van Smeden, L. Hoppel, R. Van Der Heijden, T. Hankemeier, R.J. Vreeken, J.A. Bouwstra, LC/MS analysis of stratum corneum lipids: Ceramide profiling and discovery, J. Lipid Res. 52 (2011) 1211–1221. https://doi.org/10.1194/jlr.M014456.

[13] M. Kawana, M. Miyamoto, Y. Ohno, A. Kihara, Comparative profiling and comprehensive quantification of stratum corneum ceramides in humans and mice by LC/MS/MS, J. Lipid Res. 61 (2020) 884–895. https://doi.org/10.1194/jlr.ra120000671.

[14] A. Alexaki, B.A. Clarke, O. Gavrilova, Y. Ma, H. Zhu, X. Ma, L. Xu, G. Tuymetova, B.C. Larman, M.L. Allende, T.M. Dunn, R.L. Proia, De novo sphingolipid biosynthesis is required for adipocyte survival and metabolic homeostasis, J. Biol. Chem. 292 (2017) 3929–3939. https://doi.org/10.1074/jbc.M116.756460.

[15] J. van Smeden, H. Al-Khakany, Y. Wang, D. Visscher, N. Stephens, S. Absalah, H.S. Overkleeft, J.M.F.G. Aerts, A. Hovnanian, J.A. Bouwstra, Skin barrier lipid enzyme activity in Netherton patients is associated with protease activity and ceramide abnormalities, J. Lipid Res. 61 (2020) 859–869. https://doi.org/10.1194/jlr.ra120000639.

[16] M. Janssens, Lamellar Lipid Organization and Ceramide Composition in the Stratum Corneum of Patients with Atopic Eczema, J. Invest. Dermatol. 131 (2011) 2136–2138. https://doi.org/10.1038/jid.2011.175.

[17] J. Van Smeden, J.A. Bouwstra, Stratum Corneum Lipids: Their Role for the Skin Barrier Function in Healthy Subjects and Atopic Dermatitis Patients, Curr. Probl. Dermatology. 49 (2016) 8–26. https://doi.org/10.1159/000441540.

[18] M. Boncheva, The physical chemistry of the stratum corneum lipids, Int. J. Cosmet. Sci. 36 (2014) 505–515. https://doi.org/10.1111/ics.12162.

[19] B. Školová, B. Januìššová, J. Zbytovská, G. Gooris, J. Bouwstra, P. Slepička, P. Berka, J. Roh, K. Palát, A. Hrabálek, K. Vávrová, Ceramides in the skin lipid membranes: Length matters, Langmuir. 29 (2013) 15624–15633. https://doi.org/10.1021/la4037474.

[20] J.A. Bouwstra, F.E.R. Dubbelaar, G.S. Gooris, A.M. Weerheim, M. Ponec, The role of ceramide composition in the lipid organisation of the skin barrier, Biochim. Biophys. Acta - Biomembr. 1419 (1999) 127–136. https://doi.org/10.1016/S0005-2736(99)00057-7.

[21] T. Maula, M.A. Al Sazzad, J.P. Slotte, Influence of Hydroxylation, Chain Length, and Chain Unsaturation on Bilayer Properties of Ceramides, Biophys. J. 109 (2015) 1639–1651. https://doi.org/10.1016/j.bpj.2015.08.040.

[22] D. Groen, D.S. Poole, G.S. Gooris, J.A. Bouwstra, Is an orthorhombic lateral packing and a proper lamellar organization important for the skin barrier function ?, BBA - Biomembr. 1808 (2011) 1529–1537. https://doi.org/10.1016/j.bbamem.2010.10.015.

[23] R.J. Hay, N.E. Johns, H.C. Williams, I.W. Bolliger, R.P. Dellavalle, D.J. Margolis, R. Marks, L. Naldi, M.A. Weinstock, S.K. Wulf, C. Michaud, C.J.L. Murray, M. Naghavi, The Global Burden of Skin Disease in 2010 : An Analysis of the Prevalence and Impact of Skin Conditions, J. Invest. Dermatol. 134 (2014) 1527–1534. https://doi.org/10.1038/jid.2013.446.

[24] F.T. Satimia, S.R. McBride, B. Leppard, Prevalence of skin disease in rural Tanzania and factors influencing the choice of health care, modern or traditional, Arch. Dermatol. 134 (1998) 1363–1366. https://doi.org/10.1001/archderm.134.11.1363.

[25] J. Levin, S.F. Friedlander, J.Q. Del Rosso, Atopic dermatitis and the stratum corneum part 2: Other structural and functional characteristics of the stratum corneum barrier in atopic skin, J. Clin. Aesthet. Dermatol. 6 (2013) 49–54.

[26] P. Rerknimitr, A. Otsuka, C. Nakashima, K. Kabashima, Skin Barrier Function and Atopic Dermatitis, Curr. Dermatol. Rep. 7 (2018) 209–220. https://doi.org/10.1007/s13671-018-0232-y.

[27] A.D.I. Nardo, P. Wertz, A. Giannetti, S. Seidenari, Ceramide and Cholesterol Composition of the Skin of Patients with Atopic Dermatitis, Acta Derm. Venereol. 78 (1998) 27–30.

[28] WHO, Global report on Psoriasis, 2016. http://www.who.int/about/licensing/copyright_form/index.html%0Ahttp://www.who.int/about/licensing/.

[29] S. Motta, M. Monti, S. Sesana, R. Caputo, S. Carelli, R. Ghidoni, Ceramide

composition of the psoriatic scale, BBA - Mol. Basis Dis. 1182 (1993) 147–151. https://doi.org/10.1016/0925-4439(93)90135-N.

[30] U. Yokose, J. Ishikawa, Y. Morokuma, A. Naoe, Y. Inoue, Y. Yasuda, H. Tsujimura, T. Fujimura, T. Murase, A. Hatamochi, The ceramide [NP]/[NS] ratio in the stratum corneum is a potential marker for skin properties and epidermal differentiation, BMC Dermatol. 20 (2020) 1–12. https://doi.org/10.1186/s12895-020-00102-1.

[31] B.K. Kim, J.C. Shon, H.S. Seo, K.H. Liu, J.W. Lee, S.K. Ahn, S.P. Hong, Decrease of ceramides with long-chain fatty acids in psoriasis: Possible inhibitory effect of interferon gamma on chain elongation, Exp. Dermatol. 31 (2021) 122–132. https://doi.org/10.1111/exd.14431.

[32] B.L. Lew, Y. Cho, J. Kim, W.Y. Sim, N.I. Kim, Ceramides and cell signaling molecules in psoriatic epidermis: Reduced levels of ceramides, PKC-α, and JNK, J. Korean Med. Sci. 21 (2006) 95–99. https://doi.org/10.3346/jkms.2006.21.1.95.

[33] Y. Cho, B.L. Lew, K. Seong, N.I. Kim, An inverse relationship between ceramide synthesis and clinical severity in patients with psoriasis, J. Korean Med. Sci. 19 (2004) 859–863. https://doi.org/10.3346/jkms.2004.19.6.859.

[34] J.E. Markham, D. V. Lynch, J.A. Napier, T.M. Dunn, E.B. Cahoon, Plant sphingolipids: Function follows form, Curr. Opin. Plant Biol. 16 (2013) 350–357. https://doi.org/10.1016/j.pbi.2013.02.009.

[35] L. Wang, T. Wang, W.R. Fehr, Effect of seed development stage on sphingolipid and phospholipid contents in soybean seeds, J. Agric. Food Chem. 54 (2006) 7812–7816. https://doi.org/10.1021/jf0616255.

[36] L. V. Michaelson, J.A. Napier, D. Molino, J.D. Faure, Plant sphingolipids: Their importance in cellular organization and adaption, Biochim. Biophys. Acta -. 1861 (2016) 1329–1335. https://doi.org/10.1016/j.bbalip.2016.04.003.

[37] M.O. Pata, Y.A. Hannun, C.K.-Y. Ng, Plant sphingolipids: decoding the enigma of the Sphinx, New Phytol. 185 (2010) 611–630. https://doi.org/10.1158/0008-5472.CAN-10-4002.BONE.

[38] H. Imai, M. Ohnishi, M. Kinoshita, M. Kojima, S. Ito, Structure and Distribution of Cerebroside Containing Unsaturated Hydroxy Fatty Acids in Plant Leaves, Biosci. Biotech. Biochem . 59 (1995) 1309–1313. https://doi.org/10.1271/bbb.59.1309.

[39] D. V. Lynch, T.M. Dunn, An introduction to plant sphingolipids and a review of recent advances in understanding their metabolism and function, New Phytol. 161 (2004) 677–702. https://doi.org/10.1111/j.1469-8137.2003.00992.x.

[40] IUPAC-IUB Commission on Biochemical Nomenclature, The nomenclature of lipids, Biochem.J. 171 (1978) 21–35. https://doi.org/10.1016/0003-9861(68)90152-5.

[41] P. Sperling, E. Heinz, Plant sphingolipids: Structural diversity, biosynthesis, first genes and functions, Biochim. Biophys. Acta. 1632 (2003) 1–15. https://doi.org/10.1016/S1388-1981(03)00033-7.

[42] R. Cammack, C. Lie, H. Egge, P. Karlson, H.B.F. Dixon, J.C. Rigg, Nomenclature of glycolipids, Carbohydr. Res. 312 (1998) 167–175. https://doi.org/10.1016/S0008-6215(98)00231-6.

[43] M.A. Chester, IUPAC-IUB Joint Commission on Biochemical Nomenclature (JCBN). Nomenclature of glycolipids--recommendations 1997., Eur. J. Biochem. 257 (1998) 293–298. https://doi.org/10.1046/j.1432-1327.1998.2570293.x.

[44] N. Canela, P. Herrero, S. Mariné, P. Nadal, M.R. Ras, M.Á. Rodríguez, L. Arola, Analytical methods in sphingolipidomics: Quantitative and profiling approaches in food analysis, J. Chromatogr. A. 1428 (2016) 16–38. https://doi.org/10.1016/j.chroma.2015.07.110.

[45] J.E. Markham, J. Li, E.B. Cahoon, J.G. Jaworski, Separation and identification of major plant sphingolipid classes from leaves, J. Biol. Chem. 281 (2006) 22684–22694. https://doi.org/10.1074/jbc.M604050200.

[46] J.-L. Cacas, S. Melser, F. Domergue, J. Joubès, B. Bourdenx, J.-M. Schmitter, S. Mongrand, Rapid nanoscale quantitative analysis of plant sphingolipid long-chain bases by GC-MS, Anal. Bioanal. Chem. 403 (2012) 2745–2755. https://doi.org/10.1007/s00216-012-6060-1.

[47] D. Warnecke, E. Heinz, Recently discovered functions of glucosylceramides in plants and fungi, Cell. Mol. Life Sci. 60 (2003) 919–941. https://doi.org/10.1007/s00018-003-2243-4.

[48] K.D. Luttgeharm, A.N. Kimberlin, E.B. Cahoon, Plant Sphingolipid Metabolism and Function, in: Y. Nakamura, Y. Li-Beisson (Eds.), Lipids Plant Algae Dev. Subcell. Biochem., 1st ed., Springer International Publishing, Switzerland, 2016: pp. 229–286.

https://doi.org/10.1007/978-3-319-25979-6.

[49] H. Liang, N. Yao, J.T. Song, S. Luo, H. Lu, J.T. Greenberg, Ceramides modulate programmed cell death in plants, Genes Dev. 17 (2003) 2636–2641. https://doi.org/10.1101/gad.1140503.

[50] L. Li, J. Han, Z. Wang, J. Liu, J. Wei, S. Xiong, Z. Zhao, Mass spectrometry methodology in lipid analysis, Int. J. Mol. Sci. 15 (2014) 10492–10507. https://doi.org/10.3390/ijms150610492.

[51] K. Miazek, S. Lebecque, M. Hamaidia, A. Paul, S. Danthine, L. Willems, M. Frederich, E. De Pauw, M. Deleu, A. Richel, D. Goffin, Sphingolipids: Promising lipid-class molecules with potential applications for industry. A review, Biotechnol. Agron. Soc. Environ. 20 (2016) 321–336.

[52] J. Folch, M. Lees, S.G.H. S, A simple method for the isolation and purification of total lipides from animal tissues, J. Biol.Chem. 226 (1957) 497–509.

[53] E.G. Bligh, W.J. Dyer, A rapid method of total lipid extraction and purification, Can. J. Biochem. Physiol. 37 (1959) 911–917.

[54] Y. Fujino, M. Ohnishi, Isolation and structure of diglycosylsterols and triglycosylsterols in rice bran, Biochim. Biophys. Acta. 574 (1979) 94–102. https://doi.org/10.1016/0005-2760(79)90088-2.

[55] A.M. Manich Bou, I. Garay Peral, J.L. Parra Juez, L. Coderch Negra, M. Martí Gelabert, R. Ramírez Mileo, Ceramides Extracted from Wool: Supercritical Extraction Processes, Text. Res. J. 79 (2009) 721–727. https://doi.org/10.1177/0040517508097518.

[56] P.K. Stumpf, J.B. Mudd, W. Davidnes, The Metabolism, Structure, and Function of Plant Lipids, 1st ed., PLENUM PRESS, New york, 1987.

[57] K. Yang, X. Han, Lipidomics: Techniques, applications, and outcomes related to biomedical sciences, Trends Biochem Sci. 41 (2016) 954–969. https://doi.org/10.1007/s11065-015-9294-9.Functional.

[58] T. Tanaka, T. Kida, H. Imai, J.I. Morishige, R. Yamashita, H. Matsuoka, S. Uozumi, K. Satouchi, M. Nagano, A. Tokumura, Identification of a sphingolipid-specific phospholipase D activity associated with the generation of phytoceramide-1-phosphate in cabbage leaves, FEBS J. 280 (2013) 3797–3809.

https://doi.org/10.1111/febs.12374.

[59] B. Fuchs, R. Süß, K. Teuber, M. Eibisch, J. Schiller, Lipid analysis by thin-layer chromatography—A review of the current state, J. Chromatogr. A. 1218 (2011) 2754–2774. https://doi.org/10.1016/j.chroma.2010.11.066.

[60] G. Van Echten-deckert, Sphingolipid Extraction and Analysis by Thin-Layer Chromatography, in: i G. van Echten-Deckert, K. Sandhoff (Eds.), Compr. Nat. Prod. Chem., Elsevier Science, Amsterdam, 2000: pp. 64–79.

[61] C.A. Haynes, J.C. Allegood, H. Park, M.C. Sullards, Sphingolipidomics: methods for the comprehensive analysis of sphingolipids, JJ Chromatogr B Anal. Technol Biomed Life Sci. 877 (2009) 2696–2708. https://doi.org/10.1016/j.jchromb.2008.12.057.SPHINGOLIPIDOMICS.

[62] V.L. Cebolla, C. Jarne, J. Vela, R. Garriga, L. Membrado, V.L. Cebolla, C. Jarne, J. Vela, R. Garriga, L. Membrado, J. Galb, Scanning densitometry and mass spectrometry for HPTLC analysis of lipids : The last 10 years, J. Liq. Chromatogr. Relat. Technol. 44 (2021) 148–170. https://doi.org/10.1080/10826076.2020.1866600.

[63] E.N. Tessema, T. Gebre-mariam, C.E.H. Schmelzer, R.H.H. Neubert, Isolation and structural characterization of glucosylceramides from Ethiopian plants by LC / APCI-MS / MS, J. Pharm. Biomed. Anal. 141 (2017) 241–249. https://doi.org/10.1016/j.jpba.2017.04.036.

[64] T. Gildenast, J. Lasch, Isolation of ceramide fractions from human stratum corneum lipid extracts by high-performance liquid chromatography, Biochim. Biophys. Acta. 1346 (1997) 69–74. https://doi.org/10.1016/S0005-2760(97)00019-2.

[65] H. Farwanah, R. Neubert, S. Zellmer, K. Raith, Improved procedure for the separation of major stratum corneum lipids by means of automated multiple development thin-layer chromatography, J. Chromatogr. B Anal. Technol. Biomed. Life Sci. 780 (2002) 443–450. https://doi.org/10.1016/S1570-0232(02)00654-2.

[66] H. Farwanah, K. Raith, R.H.H. Neubert, J. Wohlrab, Ceramide profiles of the uninvolved skin in atopic dermatitis and psoriasis are comparable to those of healthy skin, Arch. Dermatol. Res. 296 (2005) 514–521. https://doi.org/10.1007/s00403-005-0551-2.

[67] M. Reisberg, N. Arnold, A. Porzel, R.H.H. Neubert, B. Dräger, Production of Rare

Phyto-Ceramides from Abundant Food Plant Residues, J. Agric. Food Chem. 65 (2017) 1507–1517. https://doi.org/10.1021/acs.jafc.6b04275.

[68] M.C. McMaster, LC/MS: A Practical User's Guide, A JOHN WILEY & SONS, INC, New Jersey, 2005. https://doi.org/10.1016/j.jasms.2006.05.001.

[69] Tk. Takahashi, K. Izumi, E. Nakahata, M. Hirata, S. Kazutaka, T. Keisuke, K. Nagao, K. Hiroshi, Quantitation and Structural Determination of Glucosylceramides Contained in Sake Lees, J. Oleo Sci. 63 (2014) 15–23. https://doi.org/10.5650/jos.ess13086.

[70] S. Lee, Y.S. Lee, K.M. Choi, K.S. Yoo, D.M. Sin, W. Kim, Y.M. Lee, J.T. Hong, Y.P. Yun, H.S. Yoo, Quantitative analysis of sphingomyelin by high-performance liquid chromatography after enzymatic hydrolysis, Evidence-Based Complement. Altern. Med. 2012 (2012) 1–9. https://doi.org/10.1155/2012/396218.

[71] Z. Lin, Z. Quan, F. Xueqi, C. Guoqiang, Separation and Detection of Ceramides by HPLC Followed by Evaporative Light-Scattering Detection and Thin Layer Chromatography, TSINGHUA Sci. Technol. 7 (2002) 660–664.

[72] J. Duan, T. Sugawara, T. Hirata, Rapid Quantitative Analysis of Sphingolipids in Seafood Using HPLC with Evaporative Light-Scattering Detection: Its Application in Tissue Distribution of Sphingolipids in Fish, J. Oleo Sci. 59 (2011) 509–513. https://doi.org/10.5650/jos.59.509.

[73] L. Wang, T. Wang, W.R. Fehr, HPLC quantification of sphingolipids in soybeans with modified palmitate content, J. Agric. Food Chem. 54 (2006) 7422–7428. https://doi.org/10.1021/jf061624c.

[74] E. Gutierrez, T. Wang, W.R. Fehr, Quantification of sphingolipids in soybeans, J. Am. Oil Chem. Soc. 81 (2004) 737–742. https://doi.org/10.1007/s11746-004-0971-y.

[75] R. Rombaut, K. Dewettinck, J. Van Camp, Phospho- and sphingolipid content of selected dairy products as determined by HPLC coupled to an evaporative light scattering detector (HPLC-ELSD), J. Food Compos. Anal. 20 (2007) 308–312. https://doi.org/10.1016/j.jfca.2006.01.010.

[76] X. Yan, D.J. Vredeveld, S.R. Missler, Quantification of Glucosylceramides in Wheat Extracts Using High-Performance Liquid Chromatography with Evaporative Light-Scattering Detection, Am. J. Food Sci. Nutr. 2 (2015) 95–100.

http://www.aascit.org/journal/archive2?journalId=907&paperId=3325.

[77] M.C. Sullards, J.C. Allegood, S. Kelly, E. Wang, C.A. Haynes, H. Park, Y. Chen, A.H. Merrill, Structure-Specific, Quantitative Methods for Analysis of Sphingolipids by Liquid Chromatography-Tandem Mass Spectrometry: "Inside-Out" Sphingolipidomics, Methods Enzymol. 432 (2007) 83–115. https://doi.org/10.1016/S0076-6879(07)32004-1.

[78] E. Sisu, C. Flangea, A. Serb, A. Rizzi, A.D. Zamfir, High-performance separation techniques hyphenated to mass spectrometry for ganglioside analysis, Electrophoresis. 32 (2011) 1591–1609. https://doi.org/10.1002/elps.201100067.

[79] H. Farwanah, T. Kolter, K. Sandhoff, Mass spectrometric analysis of neutral sphingolipids: Methods, applications, and limitations, Biochim. Biophys. Acta - Mol. Cell Biol. Lipids. 1811 (2011) 854–860. https://doi.org/10.1016/j.bbalip.2011.05.011.

[80] A.H. Merrill, M.C. Sullards, J.C. Allegood, S. Kelly, E. Wang, Recent Methods in Molecular and Cell Biology of Lipids, in: D.E. Vance (Ed.), Methods, Elsevier, 2005: pp. 1–54.

[81] R.L. Shaner, J.C. Allegood, H. Park, E. Wang, S. Kelly, C.A. Haynes, J. M. Cameron Sullards, and Alfred H. Merrill, Quantitative analysis of sphingolipids for lipidomics using triple quadrupole and quadrupole linear ion trap mass spectrometers, J. Lipid Res. 50 (2009) 1692–1707. https://doi.org/10.1194/jlr.d800051-jlr200.

[82] M.H. Lee, G.H. Lee, J.S. Yoo, Analysis of ceramides in cosmetics by reversed-phase liquid chromatography/electrospray ionization mass spectrometry with collision-induced dissociation, Rapid Commun. Mass Spectrom. 17 (2003) 64–75. https://doi.org/10.1002/rcm.878.

[83] E. Tessema, T. Gebre-Mariam, G. Paulos, J. N.Wohlrab, R.H.H. Neubert, Delivery of oat-derived phytoceramides into the stratum corneum of the skin using nanocarriers: Formulation, characterization and in vitro and ex-vivo penetration studies, Eur. J. Pharm. Biopharm. 127 (2018) 260–269. https://doi.org/10.1016/j.ejpb.2018.02.037.

[84] N. Bartke, A. Fischbeck, H.U. Humpf, Analysis of sphingolipids in potatoes (Solanum tuberosum L.) and sweet potatoes (Ipomoea batatas (L.) Lam.) by reversed phase high-performance liquid chromatography electrospray ionization tandem mass spectrometry (HPLC-ESI-MS/MS), Mol. Nutr. Food Res. 50 (2006) 1201–1211.

https://doi.org/10.1002/mnfr.200600140.

[85] J.-S. Kang, Tandem Mass Spectrometry - Applications and Principles, in: J. Prasain (Ed.), Princ. Appl. LC-MS/MS Quant. Bioanal. Anal. Var. Biol. Samples, InTech, Rijeka, Croatia, 2012: pp. 441–492. https://doi.org/10.5772/32085.

[86] E. de Hoffmann, V. Stroobant, Mass Spectrometry, 3rd ed., John Wiley & Sons Ltd, 2007. https://doi.org/10.1007/978-3-319-54398-7.

[87] X. Han, Lipidomics: Comprehensive Mass Spectrometry of Lipids, Lipidomics Compr. Mass Spectrom. Lipids. (2016) 1–466. https://doi.org/10.1002/9781119085263.

[88] F. Tellier, A. Maia-Grondard, I. Schmitz-Afonso, J.D. Faure, Comparative plant sphingolipidomic reveals specific lipids in seeds and oil, Phytochemistry. 103 (2014) 50–58. https://doi.org/10.1016/j.phytochem.2014.03.023.

[89] T. Sugawara, J. Duan, K. Aida, T. Tsuduki, T. Hirata, Identification of glucosylceramides containing sphingatrienine in maize and rice using ion trap mass spectrometry, Lipids. 45 (2010) 451–455. https://doi.org/10.1007/s11745-010-3417-0.

[90] X. Han, Mass spectrometry for lipidomics, 1st ed., John Wiley & Sons, Inc, 2016. https://doi.org/10.1002/9781119085263.ch4.

[91] E.N. Tessema, T. Gebre-mariam, A. Frolov, J. Wohlrab, R.H.H. Neubert, Development and validation of LC / APCI-MS method for the quantification of oat ceramides in skin permeation studies, Anal. Bioanal. Chem. (2018).

[92] F. Fang, C.-T. Ho, S. Sang, R.T. Rosen, Determination of sphingolipids in nuts and seeds by a single quadrupole liquid chromatography-mass spectrometry method, J. Food Lipids. 12 (2005) 327–343. https://doi.org/https://doi.org/10.1111/j.1745-4522.2005.00028.x.

[93] N. Gassler, Methods in Comprehensive Mass Spectrometry-Based Measurement of Sphingolipids, J. Glycomics Lipidomics. S2 (2013) 1–3. https://doi.org/10.4172/2153-0637.s2-002.

[94] C. Buré, J.L. Cacas, S. Mongrand, J.M. Schmitter, Characterization of glycosyl inositol phosphoryl ceramides from plants and fungi by mass spectrometry, Anal. Bioanal. Chem. 406 (2014) 995–1010. https://doi.org/10.1007/s00216-013-7130-8.

[95] Y. Suzuki, M. Suzuki, E. Ito, N. Goto-Inoue, K. Miseki, J. Iida, Y. Yamazaki, M. Yamada, A. Suzuki, Convenient structural analysis of glycosphingolipids using MALDI-QIT-TOF mass spectrometry with increased laser power and cooling gas flow, J. Biochem. 139 (2006) 771–777. https://doi.org/10.1093/jb/mvj090.

[96] L.D. Sarabia, B.A. Boughton, T. Rupasinghe, A.M.L. van de Meene, D.L. Callahan, C.B. Hill, U. Roessner, High-mass-resolution MALDI mass spectrometry imaging reveals detailed spatial distribution of metabolites and lipids in roots of barley seedlings in response to salinity stress, Metabolomics. 14 (2018) 1–16. https://doi.org/10.1007/s11306-018-1359-3.

[97] J. Bielawski, J.S. Pierce, J. Snider, B. Rembiesa, Z.M. Szulc, A. Bielawska, Sphingolipid analysis by high performance liquid chromatography-tandem mass spectrometry (HPLC-MS/MS), in: C. Chalfant, M. Del Poeta (Eds.), Adv. Exp. Med. Biol. Sphingolipids as Signal. Regul. Mol., 1st ed., Springer-Verlag New York, Charleston, South Carolina, 2010: pp. 46–59. https://doi.org/10.1007/978-1-4419-6741-1_3.

[98] F. Hsu, J. Turk, Glycosphingolipids as Lithiated Adducts by Dissociation on a Triple Stage Quadrupole Instrument, J. Am. Soc. Mass Spectrom. 12 (2001) 61–79.

[99] H.I. M. Watanabe, M. Kawai-Yamada, A. Miyagi, M. Nagano, Characterization of Glucosylceramides in the Polygonaceae , Rumex obtusifolius L. Injurious Weed, Biosci. Biotechnol. Biochem. 75 (2011) 877–881. https://doi.org/10.1271/bbb.100802.

[100] C. Buré, J.L. Cacas, F. Wang, K. Gaudin, F. Domergue, S. Mongrand, J.M. Schmitter, Fast screening of highly glycosylated plant sphingolipids by tandem mass spectrometry, Rapid Commun. Mass Spectrom. 25 (2011) 3131–3145. https://doi.org/10.1002/rcm.5206.

[101] T. Sugawara, K. Aida, J. Duan, T. Hirata, Analysis of Glucosylceramides from Various Sources by Liquid Chromatography-Ion Trap Mass Spectrometry, J. Oleo Sci. 59 (2010) 387–394. https://doi.org/10.5650/jos.59.387.

[102] J.T. Watson, O.D. Sparkman, Introduction to mass spectrometry; Instrumentation, Applications and Strategies for Data Interpretation, 4th ed., John Wiley & Sons, Ltd, Chichester, England, 2007. https://doi.org/10.1088/1751-8113/44/8/085201.

[103] J. Van Smeden, L. Hoppel, R. Van Der Heijden, T. Hankemeier, R.J. Vreeken, J.A. Bouwstra, LC/MS analysis of stratum corneum lipids: Ceramide profiling and discovery, J. Lipid Res. 52 (2011) 1211–1221. https://doi.org/10.1194/jlr.M014456.

[104] A. Muñoz-Garcia, J. Ro, J.C. Brown, J.B. Williams, Identification of complex mixtures of sphingolipids in the stratum corneum by reversed-phase high-performance liquid chromatography and atmospheric pressure photospray ionization mass spectrometry, J. Chromatogr. A. 1133 (2006) 58–68. https://doi.org/10.1016/j.chroma.2006.06.067.

[105] Chen, D. Zhi, Xiong, H. Bin, Tian, Kai, Guo, J. Ming, Huang, X. Zhong, Jiang, Z. Yong, Two new sphingolipids from the leaves of Piper betle L., Molecules. 18 (2013) 11241–11249. https://doi.org/10.3390/molecules180911241.

[106] T. Sugawara, T. Tsuduki, S. Yano, M. Hirose, J. Duan, K. Aida, I. Ikeda, T. Hirata, Intestinal absorption of dietary maize glucosylceramide in lymphatic duct cannulated rats, J. Lipid Res. 51 (2010) 1761–1769. https://doi.org/10.1194/jlr.m002204.

[107] J.E. Markham, J.G. Jaworski, Rapid measurement of sphingolipids from Arabidopsis thaliana by reversed-phase high-performance liquid chromatography coupled to electrospray ionization tandem mass spectrometry, Rapid Commun. Mass Spectrom. 21 (2007) 1304–1314. https://doi.org/10.1002/rcm.

[108] V. Bizot, E. Cestone, A. Michelotti, V. Nobile, Improving skin hydration and age-related symptoms by oral administration of wheat glucosylceramides and digalactosyl diglycerides: A human clinical study, Cosmetics. 37 (2017). https://doi.org/10.3390/cosmetics4040037.

[109] Y. Tokudome, N. Masutani, S. Uchino, H. Fukai, Recovery effects of oral administration of glucosylceramide and beet extract on skin barrier destruction by UVB in hairless mice, Nutrients. 9 (2017). https://doi.org/10.3390/nu9111178.

[110] Q. Zhang, C.R. Flach, R. Mendelsohn, G. Mao, A. Pappas, M.C. Mack, R.M. Walters, M.D. Southall, Topically applied ceramide accumulates in skin glyphs, Clin. Cosmet. Investig. Dermatol. 8 (2015) 329–337. https://doi.org/10.2147/CCID.S83857.

[111] A. Takahashi, A. Kirst, U. Heinrich, A. Kiyomine, K. Ishida, H. Tronnier, H. Theis, T. Nishizaka, H. Tanabe, Evaluation of a Barrier Repair Cream Containing Pseudo-

Ceramide for Practical Use by Hairdressers with Hand Skin Disorders Due to Daily Exposure to Chemical Irritants, J. Cosmet. Dermatological Sci. Appl. 3 (2013) 263–270.

[112] S.A. Koppes, F. Charles, L.A. Lammers, M. Frings-Dresen, S. Kezic, T. Rustemeyer, Efficacy of a cream containing ceramides and magnesium in the treatment of mild to moderate atopic dermatitis: A randomized, double-blind, emollient- and hydrocortisone-controlled trial, Acta Derm. Venereol. 96 (2016) 948–953. https://doi.org/10.2340/00015555-2395.

[113] S.H. Venkataramana, N. Puttaswamy, S. Kodimule, Potential benefits of oral administration of Amorphophallus Konjac glycosylceramides on skin health – a randomized clinical study, BMC Complement. Med. Ther. 20 (2020) 1–9. https://doi.org/10.1186/s12906-019-2721-3.

[114] T. Uchiyama, Y. Nakano, O. Ueda, H. Mori, M. Nakashima, A. Noda, C. Ishizaki, M. Mizoguchi, Oral intake of glucosylceramide improves relatively higher level of transepidermal water loss in mice and healthy human subjects, J. Heal. Sci. 54 (2008) 559–566. https://doi.org/10.1248/jhs.54.559.

[115] H. Shimoda, S. Terazawa, S. Hitoe, J. Tanaka, S. Nakamura, H. Matsuda, M. Yoshikawa, Changes in Ceramides and Glucosylceramides in Mouse Skin and Human Epidermal Equivalents by Rice-Derived Glucosylceramide, J. Med. Food. 15 (2012) 1064–1072. https://doi.org/10.1089/jmf.2011.2137.

[116] Y. Tokudome, M. Endo, F. Hashimoto, Application of glucosylceramide-based liposomes increased the ceramide content in a three-dimensional cultured skin epidermis, Skin Pharmacol. Physiol. 27 (2013) 18–24. https://doi.org/10.1159/000351350.

[117] J. Ono, M. Kinoshita, K. Aida, M. Tamura, M. Ohnishi, Effects of dietary glucosylceramide on dermatitis in atopic dermatitis model mice, Eur. J. Lipid Sci. Technol. 112 (2010) 708–711. https://doi.org/10.1002/ejlt.200900268.

[118] O. Ueda, M. Hasegawa, S. Kitamura, Distribution in skin of ceramide after oral administration to rats, Drug Metab. Pharmacokinet. 24 (2009) 180–184. https://doi.org/10.2133/dmpk.24.180.

[119] O. Ueda, T. Uchiyama, M. Nakashima, Distribution and metabolism of sphingosine

in skin after oral administration to mice, Drug Metab. Pharmacokinet. 25 (2010) 456–465. https://doi.org/10.2133/dmpk.DMPK-10-RG-038.

[120] S.G. Danby, K. Brown, T. Higgs-Bayliss, J. Chittock, L. Albenali, M.J. Cork, The effect of an emollient containing urea, Ceramide NP, and lactate on skin barrier structure and function in older people with dry skin, Skin Pharmacol. Physiol. 29 (2016) 135–147. https://doi.org/10.1159/000445955.

[121] K. De Paepe, D. Roseeuw, V. Rogiers, Repair of acetone- and sodium lauryl sulphate-damaged human skin barrier function using topically applied emulsions containing barrier lipids, JEADV. 16 (2002) 587–594.

[122] U. Wollenweber, M. Farwick, Application of Skin-Identical Ceramide 3 for Enhanced Skin Moisturization and Smoothness: Latest Results, Euro. Cosmet. (2006) 1–5.

[123] T. Berkers, D. Visscher, G.S. Gooris, J.A. Bouwstra, Topically Applied Ceramides Interact with the Stratum Corneum Lipid Matrix in Compromised Ex Vivo Skin, Pharm. Res. 35 (2018) 1–13. https://doi.org/10.1007/s11095-017-2288-y.

[124] M. Liu, X. Li, X. Chen, F. Xue, J. Zheng, Topical application of a linoleic acid-ceramide containing moisturizer exhibit therapeutic and preventive benefits for psoriasis vulgaris : a randomized controlled trial, Dermatol. Ther. 28 (2015) 373–382.

[125] A. Licari, A. Marseglia, F. Agostinis, M. Milani, G. Luigi, G.L. Marseglia, Barrier Repair Therapy in Atopic Eczema : Effects of Isoleucine , Rhamnosoft , Ceramides and Niacinamide Facial and Body Creams on Clinical , Itch and Staphylococcus aureus Skin Colonization : A Prospective Assessor-Blinded Study, Clin. Pediatr. Dermatology. 2 (2016) 1–5. https://doi.org/10.21767/2472-0143.100010.

[126] T.M. Weber, M. Kausch, F. Rippke, A.M. Schoelermann, A.W. Filbry, Treatment of Xerosis with a Topical formulation Containing Glyceryl Glucoside, Natural Moisturizing Factors, and Ceramide, J. Clin. Aesthet. Dermatol. 5 (2012) 29–39.

[127] W. Gehring, J. Wenz, M.. Gloor, Influence of topically applied ceramide / phospholipid mixture on the barrier function of intact skin , atopic skin and experimentally induced barrier damage, Int. J. Cosmet. Sci. 19 (1997) 143–156.

[128] Y. Tokudome, R. Uchida, T. Yokote, H. Todo, N. Hada, J. Yasuda, H. Hayashi, F. Hashimoto, K. Sugibayashi, Effect of topically applied sphingomyelin-based

liposomes on the ceramide level in a three-dimensional cultured human skin model, J. Liposome Res. 20 (2010) 49–54. https://doi.org/10.3109/08982100903062597.

[129] A. Vovesná, A. Zhigunov, M. Balouch, J. Zbytovská, Ceramide liposomes for skin barrier recovery: A novel formulation based on natural skin lipids, Int. J. Pharm. 596 (2021) 1–10. https://doi.org/10.1016/j.ijpharm.2021.120264.

[130] C.-K. Zhoh, C.-G. Han, S.-H. Hong, I.-Y. Kim, H.-S. Lee, Nano Capsulization of Ceramide and the Efficacy of Atopy Skin, (n.d.).

[131] S.M. Jung, G.H. Yoon, H.C. Lee, M.H. Jung, S. Il Yu, S.J. Yeon, S.K. Min, Y.S. Kwon, J.H. Hwang, H.S. Shin, Thermodynamic Insights and Conceptual Design of Skin-Sensitive Chitosan Coated Ceramide/PLGA Nanodrug for Regeneration of Stratum Corneum on Atopic Dermatitis, Sci. Rep. 5 (2015) 1–12. https://doi.org/10.1038/srep18089.

[132] K. Nomoto, F. Hashimoto, K. Sugibayashi, Y. Tokudome, Increasing effect of ceramides in skin by topical application of sphingosine, Glob. Dermatology. 2 (2015) 154–158. https://doi.org/10.15761/god.1000143.

[133] Y. Tokudome, M. Jinno, H. Todo, T. Kon, K. Sugibayashi, F. Hashimoto, Increase in ceramide level after application of various sizes of sphingomyelin liposomes to a cultured human skin model, Skin Pharmacol. Physiol. 24 (2011) 218–223. https://doi.org/10.1159/000324886.

[134] Z.D. Draelos, The effect of ceramide-containing skin care products on eczema resolution duration, Cutis. 81 (2008) 87–91.

[135] K.O. Shin, H. Mihara, K. Ishida, Y. Uchida, K. Park, Exogenous Ceramide Serves as a Precursor to Endogenous Ceramide Synthesis and as a Modulator of Keratinocyte Differentiation, Cells. 11 (2022) 1–12. https://doi.org/10.3390/cells11111742.

[136] R.H.H. Neubert, S. Sonnenberger, B. Dobner, C.W. Gray, K.N. Barger, K. Sevi-Maxwell, E. Sommer, J. Wohlrab, Controlled penetration of a novel dimeric ceramide into and across the stratum corneum using microemulsions and various types of semisolid formulations, Skin Pharmacol. Physiol. 29 (2016) 130–134. https://doi.org/10.1159/000445776.

[137] J.B. Lee, M. Sung, M. Noh, J.E. Kim, J. Jang, S.J. Kim, J.W. Kim, Effective association of ceramide-coassembled lipid nanovehicles with stratum corneum for

improved skin barrier function and enhanced skin penetration, Int. J. Pharm. 579 (2020) 119162. https://doi.org/10.1016/j.ijpharm.2020.119162.

[138] E. Gutierrez, T. Wang, W.R. Fehr, Quantification of Sphingolipids in Soybeans, J. Am. Oil Chem. Soc. 81 (2004) 737–742. https://doi.org/10.1007/s11746-004-0971-y.

[139] F.F. Sahle, S. Lange, B. Dobner, J. Wohlrab, R.H.H. Neubert, Development and validation of LC/ESI-MS method for the detection and quantification of exogenous ceramide NP in stratum corneum and other layers of the skin, J. Pharm. Biomed. Anal. 60 (2012) 7–13. https://doi.org/10.1016/j.jpba.2011.10.032.

[140] P. Sengupta, B. Chatterjee, Potential and future scope of nanoemulgel formulation for topical delivery of lipophilic drugs, Int. J. Pharm. 526 (2017) 353–365. https://doi.org/10.1016/j.ijpharm.2017.04.068.

[141] H. Choudhury, B. Gorain, M. Pandey, L.A. Chatterjee, P. Sengupta, A. Das, N. Molugulu, P. Kesharwani, Recent Update on Nanoemulgel as Topical Drug Delivery System, J. Pharm. Sci. 106 (2017) 1736–1751. https://doi.org/10.1016/j.xphs.2017.03.042.

[142] L. Thomas, F. Zakira, M.A. Mirza, K. Anwer, F.J. Ahmad, Z. Iqbal, Development of Curcumin loaded chitosan polymer based nanoemulsion gel: In vitro, ex vivo evaluation and in vivo wound healing studies, Int. J. Biol. Macromol. (2017). https://doi.org/10.1016/j.ijbiomac.2017.03.066.

[143] N. Uson, M.J. Garcia, C. Solans, Formation of water-in-oil (W / O) nano-emulsions in a water / mixed non-ionic surfactant / oil systems prepared by a low-energy emulsification method, Colloids Surfaces A Physicochem. Eng. Asp. 250 (2004) 415–421. https://doi.org/10.1016/j.colsurfa.2004.03.039.

[144] P. Choudhary, C. Aparna, P. Srinivas, Formulation and evaluation of zaltoprofen nanoemulsion gel, Int. J. Pharm. Technol. 6 (2014) 6552–6571.

[145] V.P. Chavda, D. Shah, A Review on Novel Emulsification Technique: A Nanoemulsion, J. Pharmacol. Toxicol. Stud. 5 (2017) 29–37.

[146] J. Dal Mas, T. Zermiani, L.C. Thiesen, J.L.M. Silveira, K.A.B.S. Da Silva, M.M. De Souza, A. Malheiros, T.M.B. Bresolin, R.M. Lucinda-Silva, Nanoemulsion as a carrier to improve the topical anti-inflammatory activity of stem bark extract of Rapanea ferruginea, Int. J. Nanomedicine. 11 (2016) 4495–4507.

https://doi.org/10.2147/IJN.S110486.

[147] M. Sivakumar, S. Ying, K. Wei, Cavitation technology -A greener processing technique for the generation of pharmaceutical nanoemulsions, Ultrason. Sonochem. (2014) 1–15. https://doi.org/10.1016/j.ultsonch.2014.03.025.

[148] A. Vogt, C. Wischke, A.T. Neffe, N. Ma, U. Alexiev, A. Lendlein, Nanocarriers for drug delivery into and through the skin — Do existing technologies match clinical challenges?, J. Control. Release. 242 (2016) 3–15. https://doi.org/10.1016/j.jconrel.2016.07.027.

[149] T. Tadros, P. Izquierdo, J. Esquena, C. Solans, Formation and stability of nano-emulsions, Adv. Colloid Interface Sci. 108–109 (2004) 303–318. https://doi.org/10.1016/j.cis.2003.10.023.

[150] S. Bhattacharya, B.G. Prajapati, Formulation and optimization of celecoxib nanoemulgel, Asian J Pharm Clin Res. 10 (2017) 353–365. https://doi.org/10.22159/ajpcr.2017.v10i8.19510.

[151] M.S. Alam, M.S. Ali, F. Zaki, N. Alam, M.I. Alam, F. Ahmad, M.R. Siddiqui, M.D. Ali, M.S. Ansari, S. Ahmad, M. Ali, Enhancement of Anti-Dermatitis Potential of Clobetasol Propionate by DHA [Docosahexaenoic Acid] Rich Algal Oil Nanoemulsion Gel, Iran. J. Pharm. Res. 15 (2016) 35–52.

[152] M. Srivastava, K. Kohli, M. Ali, Formulation development of novel in situ nanoemulgel (NEG) of ketoprofen for the treatment of periodontitis, Drug Deliv. 23 (2016) 154–166. https://doi.org/10.3109/10717544.2014.907842.

[153] U. Syamala, Development & optimization of allyl amine antifungal nanoemulgel using 2-3 factorial design: for the treatment of tinea pedis, Eur. Sci. J. 4 (2013) 597–605. https://eujournal.org/index.php/esj/article/view/2515.

[154] R.C. De Azevedo Ribeiro, S.M.A.G. Barreto, E.A. Ostrosky, P.A. Da Rocha-Filho, L.M. Veríssimo, M. Ferrari, Production and characterization of cosmetic nanoemulsions containing Opuntia ficus-indica (L.) Mill extract as moisturizing agent, Molecules. 20 (2015) 2492–2509. https://doi.org/10.3390/molecules20022492.

[155] D.S. Bernardi, T.A. Pereira, N.R. Maciel, J. Bortoloto, G.S. Viera, G.C. Oliveira, P.A. Rocha-filho, Formation and stability of oil-in-water nanoemulsions containing

rice bran oil : in vitro and in vivo assessments, J. Nanobiotechnology. 9 (2011) 1–9.

[156] R. Mohammadi, M. Khoobdel, M. Negahban, S. Khani, Nanoemulsified Mentha piperita and Eucalyptus globulus oils exhibit enhanced repellent activities against Anopheles stephensi, Asian Pac. J. Trop. Med. 12 (2019) 520–527. https://doi.org/10.4103/1995-7645.271292.

[157] O. Samia, R. Hanan, E.T. Kamal, Carbamazepine Mucoadhesive Nanoemulgel (MNEG) as brain targeting delivery system via the olfactory mucosa, Drug Deliv. 19 (2012) 58–67. https://doi.org/10.3109/10717544.2011.644349.

[158] M.R. Patel, M.H. Patel, R.B. Patel, Preparation and in vitro/ex vivo evaluation of nanoemulsion for transnasal delivery of paliperidone, Appl. Nanosci. 6 (2016) 1095–1104. https://doi.org/10.1007/s13204-016-0527-x.

[159] D.J. Mcclements, J. Rao, Food-Grade Nanoemulsions : Formulation , Fabrication , Properties , Performance , Biological Fate , and Potential Toxicity, Crit. Rev. FoodScience AndNutrition. 51 (2011) 285–330. https://doi.org/10.1080/10408398.2011.559558.

[160] R. Tungadi, W. Susanty, P. Wicita, E. Pido, Transdermal delivery of snakehead fish (ophiocephalus striatus) nanoemulgel containing hydrophobic powder for burn wound, Pharm. Sci. 24 (2018) 313–323. https://doi.org/10.15171/PS.2018.45.

[161] K. Mulia, R.M.A. Ramadhan, E. Krisanti, Encapsulation of mangosteen extract in virgin coconut oil based nanoemulsions: Preparation and characterization for topical formulation, Mater. Sci. Forum. 929 (2018) 234–242. https://doi.org/10.4028/www.scientific.net/MSF.929.234.

[162] S. Kotta, A.W. Khan, S.H. Ansari, R.K. Sharma, J. Ali, Formulation of nanoemulsion: A comparison between phase inversion composition method and high-pressure homogenization method, Drug Deliv. 22 (2015) 455–466. https://doi.org/10.3109/10717544.2013.866992.

[163] Abdul-Qadir, M.D. Faiyazuddin, M.D. Talib Hussain, T.M. Alshammari, F. Shakeel, Critical steps and energetics involved in a successful development of a stable nanoemulsion, J. Mol. Liq. 214 (2016) 7–18. https://doi.org/10.1016/j.molliq.2015.11.050.

[164] E. saleh Mahdi, A.M. Noor, M. hameem Sakeena, G.Z. Abdullah, M.F. Abdulkarim,

M.A. Sattar, Formulation and in vitro release evaluation of newly synthesized palm kernel oil esters-based nanoemulsion delivery system for 30 % ethanolic dried extract derived from local Phyllanthus urinaria for skin antiaging, Int. J. Nanomedicine. 6 (2011) 2499–2512.

[165] A. Junkum, W. Maleewong, A. Saeung, D. Champakaew, A. Chansang, D. Amornlerdpison, A.K. Aldred, U. Chaithong, A. Jitpakdi, D. Riyong, B. Pitasawat, Ligusticum sinense Nanoemulsion Gel as Potential Repellent, (2021).

[166] Y. Zheng, W.-Q. Ouyang, Y.-P. Wei, shahid F. Syed, C. Hao, B.-Z. Wang, Y. Shang, Effects of Carbopol ® 934 proportion on nanoemulsion gel for topical and transdermal drug delivery : a skin permeation study, Int. J. Nanomedicine. 11 (2016) 5971–5987.

[167] cheng loong Ngan, M. Basri, F.F. Lye, H. reza F. Masoumi, M. Tripathy, R. abedi Karjiban, E. Abdul-Malek, Comparison of process parameter optimization using different designs in nanoemulsion-based formulation for transdermal delivery of fullerene, Int. J. Nanomedicine. 9 (2014) 4375–4386.

[168] G. Deli, S. Hatziantoniou, Y. Nikas, C. Demetzos, Solid lipid nanoparticles and nanoemulsions containing ceramides : Preparation and physicochemical characterization Solid lipid nanoparticles and nanoemulsions containing ceramides : Preparation and physicochemical characterization, J. Liposome Res. 19 (2009) 180–188. https://doi.org/10.1080/08982100802702046.

[169] S. Zainol, M. Basri, H. Bin Basri, A.F. Shamsuddin, S.S. Abdul-Gani, R.A. Karjiban, E. Abdul-Malek, Formulation Optimization of a Palm-Based Nanoemulsion System Containing Levodopa, Int. J. Mol. Sci. 13 (2012) 13049–13064. https://doi.org/10.3390/ijms131013049.

[170] O. Campolo, G. Giunti, M. Laigle, T. Michel, V. Palmeri, Essential oil-based nano-emulsions: Effect of different surfactants, sonication and plant species on physicochemical characteristics, Ind. Crops Prod. 157 (2020) 112935. https://doi.org/10.1016/j.indcrop.2020.112935.

[171] H.K. Syed, K.K. Peh, Identification of phases of various oil, surfactant/co-surfactants and water system by ternary phase diagram, Acta Pol. Pharm. - Drug Res. 71 (2014) 301–309.

[172] A. Hussain, A. Samad, S.K. Singh, M.N. Ahsan, M.W. Haque, A. Faruk, F.J. Ahmed, Nanoemulsion gel-based topical delivery of an antifungal drug: In vitro activity and in vivo evaluation, Drug Deliv. 23 (2016) 652–667. https://doi.org/10.3109/10717544.2014.933284.

[173] N. Sadurní, C. Solans, N. Azemar, M.J. García-Celma, Studies on the formation of O/W nano-emulsions, by low-energy emulsification methods, suitable for pharmaceutical applications, Eur. J. Pharm. Sci. 26 (2005) 438–445. https://doi.org/10.1016/j.ejps.2005.08.001.

[174] M. Kumar, R.S. Bishnoi, A.K. Shukla, C.P. Jain, Techniques for Formulation of Nanoemulsion Drug Delivery System: A Review., Prev. Nutr. Food Sci. 24 (2019) 225–234. https://doi.org/10.3746/pnf.2019.24.3.225.

[175] H. Jasmina, O. Džana, E. Alisa, V. Edina, R. Ognjenka, Preparation of nanoemulsions by high-energy and low- energy emulsification methods, in: IFMBE Proc. Vol., 2017: pp. 317–322. https://doi.org/10.1007/978-981-10-4166-2.

[176] D.J. Mcclements, Edible nanoemulsions : fabrication, properties, and functional performance, R. Soc. Chem. 7 (2011) 2297–2316. https://doi.org/10.1039/c0sm00549e.

[177] N.A.N. Azmi, A.A.M. Elgharbawy, S.R. Motlagh, N. Samsudin, H.M. Salleh, Nanoemulsions: Factory for food, pharmaceutical and cosmetics, Processes. 7 (2019) 1–34. https://doi.org/10.3390/pr7090617.

[178] U. Sakulku, O. Nuchuchua, N. Uawongyart, S. Puttipipatkhachorn, A. Soottitantawat, U. Ruktanonchai, Characterization and mosquito repellent activity of citronella oil nanoemulsion, Int. J. Pharm. 372 (2009) 105–111. https://doi.org/10.1016/j.ijpharm.2008.12.029.

[179] W.T. Chong, C.P. Tan, Y.K. Cheah, A.F.B. Lajis, N.L.H.M. Dian, S. Kanagaratnam, O.M. Lai, Optimization of process parameters in preparation of tocotrienol-rich red palm oil-based nanoemulsion stabilized by Tween80-Span 80 using response surface methodology, PLoS One. 13 (2018) 1–22. https://doi.org/10.1371/journal.pone.0202771.

[180] S.N. Afifah, S. Azhar, S.E. Ashari, N. Salim, Development of a kojic monooleate-enriched oil-in-water nanoemulsion as a potential carrier for hyperpigmentation

treatment, Int. J. Nanomedicine. 13 (2018) 6465–6479. https://doi.org/10.2147/IJN.S171532.

[181] O. Nuchuchua, U. Sakulku, N. Uawongyart, S. Puttipipatkhachorn, A. Soottitantawat, U. Ruktanonchai, In vitro characterization and mosquito (Aedes aegypti) repellent activity of essential-oils-loaded nanoemulsions, AAPS PharmSciTech. 10 (2009) 1234–1242. https://doi.org/10.1208/s12249-009-9323-1.

[182] A.A. Ochoa, J.A. Hernández-Becerra, A. Cavazos-Garduño, H.S. GarcÍa, E.J. Vernon-Carter, Preparation and characterization of curcumin nanoemulsions obtained by thin-film hydration emulsification and ultrasonication methods, Rev. Mex. Ing. Quim. 15 (2016) 79–90.

[183] L.J. Danielli, M. dos Reis, M. Bianchini, G.S. Camargo, S.A.L. Bordignon, I.K. Guerreiro, A. Fuentefria, M.A. Apel, Antidermatophytic activity of volatile oil and nanoemulsion of Stenachaenium megapotamicum (Spreng.) Baker, Ind. Crops Prod. 50 (2013) 23–28. https://doi.org/10.1016/j.indcrop.2013.07.027.

[184] R. Su, L. Yang, Y. Wang, S. Yu, Y. Guo, J. Deng, Q. Zhao, X. Jin, Formulation, development, and optimization of a novel octyldodecanol-based nanoemulsion for transdermal delivery of ceramide IIIB, Int. J. Nanomedicine. 12 (2017) 5203–5221. https://doi.org/10.2147/IJN.S139975.

[185] A.M. Eid, H.A. El-Enshasy, R. Aziz, N.A. Elmarzugi, Preparation, characterization and anti-inflammatory activity of Swietenia macrophylla nanoemulgel, J. Nanomedicine Nanotechnol. 5 (2014) 1–10. https://doi.org/10.4172/2157-7439.1000190.

[186] N.P. Yadav, V.K. Rai, N. Mishra, P. Sinha, D.U. Bawankule, A. Pal, A.K. Tripathi, C.S. Chanotiya, A novel approach for development and characterization of effective mosquito repellent cream formulation containing citronella oil, Biomed Res. Int. 2014 (2014). https://doi.org/10.1155/2014/786084.

[187] N. Dasgupta, S. Ranjan, An Introduction to Food Grade Nanoemulsions, Springer Nature, Singapore, 2018.

[188] S.B. Pratap, K. Brajesh, S.K. Jain, S. Kausar, Development and Characterization of A Nanoemulsion Gel formulation for Transdermal delivery of Carvedilol, Int. J. Drug Dev. Res. 4 (2012) 151–161.

[189] R. Ramasamy, R. Rajan, R. Velmurugan, Development of Mosquito Repellent Fabrics using Vitex negundo loaded Nanoparticles, Malaya J. Biosci. 1 (2014) 19–23. www.malayabiosciences.com.

[190] A. Chebil, J. Desbrières, C. Nouvel, J.L. Six, A. Durand, Ostwald ripening of nanoemulsions stopped by combined interfacial adsorptions of molecular and macromolecular nonionic stabilizers, Colloids Surfaces A Physicochem. Eng. Asp. 425 (2013) 24–30. https://doi.org/10.1016/j.colsurfa.2013.02.028.

[191] C. Preetz, A. Hauser, G. Hause, A. Kramer, K. Mäder, Application of atomic force microscopy and ultrasonic resonator technology on nanoscale: Distinction of nanoemulsions from nanocapsules, Eur. J. Pharm. Sci. 39 (2010) 141–151. https://doi.org/10.1016/j.ejps.2009.11.009.

[192] H.K. Drais, A.A. Hussein, Formulation characterization and evaluation of meloxicam nanoemulgel to be used topically, Iraqi J. Pharm. Sci. 26 (2017) 9–16. https://doi.org/10.1234/ijps.v26i1.681.

[193] V. Bali, M. Ali, J. Ali, Study of surfactant combinations and development of a novel nanoemulsion for minimising variations in bioavailability of ezetimibe, Colloids Surfaces B Biointerfaces. 76 (2010) 410–420. https://doi.org/10.1016/j.colsurfb.2009.11.021.

[194] M.M. Ahmed, K. Anwer, F. Fatima, A.S. Alali, M.A. Kalam, A. Zafar, S. Alshehri, M.M. Ghoneim, Development of Apremilast Nanoemulsion-Loaded Chitosan Gels : In Vitro Evaluations and Anti-Inflammatory and Wound Healing Studies on a Rat Model, Gels. 8 (2022) 1–17. https://doi.org/https://doi.org/ 10.3390/gels8050253.

[195] A. Mahtab, M. Anwar, N. Mallick, Z. Naz, G.K. Jain, F.J. Ahmad, Transungual Delivery of Ketoconazole Nanoemulgel for the Effective Management of Onychomycosis, AAPS PharmSciTech. 17 (2016) 1477–190. https://doi.org/10.1208/s12249-016-0488-0.

[196] M.K. Jeengar, S.V.K. Rompicharla, S. Shrivastava, N. Chella, N.R. Shastri, V.G.M. Naidu, R. Sistla, Emu oil based nano-emulgel for topical delivery of curcumin, Int. J. Pharm. 506 (2016) 222–236. https://doi.org/10.1016/j.ijpharm.2016.04.052.

[197] R. Neubert, C. Bendas, W. Wohlrab, B. Gienau, W. Fuerst, A multilayer membrane system for modelling drug penetration into skin *, Int. J. Pharm. 75 (1991) 89–94.

[198] P. Chellapa, A.T. Mohamed, E.I. Keleb, A. Elmahgoubi, A.M. Eid, Y.S. Issa, N.A. Elmarzugi, Nanoemulsion and Nanoemulgel as a Topical Formulation, IOSR J. Pharm. 5 (2015) 43–47. http://www.iosrphr.org/papers/v5i10/F0510043047.pdf.

[199] Y. Mao, X. Chen, B. Xu, Y. Shen, Z. Ye, B. Chaurasiya, L. Liu, Y. Li, X. Xing, D. Chen, Eprinomectin nanoemulgel for transdermal delivery against endoparasites and ectoparasites: preparation, in vitro and in vivo evaluation, Drug Deliv. 26 (2019) 1104–1114. https://doi.org/10.1080/10717544.2019.1682720.

[200] M. Bashir, J. Ahmad, M. Asif, S.U.D. Khan, M. Irfan, A.Y. Ibrahim, S. Asghar, I.U. Khan, M.S. Iqbal, A. Haseeb, S.H. Khalid, M.A.S. Abourehab, Nanoemulgel, an innovative carrier for diflunisal topical delivery with profound anti-inflammatory effect: In vitro and in vivo evaluation, Int. J. Nanomedicine. 16 (2021) 1457–1472. https://doi.org/10.2147/IJN.S294653.

[201] D.E. Ermawati, F. Alya, F. Prihapsara, Optimization of Gold Particle-Vitamin E Nanoemulgel and in Vivo Test, Adv. Heal. Sci. Res. 18 (2019) 1–5.

[202] WHO, World malaria report 2020- WHO, 2020.

[203] FMOH, National Strategic Plan for Malaria Prevention Control and Elimination in Ethiopia 2011-2015, 2010. http://www.nationalplanningcycles.org/sites/default/files/country_docs/Ethiopia/ethiopia_malaria_national_strategic_plan_2011-2015_130810.pdf.

[204] WHO, WHO Guidelines for malaria - 14 March 2023, Geneva, 2023.

[205] WHO, Global technical strategy for malaria 2016-2030, 2021 update, 2021. https://apps.who.int/iris/rest/bitstreams/1357541/retrieve.

[206] PMI, 17th Annual Report to congress, 2023.

[207] C. Kongkaew, I. Sakunrag, N. Chaiyakunapruk, A. Tawatsin, Effectiveness of citronella preparations in preventing mosquito bites : systematic review of controlled laboratory experimental studies, Trop. Med. Int. Heal. 16 (2011) 802–810. https://doi.org/10.1111/j.1365-3156.2011.02781.x.

[208] D. Musoke, E. Atusingwize, C. Namata, R. Ndejjo, R.K. Wanyenze, M.R. Kamya, Integrated malaria prevention in low- and middle-income countries: a systematic review, Malar. J. 22 (2023) 1–37. https://doi.org/10.1186/s12936-023-04500-x.

[209] L.A. Messenger, J. Furnival-Adams, K. Chan, B. Pelloquin, L. Paris, M. Rowland,

Vector control for malaria prevention during humanitarian emergencies: a systematic review and meta-analysis, Lancet Glob. Heal. 11 (2023) e534–e545. https://doi.org/10.1016/s2214-109x(23)00044-x.

[210] WHO, Malaria vector control and personal protection, Geneva, 2006.

[211] H.F. Khater, A.M. Selim, G.A. Abouelella, N.A. Abouelella, K. Murugan, N.P. Vaz, M. Govindarajan, Commercial Mosquito Repellents and Their Safety Concerns, Malaria. (2019). https://doi.org/DOI: http://dx.doi.org/10.5772/intechopen.87436.

[212] WHO, Vectrol control for malaria and other mosquito borne diseases, (1995).

[213] L.C. Rutledge, R.K. Gupta, Z.A. Mehr, M.D. Buescher, W.G. Reifenrath, Evaluation of controlled-release mosquito repellent formulations, J. Am. Mosq. Control Assoc. 12 (1996) 39–44.

[214] M.S. Fradin, Mosquitoes and Mosquito Repellents: A Clinician's Guide, Ann Intern Med. 128 (1998) 931–940.

[215] J.K. Yoon, K. Kim, Y. Cho, Y. Gwon, H.S. Cho, Y. Heo, K. Park, Y. Lee, M. Kim, Y. Oh, Y.B. Kim, Comparison of Repellency Effect of Mosquito Repellents for DEET , Citronella , and Fennel Oil, J. Parasitol. Res. 2015 (2015) 1–6. https://doi.org/10.1155/2015/361021.

[216] J.K. Yoon, K.C. Kim, Y. Cho, Y.D. Gwon, H.S. Cho, Y. Heo, K. Park, Y.W. Lee, M. Kim, Y.K. Oh, Y.B. Kim, Comparison of Repellency Effect of Mosquito Repellents for DEET, Citronella, and Fennel Oil, J. Parasitol. Res. (2015) 1–7. https://doi.org/10.1155/2015/361021.

[217] M.M.M. Specos, J.J. García, J. Tornesello, P. Marino, D.M. Vecchia, D.M.V. Tesoriero, L.G. Hermida, Microencapsulated citronella oil for mosquito repellent finishing of cotton textiles, Trans. R. Soc. Trop. Med. Hyg. 104 (2010) 653–658. https://doi.org/10.1016/j.trstmh.2010.06.004.

[218] B. Solomon, T. Gebre-mariam, K. Asres, Mosquito Repellent Actions of the Essential Oils of Cymbopogon citratus , Cymbopogon nardus and Eucalyptus citriodora : Evaluation and Formulation Studies, J. Essent. Oil Bear. Plants. 15 (2012) 766–773. https://doi.org/10.1080/0972060X.2012.10644118.

[219] R. Ghalandari, H. Vatandoost, M. Shayeghi, M. Abolhassani, M. Hashemzadeh, Repellent Effect of Extracts and Essential Oils of Citrus limon (Rutaceae) and

Melissa officinalis (Labiatae) Against Main Malaria Vector , Anopheles stephensi (Diptera : Culicidae), Iran. J Publ Heal. 32 (2003) 47–52.

[220] A.O. Oyedele, A.A. Gbolade, M.B. Sosan, F.B. Adewoyin, O.L. Soyelu, O.O. Orafidiya, Formulation of an effective mosquito-repellent topical product from lemongrass oil, Phytomedicine. 9 (2002) 259–262. https://doi.org/10.1078/0944-7113-00120.

[221] M.K. Das, M.A. Ansari, Evaluation of repellent action of Cymbopogan martinii martinii Stapf var sofia oil against Anopheles sundaicus in tribal villages of Car Nicobar Island , Andaman & Nicobar Islands , India, J Vect Borne Dis. 40 (2003) 100–104.

[222] A. Navayan, E. Moghimipour, M.J. Khodayar, B. Vazirianzadeh, A. Siahpoosh, M. Valizadeh, Z. Mansourzadeh, Evaluation of the mosquito repellent activity of nano-sized microemulsion of Eucalyptus globulus essential oil against Culicinae, Jundishapur J. Nat. Pharm. Prod. 12 (2017) 0–5. https://doi.org/10.5812/jjnpp.55626.

[223] H. Wu, C.C. Fu, D.D. Yu, J.T. Feng, X. Zhang, Z.Q. Ma, Repellent activity screening of 11 kinds of essential oils against Aedes albopictus Skuse: Microcapsule preparation of Herba Schizonepetae oil and repellent bioassay on hand skin, Trans. R. Soc. Trop. Med. Hyg. 107 (2013) 471–479. https://doi.org/10.1093/trstmh/trt045.

[224] Y. Trongtokit, Y. Rongsriyam, N. Komalamisra, C. Apiwathnasorn, Comparative Repellency of 38 Essential Oils against Mosquito Bites, Phytother. Res. 19 (2005) 303–309. https://doi.org/10.1002/ptr.1637.

[225] N. Misni, Z. Mohamed Nor, R. Ahmad, N.R. Ithnin, N.Z. Unyah, Microencapsulation preservation of the stability and efficacy of citrus grandis oil-based repellent formulation against aedes aegypti during storage, Molecules. 26 (2021). https://doi.org/10.3390/molecules26123599.

[226] W. Hsu, J. Yen, Y. Wang, Formulas of components of citronella oil against mosquitoes (Aedes aegypti), J. Environ. Sci. Heal. , Part B . 48 (2013) 37–41. https://doi.org/10.1080/03601234.2013.816613.

[227] B. Solomon, F.F. Sahle, T. Gebre-Mariam, K. Asres, R.H.H. Neubert, Microencapsulation of citronella oil for mosquito-repellent application: Formulation

and in vitro permeation studies, Eur. J. Pharm. Biopharm. 80 (2012) 61–66. https://doi.org/10.1016/j.ejpb.2011.08.003.

[228] H. Kaur, U. Bhardwaj, R. Kaur, H. Kaur, Chemical Composition and Antifungal Potential of Citronella (Cymbopogon nardus) Leaves Essential Oil and its Major Compounds Journal of Essential Oil-Bearing Plants, J. Essent. Oil Bear. Plants. 24 (2021) 571–581. https://doi.org/10.1080/0972060X.2021.1942231.

[229] P.S. Kakaraparthi, K.V.N.S. Srinivas, J.K. Kumar, A.N. Kumar, D.K. Rajput, S. Anubala, Changes in the essential oil content and composition of palmarosa (Cymbopogon martini) harvested at different stages and short intervals in two different seasons, Ind. Crops Prod. 69 (2015) 348–354. https://doi.org/10.1016/j.indcrop.2015.02.020.

[230] G.R. Smitha, H.L. Dhaduk, A new chemotype of palmarosa [Cymbopogon martini (Roxb.) W. Watson] identified from 'The Aravali Range' of Rajasthan, India, Med. Plants. 10 (2018) 203–209. https://doi.org/10.5958/0975-6892.2018.00033.3.

[231] N. Dayan, Stratum Corneum: The Role of Lipids and Ceramides, Cosmet. Toilet. 121 (2006) 37–42. http://www.alluredbooks.com/sample_pages/ca_ch1.pdf.

[232] R. Darlenski, J. Kazandjieva, N. Tsankov, Skin barrier function: morphological basis and regulatory mechanisms, J. Clin. Med. 4 (2011) 36–45.

[233] M. Hirata, K. Tsuge, L.N. Jayakody, Y. Urano, K. Sawada, S. Inaba, K. Nagao, H. Kitagaki, Structural determination of glucosylceramides in the distillation remnants of shochu, the japanese traditional liquor, and its production by aspergillus kawachii, J. Agric. Food Chem. 60 (2012) 11473–11482. https://doi.org/10.1021/jf303117e.

[234] E.N. Tessema, T. Gebre-mariam, S. Lange, B. Dobner, R.H.H. Neubert, Potential application of oat-derived ceramides in improving skin barrier function : Part 1 . Isolation and structural characterization, J. Chromatogr. B. 1065–1066 (2017) 87–95. https://doi.org/10.1016/j.jchromb.2017.09.029.

[235] N. Takakuwa, K. Saito, M. Ohnishi, Y. Oda, Determination of glucosylceramide contents in crop tissues and by-products from their processing, Bioresour. Technol. 96 (2005) 1089–1092. https://doi.org/10.1016/j.biortech.2004.09.019.

[236] M.C. Sullards, D. V. Lynch, A.H. Merrill, J. Adams, Structure determination of soybean and wheat glucosylceramides by tandem mass spectrometry, J. Mass

Spectrom. 35 (2000) 347–353. https://doi.org/10.1002/(SICI)1096-9888(200003)35:3<347::AID-JMS941>3.0.CO;2-3.

[237] E. Bartkiene, V. Bartkevics, V. Starkute, V. Krungleviciute, D. Cizeikiene, D. Zadeike, G. Juodeikiene, Z. Maknickiene, Chemical composition and nutritional value of seeds of Lupinus luteus L ., L . angustifolius L . and new hybrid lines of L . angustifoliu s L ., Zemdirbyste-Agriculture. 103 (2016) 107–114. https://doi.org/10.13080/z-a.2016.103.014.

[238] Getachew P, Chemical Composition and The Effects of Traditional Processing on Nutritional Composition of Gibto (Lupinus Albus. L) Grown In, Gojam Area, 2009.

[239] H. Shewayrga, P.A. Sopade, Ethnobotany, diverse food uses, claimed health benefits and implications on conservation of barley landraces in North Eastern Ethiopia highlands, J. Ethnobiol. Ethnomed. 7 (2011) 1–15. https://doi.org/10.1186/1746-4269-7-19.

[240] L.R. Chen, C.Y. Ko, W.R. Folk, T.Y. Lin, Chilling susceptibility in mungbean varieties is associated with their differentially expressed genes, Bot. Stud. 58 (2017) 1–9. https://doi.org/10.1186/s40529-017-0161-2.

[241] H. Goto, K. Nishikawa, N. Shionoya, M. Taniguchi, T. Igarashi, Determination of sphingoid bases from hydrolyzed glucosylceramide in rice and wheat by online post-column high-performance liquid chromatography with O-phthalaldehyde derivatization, J. Oleo Sci. 61 (2012) 681–688. https://doi.org/10.5650/jos.61.681.

[242] Y. Fujino, M. Ohnishi, Constituents of ceramide and ceramide monohexoside in rice bran, Chem. Phys. Lipids. 17 (1976) 275–289. https://doi.org/10.1016/0009-3084(76)90073-6.

[243] I. Hedberg and S. Edwards, Flora of Ethiopia, vol 3, Addis Ababa and Asmera, Ethiopia, 1989.

[244] EMA, Guideline on bioanalytical method validation Guideline on bioanalytical method validation, (2012) 1–20.

[245] H.E. Carter, J.A. Rothfus, R. Gigg, Biochemistry of the sphingolipids: XII. conversion of cerebrosides to ceramides and sphingosine; structure of Gaucher cerebroside, J. Lipid Res. 2 (1961) 228–234.

[246] A. Gunnarsson, J. Lundsten, S. Svensson, Specific cleavage of the glycosidic bond

between the carbohydrate and ceramide portions in glycosphingolipids using trifluoroacetolysis., Acta Chem. Scand. B. 38 (1984) 603–609. https://doi.org/10.3891/acta.chem.scand.38b-0603.

[247] A.F. Bochkov, G.E. Zaikov, Cleavage of O-glycosidic Bonds, 1st ed., Pergamon Press, Oxford [England], 1979. https://doi.org/10.1016/b978-0-08-022949-2.50011-3.

[248] J.M. Jungersted, L.I. Hellgren, J.K. Høgh, T. Drachmann, G.B.E. Jemec, T. Agner, Ceramides and barrier function in healthy skin, Acta Derm. Venereol. 90 (2010) 350–353. https://doi.org/10.2340/00015555-0894.

[249] H.J. Cha, C. He, H. Zhao, Y. Dong, I.S. An, S. An, Intercellular and intracellular functions of ceramides and their metabolites in skin (Review), Int. J. Mol. Med. 38 (2016) 16–22. https://doi.org/10.3892/ijmm.2016.2600.

[250] W.M. Holleran, Y. Takagi, G.K. Menon, G. Legler, K.R. Feingold, P.M. Elias, Processing of epidermal glucosylceramides is required for optimal mammalian cutaneous permeability barrier function, J. Clin. Invest. 91 (1993) 1656–1664. https://doi.org/10.1172/JCI116374.

[251] N. Jonca, Ceramides metabolism and impaired epidermal barrier in cutaneous diseases and skin aging: focus on the role of the enzyme PNPLA1 in the synthesis of ω-O-acylceramides and its pathophysiological involvement in some forms of congenital ichthyoses, OCL. 26 (2019) 1–7.

[252] Y. Takagi, E. Kriehuber, G. Imokawa, P.M. Elias, W.M. Holleran, β-Glucocerebrosidase activity in mammalian stratum corneum, J. Lipid Res. 40 (1999) 861–869.

[253] K. Akimoto, N. Yoshikawa, Y. Higaki, M. Kawashima, G. Imokawa, Quantitative analysis of stratum corneum lipids in xerosis and asteatotic eczema, J. Dermatol. 20 (1993) 1–6. https://doi.org/10.1111/j.1346-8138.1993.tb03820.x.

[254] K. Jin, Y. Higaki, Y. Takagi, K. Higuchi, Y. Yada, M. Kawashima, G. Imokawa, Analysis of beta-glucocerebrocidase and ceramidase activities in atoic and aged dry skin, Acta Derm Venereol. 74 (1994) 337–340.

[255] P.D. Mier, J.J.M.A. Van den Hurk, Lysosomal hydrolases of the epidermis: Changes in Disease, Br. J. Dermatol. 95 (1976) 271–274. https://doi.org/10.1111/j.1365-

2133.1976.tb07014.x.

[256] E. Kahraman, M. Kaykın, H. Şahin Bektay, S. Güngör, Recent Advances on Topical Application of Ceramides to Restore Barrier Function of Skin, Cosmetics. 6 (2019) 52. https://doi.org/10.3390/cosmetics6030052.

[257] A.A. Adem, A. Belete, A. Soboleva, A. Frolov, E.N. Tessema, T. Gebre-Mariam, R.H.H. Neubert, Structural Characterization of Plant Glucosylceramides and the Corresponding Ceramides by UHPLC-LTQ-Orbitrap Mass Spectrometry, J. Pharm. Biomed. Anal. 192 (2020) 113677. https://doi.org/10.1016/j.jpba.2020.113677.

[258] E.M. Willsteed, B.S. Bhogal, A. Das, S.S. Bekir, F. Wojnarowska, M.M. Black, P.H. Mckee, An ultrastructural comparison of dermo-epidermal separation techniques, J. Cutan. Pathol. 18 (1991) 8–12. https://doi.org/10.1111/j.1600-0560.1991.tb00595.x.

[259] D.W. Burden, Guide to the Homogenization of Biological Samples, Random Prim. (2008) 1–14.

[260] S. Handa, T. Yamakaw, Biochemical studies in cat and human gangliosidosis, J. Neurochem. 18 (1971) 1275–1280.

[261] O.T. Mueller, A. Rosenberg, Beta Glucoside Hydrolase Activity of Normal and Glucosylceramidotic Cultured Human Skin Fibroblasts, J. Biol. Chem. 252 (1977) 825–829. https://doi.org/10.1016/S0021-9258(19)75171-0.

[262] M. Sargent, Guide to achieving reliable quantitative LC-MS measurements, RSC Anal. Methods Comm. (2013) 1–69.

[263] Y. Zou, H.I. Maibach, Dermal–epidermal separation methods: research implications, Arch. Dermatol. Res. 310 (2017) 1–9. https://doi.org/10.1007/s00403-017-1774-8.

[264] J.P. Baumberger, V. Suntzeff, E. V. Cowdry, Methods for the separation of epidermis from dermis and some physiologic and chemical properties of isolated epidermis, J. Natl. Cancer Inst. 2 (1942) 413–423. https://doi.org/10.1093/jnci/2.5.413.

[265] E.J.V. an Scott, Preliminary and Short Reports: Mechanical Separation of the Epidermis From the Corium, J. Invest. Dermatol. (1952) 377–380.

[266] F. Chang, P.W. Wertz, C.A. Squier, Comparison of glycosidase activities in

epidermis, palatal epithelium and buccal epithelium, Comp. Biochem. Physiol. 100B (1991) 137–139. https://doi.org/10.1016/0305-0491(91)90096-V.

[267] Y. Kitano, N. Okada, Separation of the epidermal sheet by dispase, Br. J. Dermatol. 108 (1983) 555–560. https://doi.org/10.1111/j.1365-2133.1983.tb01056.x.

[268] H. Kim, S.-H. Jin, Studies in epidermal-dermal separation and enzyme activities in neonatal rat epidermis, Korean J. Toxicol. 5 (1989) 89–96.

[269] W.R. Gammon, R.A. Briggaman, A.O. Inman, Differentiating anti-lamina lucida and anti-sublamina densa anti-BMZ antibodies by indirect immunofluorescence on 1.0 M sodium chloride-separated skin, J. Invest. Dermatol. 82 (1984) 139–144. https://doi.org/10.1111/1523-1747.ep12259692.

[270] M.W.K. Wong, N. Braidy, R. Pickford, P.S. Sachdev, A. Poljak, Comparison of single phase and biphasic extraction protocols for lipidomic studies using human plasma, Front. Neurol. 10 (2019) 1–11. https://doi.org/10.3389/fneur.2019.00879.

[271] V. Matyash, G. Liebisch, T. V. Kurzchalia, A. Shevchenko, D. Schwudke, Lipid extraction by methyl-terf-butyl ether for high-throughput lipidomics, J. Lipid Res. 49 (2008) 1137–1146. https://doi.org/10.1194/jlr.D700041-JLR200.

[272] P. Araujo, Key aspects of analytical method validation and linearity evaluation, J. Chromatogr. B. 877 (2009) 2224–2234. https://doi.org/10.1016/j.jchromb.2008.09.030.

[273] ICH, ICH Harmonized Tripartite Guideline, Validation of Analytical Procedures: Text and Methodology Q2(R1), (2005).

[274] J. Mark Green, A practical guide to analytical method validation, 1996.

[275] V.P. Shah, K.K. Midha, J.W.A. Findlay, H.M. Hill, J.D. Hulse, I.J. McGilveray, G. McKay, K.J. Miller, R.N. Patnaik, M.L. Powell, A. Tonelli, C.T. Viswanathan, A. Yacobi, Bioanalytical Method Validation-A Revisit with a Decade of Progress, Pharm. Res. 17 (2000) 1551–1557. https://doi.org/10.1023/A.

[276] S. Walfish, Analytical Methods : A Statistical Perspective on the ICH Q2A and Q2B Guidelines for Validation of Analytical Methods, BioPharm Int. (2006) 1–6.

[277] EMA, Validation of analytical procedures: Methodology. ICH harmonized tripartite guideline, 1995. https://doi.org/10.1016/B978-0-12-386454-3.00861-7.

[278] P. Panuwet, R.E. Hunter, P.E. D'Souza, X. Chen, S.A. Radford, J.R. Cohen, M.E.

Marder, K. Kartavenka, P.B. Ryan, D.B. Barr, Biological Matrix Effects in Quantitative Tandem Mass Spectrometry-Based Analytical Methods: Advancing Biomonitoring, Crit. Rev. Anal. Chem. 46 (2016) 93–105. https://doi.org/10.1080/10408347.2014.980775.

[279] H. Trufelli, P. Palma, G. Famiglini, A. Cappiello, An overview of matrix effects in liquid chromatography-mass spectrometry, Mass Spectrom. Rev. 30 (2011) 491–509. https://doi.org/10.1002/mas.20298.

[280] W. Zhou, S. Yang, P.G. Wang, Matrix effects and application of matrix effect factor, Bioanalysis. 9 (2017) 1839–1844. https://doi.org/10.4155/bio-2017-0214.

[281] E.L.I. Robins, H.E. Hirsch, S.S. Emmons, Glycosidases in the Nervous, J. Biol. Chem. 243 (1968) 4246–4252. https://doi.org/10.1016/S0021-9258(18)93249-7.

[282] E. Shimada, K. Aida, T. Sugawara, T. Hirata, Inhibitory effect of topical maize glucosylceramide on skin photoaging in UVA-irradiated hairless mice, J. Oleo Sci. 60 (2011) 321–325. https://doi.org/10.5650/jos.60.321.

[283] P.W. Wertz, Current understanding of skin biology pertinent to skin penetration: Skin biochemistry, Skin Pharmacol. Physiol. 26 (2013) 217–226. https://doi.org/10.1159/000351949.

[284] A. Hussain, A. Samad, S.K. Singh, M.N. Ahsan, M.W. Haque, A. Faruk, F.J. Ahmed, Nanoemulsion gel-based topical delivery of an antifungal drug : in vitro activity and in vivo evaluation, Drug Deliv. 23 (2016) 1–16. https://doi.org/10.3109/10717544.2014.933284.

[285] G. Deli, S. Hatziantoniou, Y. Nikas, C. Demetzos, Solid lipid nanoparticles and nanoemulsions containing ceramides: Preparation and physicochemical characterization, J. Liposome Res. 19 (2009) 180–188. https://doi.org/10.1080/08982100802702046.

[286] S. Cafaggi, R. Leardi, B. Parodi, G. Caviglioli, G. Bignardi, An example of application of a mixture design with constraints to a pharmaceutical formulation, Chemom. Intell. Lab. Syst. 65 (2003) 139–147.

[287] T. Lundstedt, E. Seifert, L. Abramo, B. Thelin, A. Nystrom, J. Pettersen, R. Bergman, Experimental design and optimization, Chemom. Intell. Lab. Syst. 42 (1998) 3–40.

[288] J.A. Cornell, Experiments with mixtures: Design, Models, and the analysis of mixture data, 3rd ed., John Wiley & Sons, Inc, New York, 2018. https://doi.org/10.18805/bkap112.

[289] A.A. Date, M.S. Nagarsenker, Design and evaluation of self-nanoemulsifying drug delivery systems (SNEDDS) for cefpodoxime proxetil, Int. J. Pharm. 329 (2007) 166–172. https://doi.org/10.1016/j.ijpharm.2006.08.038.

[290] A.S. Dhoot, A. Naha, J. Priya, N. Xalxo, Phase diagrams for three component mixtures in pharmaceuticals and its applications, J. Young Pharm. 10 (2018) 132–137. https://doi.org/10.5530/jyp.2018.10.31.

[291] P. Chellapa, A.M. Eid, N.A. Elmarzugi, Preparation and characterization of virgin coconut oil nanoemulgel, J. Chem. Pharm. Res. 7 (2015) 787–793.

[292] F.F. Sahle, H. Metz, J. Wohlrab, R.H.H. Neubert, Polyglycerol fatty acid ester surfactant-based microemulsions for targeted delivery of ceramide AP into the stratum corneum: Formulation, characterisation, in vitro release and penetration investigation, Eur. J. Pharm. Biopharm. 82 (2012) 139–150. https://doi.org/10.1016/j.ejpb.2012.05.017.

[293] A. Azeem, M. Rizwan, F.J. Ahmad, Z. Iqbal, R.K. Khar, M. Aqil, S. Talegaonkar, Nanoemulsion components screening and selection: A technical note, AAPS PharmSciTech. 10 (2009) 69–76. https://doi.org/10.1208/s12249-008-9178-x.

[294] S. Bhattacharya, B.G. Prajapati, Formulation and optimization of celecoxib nanoemulgel, Asian J. Pharm. Clin. Res. 10 (2017) 353–365. https://doi.org/10.22159/ajpcr.2017.v10i8.19510.

[295] A. Eichner, S. Stahlberg, S. Sonnenberger, S. Lange, B. Dobner, A. Ostermann, T.E. Schrader, T. Hauß, A. Schroeter, D. Huster, R.H.H. Neubert, Influence of the penetration enhancer isopropyl myristate on stratum corneum lipid model membranes revealed by neutron diffraction and 2H NMR experiments, Biochim. Biophys. Acta - Biomembr. 1859 (2017) 745–755. https://doi.org/10.1016/j.bbamem.2017.01.029.

[296] D.W. Osborne, J. Musakhanian, Skin Penetration and Permeation Properties of Transcutol- Neat or Diluted Mixtures, AAPS PharmSciTech. 19 (2018) 3512–3533. https://doi.org/10.1208/s12249-018-1196-8.

[297] J.W. Fluhr, M. Gloor, L. Lehmann, S. Lazzerini, F. Distante, E. Berardesca, Glycerol accelerates recovery of barrier function in vivo, Acta Derm. Venereol. 79 (1999) 418–421. https://doi.org/10.1080/000155599750009825.

[298] S. Nafisi, H.I. Maibach, Nanotechnology in cosmetics, in: K. Sakamoto, R. Lochhead, H. Maibach, Y. Yamashita (Eds.), Cosmet. Sci. Technol. Theor. Princ. Appl., 1 st, Elsevier, california, 2017: pp. 337–361. https://doi.org/10.1016/B978-0-12-802005-0.00022-7.

[299] T.J. Wooster, M. Golding, P. Sanguansri, Ripening Stability, Langmuir. 24 (2008) 12758–12765. https://doi.org/10.1021/la801685v.

[300] R.N. Dash, M. Habibuddin, T. Humaira, D. Ramesh, Design , optimization and evaluation of glipizide solid self-nanoemulsifying drug delivery for enhanced solubility and dissolution, Saudi Pharm. J. 23 (2015) 528–540. https://doi.org/10.1016/j.jsps.2015.01.024.

[301] M. Rezaee, M. Basri, R.N.Z. Raja, Abdul-rahman, A.B. Salleh, N. Chaibakhsh, R. abedi Karjiban, Formulation development and optimization of palm kernel oil esters-based nanoemulsions containing sodium diclofenac, Int. J. Nanomedicine. 9 (2014) 539–548.

[302] N.A. Wahgiman, N. Salim, M.B. Abdul-Rahman, S.E. Ashari, Optimization of nanoemulsion containing gemcitabine and evaluation of its cytotoxicity towards human fetal lung fi broblast (MRC5) and human lung carcinoma (A549) cells, (2019) 7323–7338.

[303] Z. Mori, N. Anarjan, Preparation and characterization of nanoemulsion based b -carotene hydrogels, J. Food Sci. Technol. 55 (2018) 5014–5024. https://doi.org/10.1007/s13197-018-3440-3.

[304] A. Gupta, H.B. Eral, T.A. Hatton, P.S. Doyle, Nanoemulsions: Formation, properties and applications, Soft Matter. 12 (2016) 2826–2841. https://doi.org/10.1039/c5sm02958a.

[305] K. Soni, A. Mujtaba, H. Akhter, A. Zafar, K. Kohli, Optimisation of ethosomal nanogel for topical nano-CUR and sulphoraphane delivery in effective skin cancer therapy, J. Microencapsul. 37 (2020) 91–108. https://doi.org/10.1080/02652048.2019.1701114.

[306] T. Miyazawa, S. Ito, Y. Fujino, Isolation of Cerebroside from Pea Seeds, Agric. Biol. Chem. 38 (1974) 1387–1391.

[307] M. Kojima, M. Ohnishi, S. Ito, Composition and Molecular Species of Ceramide and Cerebroside in Scarlet Runner Beans (Phaseolus coccineus L .) and Kidney Beans (Phaseolus vulgaris L .), J. Agric. Food Chem. 39 (1991) 1709–1714.

[308] J.N. Kanfer, S. Hakomori, Handbook of lipid research, 1st ed., Plenum press, New York, 2012. https://doi.org/10.1007/978-1-4757-0396-2.

[309] R.B. Patel, M.R. Patel, K.K. Bhatt, B.G. Patel, Risperidone-loaded mucoadhesive microemulsion for intranasal delivery: Formulation development, physicochemical characterization and ex vivo evaluation, J. Drug Deliv. Sci. Technol. 23 (2013) 561–567. https://doi.org/10.1016/S1773-2247(13)50085-2.

[310] S.R. Derkach, S.O. Ilyin, A.A. Maklakova, V.G. Kulichikhin, A.Y. Malkin, The rheology of gelatin hydrogels modified by κ-carrageenan, LWT- Food Sci. Technol. 63 (2015) 612–619. https://doi.org/10.1016/j.lwt.2015.03.024.

[311] M.N. Abdul Rahman, O.A.J. Abdul-Qader, S. Sukmasari, A.F. Ismail, A.A. Doolaanea, Rheological characterization of different gelling polymers for dental gel formulation, J. Pharm. Sci. Res. 9 (2017) 2633–2640.

[312] L. Qiao, Y. Li, Y. Chi, Y. Ji, Y. Gao, H. Hwang, W.G. Aker, P. Wang, Rheological properties, gelling behavior and texture characteristics of polysaccharide from Enteromorpha prolifera, Carbohydr. Polym. 136 (2016) 1307–1314. https://doi.org/10.1016/j.carbpol.2015.10.030.

[313] S. Hamanaka, M. Hara, H. Nishio, F. Otsuka, A. Suzuki, Y. Uchida, Human epidermal glucosylceramides are major precursors of stratum corneum ceramides, J. Invest. Dermatol. 119 (2002) 416–423. https://doi.org/10.1046/j.1523-1747.2002.01836.x.

[314] F.F. Sahle, H. Metz, J. Wohlrab, R.H.H. Neubert, Lecithin-based microemulsions for targeted delivery of Ceramide AP into the stratum corneum: Formulation, characterizations, and in vitro release and penetration studies, Pharm. Res. 30 (2013) 538–551. https://doi.org/10.1007/s11095-012-0899-x.

[315] PMI, President's Malaria Initiative Ethiopia, Malaria operational plan 2017, (2017) 9–11.

[316] Ulesido Fekadu Massebo, Malaria vectors in southern Ethiopia, University of Bergen, 2017.

[317] S. Naseem, T. Munir, M. Faheem Malik, Mosquito management: A review, J. Entomol. Zool. Stud. 4 (2016) 73–79.

[318] WHO, Global technical strategy for malaria 2016–2030, (2015) 1–35.

[319] M. Tavares, M.R.M. da Silva, L.B. de Oliveira de Siqueira, R.A.S. Rodrigues, L. Bodjolle-d'Almeira, E.P. dos Santos, E. Ricci-Júnior, Trends in insect repellent formulations: A review, Int. J. Pharm. 539 (2018) 190–209. https://doi.org/10.1016/j.ijpharm.2018.01.046.

[320] K. Karunamoorthi, T. Hailu, Insect repellent plants traditional usage practices in the Ethiopian malaria epidemic-prone setting: An ethnobotanical survey, J. Ethnobiol. Ethnomed. 10 (2014) 1–11. https://doi.org/10.1186/1746-4269-10-22.

[321] T.N. Barradasa, L.M.A. Lopes, E. Ricci-Júnior, K.G. de H. e Silva, C.R.E. Mansur, Development and characterization of micellar systems for application as insect repellents, Int. J. Pharm. 454 (2013) 633–640. https://doi.org/10.1016/j.ijpharm.2013.05.050.

[322] M.F. Maia, S.J. Moore, Plant-based insect repellents : a review of their efficacy , development and testing, 10 (2011) 1–15.

[323] D. Sritabutra, M. Soonwera, R epellent activity of herbal essential oils against Aedes aegypti (L inn .) and Culex quinquefasciatus (Say.), Asian Pacific J. Trop. Dis. 3 (2013) 271–276. https://doi.org/10.1016/S2222-1808(13)60069-9.

[324] J.J. Tibenda, Q. Yi, X. Wang, Q. Zhao, Review of phytomedicine, phytochemistry, ethnopharmacology, toxicology, and pharmacological activities of Cymbopogon genus, Front. Pharmacol. 13 (2022) 1–22. https://doi.org/10.3389/fphar.2022.997918.

[325] B.R. Rajeswara Rao, D.K. Rajput, R.P. Patel, Essential oil profiles of different parts of palmarosa (cymbopogon martinii (roxb.) wats. var. motia burk.), J. Essent. Oil Res. 21 (2009) 519–521. https://doi.org/10.1080/10412905.2009.9700233.

[326] V.K. Raina, S.K. Srivastava, K.K. Aggarwal, K. V. Syamasundar, S.P.S. Khanuja, Essential oil composition of Cymbopogon martinii from different places in India, Flavour Fragr. J. 18 (2003) 312–315. https://doi.org/10.1002/ffj.1222.

[327] M.R.M. da Silva, E. Ricci-Júnior, An approach to natural insect repellent formulations: from basic research to technological development, Acta Trop. 212 (2020) 105419. https://doi.org/10.1016/j.actatropica.2020.105419.

[328] N. Misni, Z.M. Nor, R. Ahmad, Microencapsulation of Citrus Grandis peel oil using interfacial precipitation chemistry technique for repellent application, Iran. J. Pharm. Res. 18 (2019) 198–209. https://doi.org/10.22037/ijpr.2019.2351.

[329] A.D. Ribeiro, J. Marques, M. Forte, F.C. Correia, P. Parpot, C. Oliveira, A.I. Pereira, L. Andrade, C. Azenha, A. Mendes, G.M. Alves, C.A. Sousa, C.J. Tavares, Microencapsulation of citronella oil for solar-activated controlled release as an insect repellent, Appl. Mater. Today. 5 (2016) 90–97. https://doi.org/10.1016/j.apmt.2016.09.003.

[330] S.N.H. Mamood, O. Hidayatulfathi, S.B. Budin, G. Ahmad Rohi, M.H. Zulfakar, The formulation of the essential oil of Piper aduncum Linnaeus (Piperales: Piperaceae) increases its efficacy as an insect repellent, Bull. Entomol. Res. 107 (2017) 49–57. https://doi.org/10.1017/S0007485316000614.

[331] S. Kotta, A.W. Khan, S.H. Ansari, R.K. Sharma, J. Ali, Formulation of nanoemulsion: a comparison between phase inversion composition method and high-pressure homogenization method, Drug Deliv. 22 (2015) 455–466. https://doi.org/10.3109/10717544.2013.866992.

[332] D.C. Abrantes, C.B. Rogerio, J.L. de Oliveira, E.V.R. Campos, D.R. de Araújo, L.C. Pampana, M.J. Duarte, G.F. Valadares, L.F. Fraceto, Development of a Mosquito Repellent Formulation Based on Nanostructured Lipid Carriers, Front. Pharmacol. 12 (2021) 1–13. https://doi.org/10.3389/fphar.2021.760682.

[333] G. Kaur, TPGS Loaded Topical Nanoemulgel of Mefenamic Acid for the Treatment of Rheumatoid Arthritis, IJPPR. 15 (2019) 64–107.

[334] K.B. Almeida, J.L. Araujo, J.F. Cavalcanti, M.T. V. Romanos, S.C. Mourão, A.C.F. Amaral, D.Q. Falcão, In vitro release and anti-herpetic activity of Cymbopogon citratus volatile oil-loaded nanogel, Rev. Bras. Farmacogn. 28 (2018) 495–502. https://doi.org/10.1016/j.bjp.2018.05.007.

[335] L.S. Wei, W. Wee, Chemical composition and antimicrobial activity of Cymbopogon nardus citronella essential oil against systemic bacteria of aquatic

animals, Iran. J. Microbiol. 5 (2013) 147–152.

[336] B. Bayala, A.Y. Coulibaly, F.W. Djigma, B.M. Nagalo, S. Baron, G. Figueredo, J.A. Lobaccaro, J. Simpore, Chemical composition , antioxidant , anti- inflammatory and antiproliferative activities of the essential oil of Cymbopogon nardus , a plant used in traditional medicine, (2020) 86–96.

[337] A.C. Ahouansou, S.R.M. Fagla, J.M. Tokoudagba, H. Toukourou, Y.K. Badou, F.A. Gbaguidi, Chemical composition and larvicidal activity of the essential oil of Cymbopogon nardus (L .) Rendle on Anopheles gambiae, 13 (2019) 1861–1869.

[338] N. Jain, M. Sharma, Chemical Composition of the Leaf Oil of Cymbopogon martinii var. sofia Collected from Udaipur, Rajasthan and their Screening Against Fungi Causing Dermatophytosis in Human Beings, J. Essent. Oil-Bearing Plants. 20 (2017) 801–808. https://doi.org/10.1080/0972060X.2017.1341344.

[339] A. Prashara, P. Hili, R.G. Veness, C.S. Evans, Antimicrobial action of palmarosa oil (Cymbopogon martinii) on Saccharomyces cerevisiae, Phytochemistry. 63 (2003) 569–575. https://doi.org/10.1016/S0031-9422(03)00226-7.

[340] H.R. Kelidari, M.D. Moemenbellah-Fard, K. Morteza-Semnani, F. Amoozegar, M. Shahriari-Namadi, M. Saeedi, M. Osanloo, Solid-lipid nanoparticles (SLN)s containing Zataria multiflora essential oil with no-cytotoxicity and potent repellent activity against Anopheles stephensi, J. Parasit. Dis. 45 (2021) 101–108. https://doi.org/10.1007/s12639-020-01281-x.

[341] S. Sinha, M. Jothiramajayam, M. Ghosh, A. Mukherjee, Evaluation of toxicity of essential oils palmarosa , citronella , lemongrass and vetiver in human lymphocytes, FOOD Chem. Toxicol. 68 (2014) 71–77. https://doi.org/10.1016/j.fct.2014.02.036.

[342] N. Agrawal, G.L. Maddikeri, A.B. Pandit, Sustained release formulations of citronella oil nanoemulsion using cavitational techniques, Ultrason. - Sonochemistry. 36 (2017) 367–374. https://doi.org/10.1016/j.ultsonch.2016.11.037.

[343] V. Ghosh, S. Saranya, A. Mukherjee, N. Chandrasekaran, Cinnamon Oil Nanoemulsion Formulation by Ultrasonic Emulsification : Investigation of Its Bactericidal Activity, J. Nanosci. Nanotechnol. 13 (2013) 114–122. https://doi.org/10.1166/jnn.2013.6701.

[344] M.J. Nirmala, L. Durai, K.A. Rao, R. Nagarajan, Ultrasonic Nanoemulsi fi cation of

Cuminum cyminum Essential Oil and Its Applications in Medicine, (2020).

[345] M.H. Shahavi, M. Hosseini, M. Jahanshahi, R.L. Meyer, G.N. Darzi, Evaluation of critical parameters for preparation of stable clove oil nanoemulsion, Arab. J. Chem. (2015). https://doi.org/10.1016/j.arabjc.2015.08.024.

[346] S. Abbas, K. Hayat, E. Karangwa, M. Bashari, X. Zhang, An Overview of Ultrasound-Assisted Food-Grade Nanoemulsions, Food Eng Rev. 5 (2013) 139–157. https://doi.org/10.1007/s12393-013-9066-3.

[347] A.M. Hashtjin, S. Abbasi, Optimization of ultrasonic emulsification conditions for the production of orange peel essential oil nanoemulsions, J Food Sci Technol. (2014). https://doi.org/10.1007/s13197-014-1322-x.

[348] W. Lu, D. Huang, C.C.R. Wang, C. Yeh, J. Tsai, Y. Huang, P. Li, Preparation, characterization, and antimicrobial activity of nanoemulsions incorporating citral essential oil, J. Food Drug Anal. (2017) 1–8. https://doi.org/10.1016/j.jfda.2016.12.018.

[349] S. Sugumar, S. Singh, A. Mukherjee, N. Chandrasekaran, Nanoemulsion of orange oil with non ionic surfactant produced emulsion using ultrasonication technique : evaluating against food spoilage yeast, Appl. Nanosci. (2016) 113–120. https://doi.org/10.1007/s13204-015-0412-z.

[350] E. Truzzi, C. Durante, D. Bertelli, B. Catellani, S. Pellacani, S. Benvenuti, Rapid Classification and Recognition Method of the Species and Chemotypes of Essential Oils by ATR-FTIR Spectroscopy Coupled with Chemometrics, Molecules. 77 (2022) 1–21.

[351] W.T. Eden, D. Alighiri, K.I. Supardi, E. Cahyono, The Mosquito Repellent Activity of the Active Component of Air Freshener Gel from Java Citronella Oil (Cymbopogon winterianus), J. Parasitol. Res. 2020 (2020). https://doi.org/10.1155/2020/9053741.

Appendix

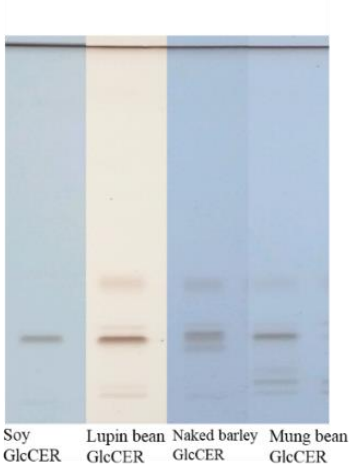

Figure A1: TLC chromatograms of soya GlcCERs (standard), lupin bean, naked barley and mung bean. The development solvent was CHCl3/MeOH (85:15, *v/v*).

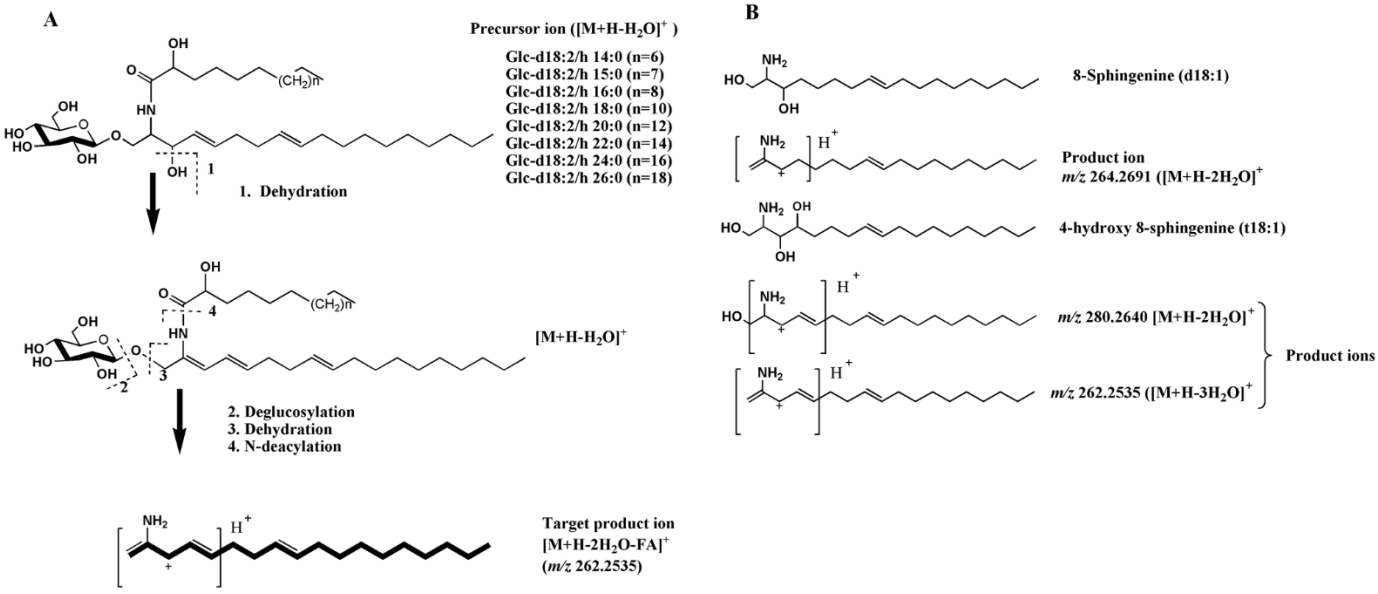

Figure A2: Fragmentation patterns of GlcCERs with d18:2 sphingoid base (A) and the product ions of GlcCER species containing d18:1 and t18:1 sphingoid bases (B). The dash line depicts the site of fragmentation.

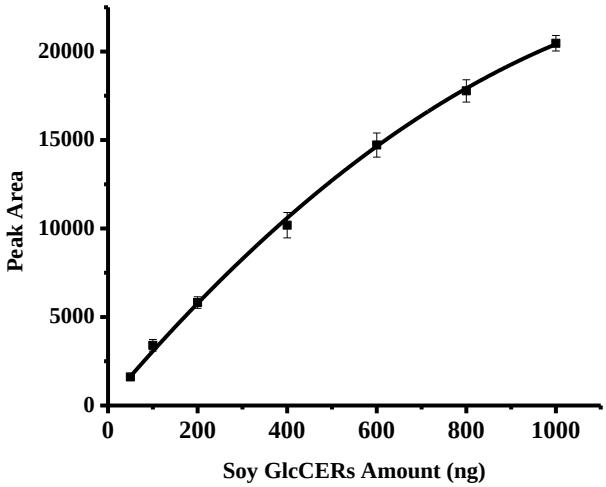

Figure A3: Calibration curve for linearity of Soy GlcCER for quantification of plant GlcCERs with AMD-HPTLC. Equation Y=170.12 + 29.94X - 0.0097X2, (R2 0.9997).

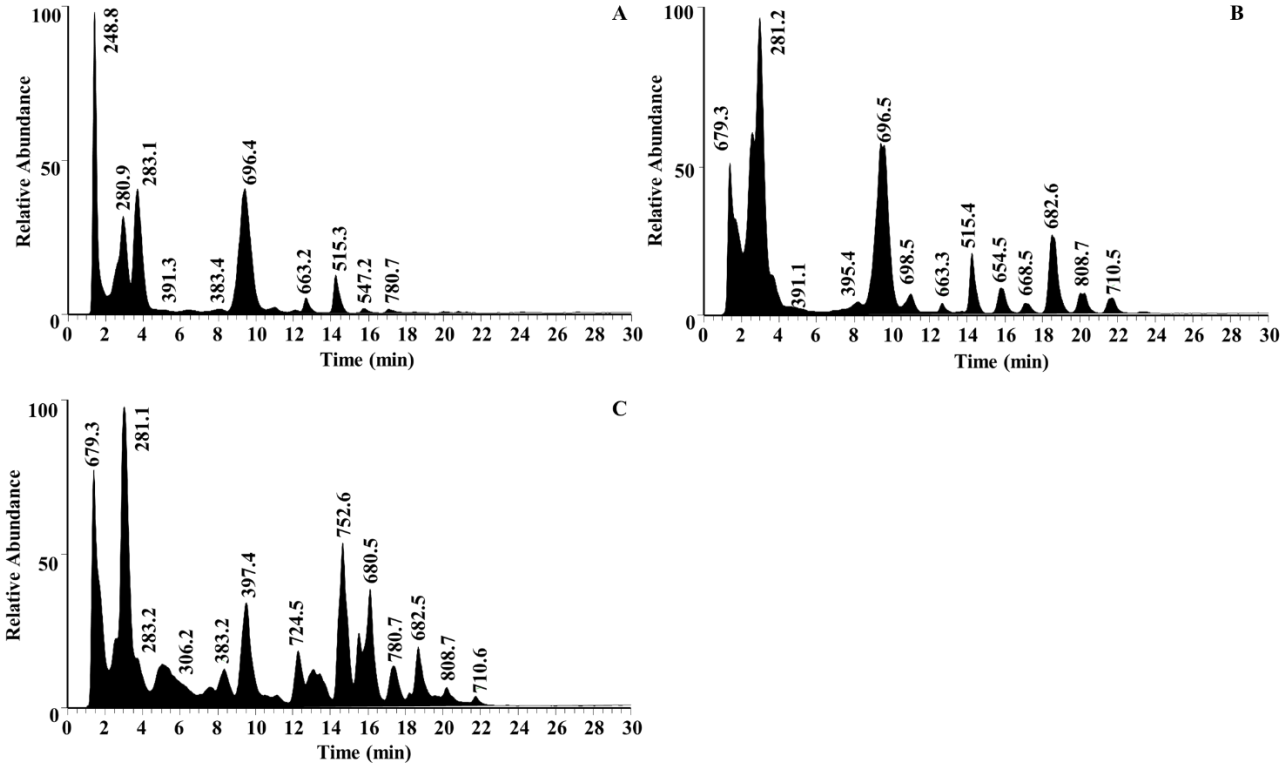

Figure A4: Base peak chromatograms (full scan: *m/z* 100 -1000) of 4N NaOH treated GlcCERs of lupin bean (A), mung bean (B) and naked barley (C) (2 h, 80 °C) using UHPLC-Triple Quadrupole MS.

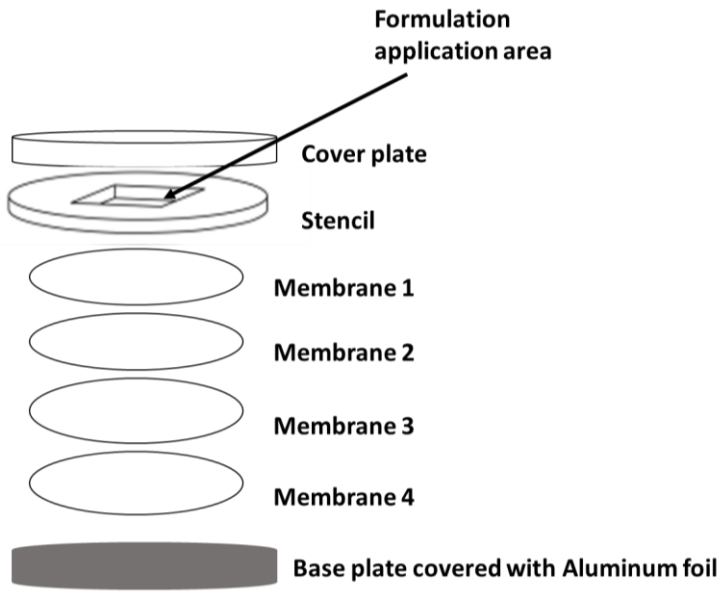

Figure A5: Schematic diagram of in-vitro multi-layer membrane release assembly.

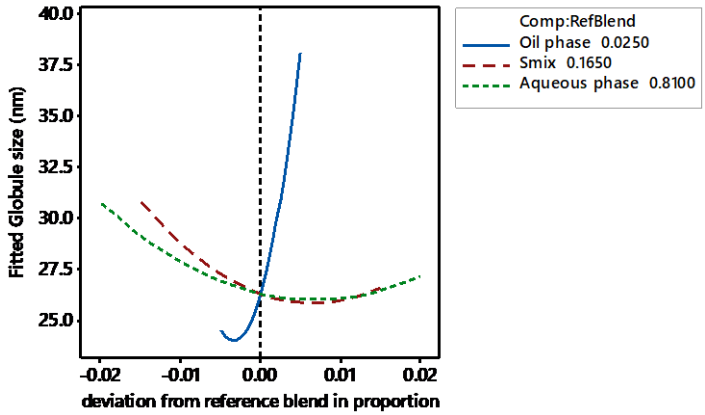

Figure A 6: Cox response trace plot showing the influence of each formulation components on NEs globule size in reference to the reference blend (RefBlend).

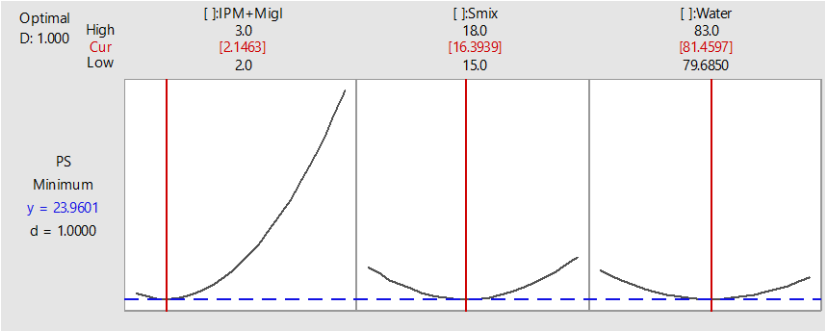

Figure A7: Optimization plot of IPM: Miglyol (1:1, *v/v*) NEs showing the optimized level of oil phase, Smix and aqueous phase with predicted globule size and formulation desirability generated using Minitab software (version 7.1.0).

		Size (d.nm):	% Intensity:	St Dev (d.n...
Z-Average (d.nm): 24.73	Peak 1:	25.41	100.0	3.443
PdI: 0.050	Peak 2:	0.000	0.0	0.000
Intercept: 0.937	Peak 3:	0.000	0.0	0.000
Result quality : Good				

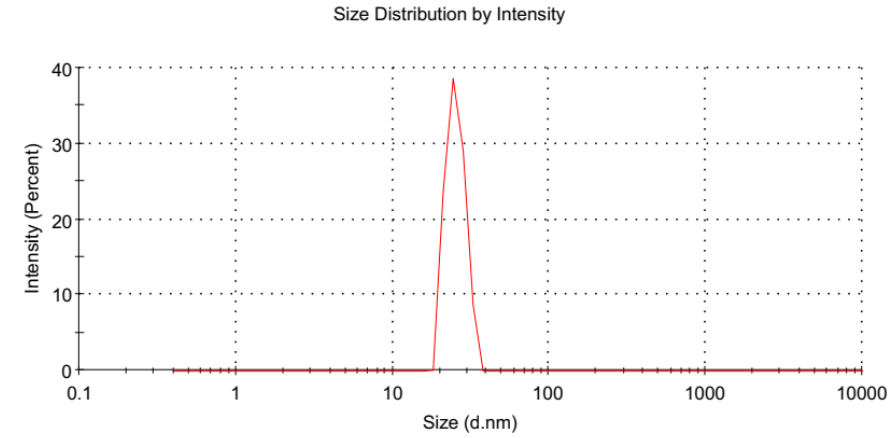

Figure A8: Particle size distribution of optimized lupin GlcCER nanoemulsion.

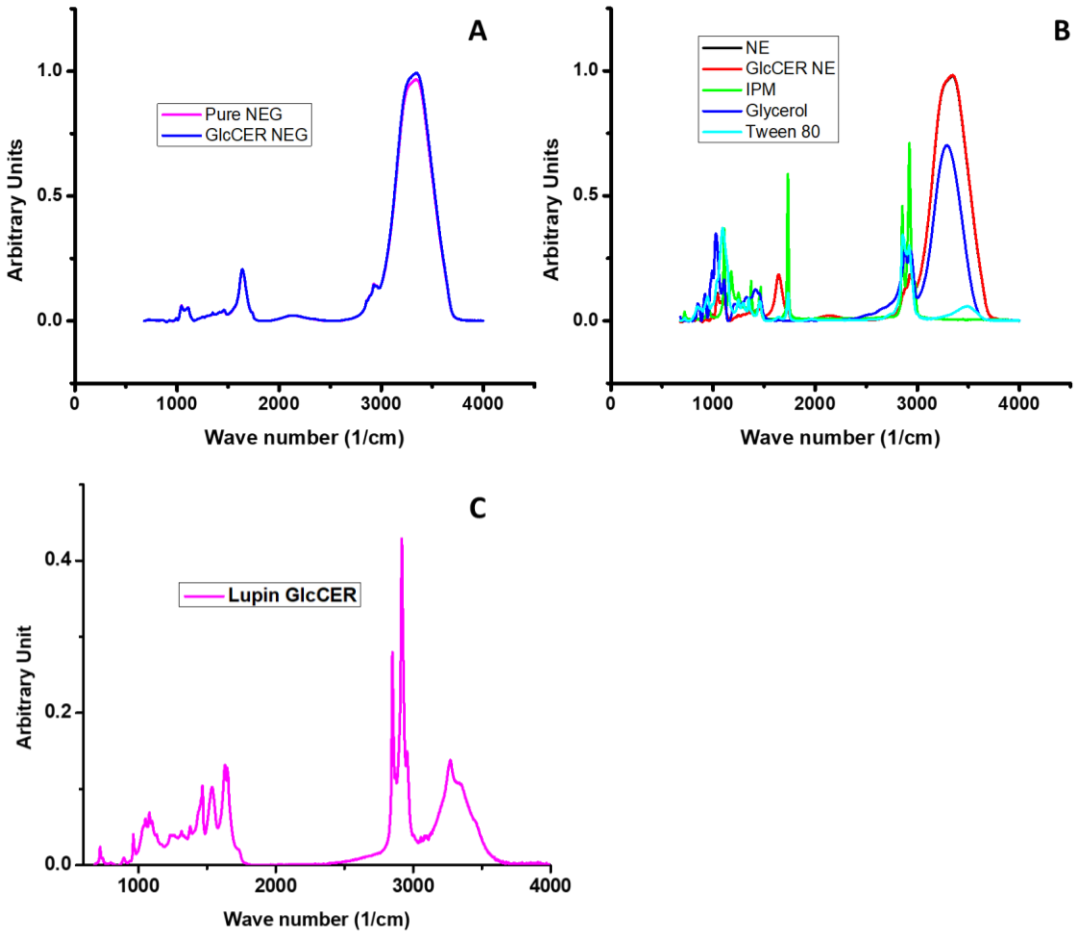

Figure A 9: FTIR spectra of pure NEG and lupin GlcCER NEG (A), pure NE, lupin GlcCER NE, and other formulation components (B) and lupin GlcCER (C).

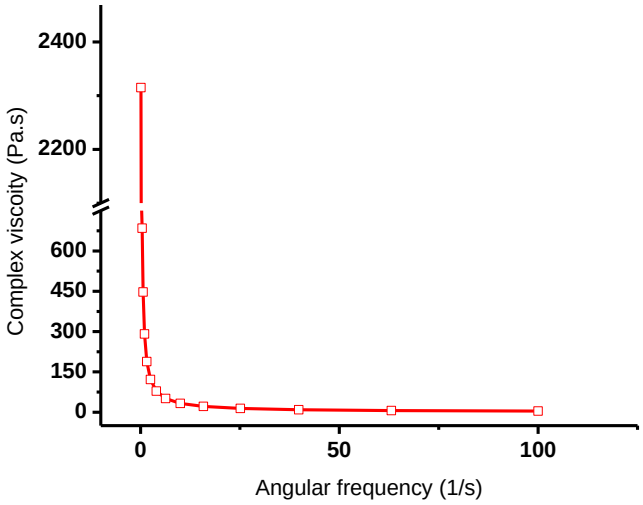

Figure A 10: the complex viscosity vs angular frequency of lupin GlcCER NEG.

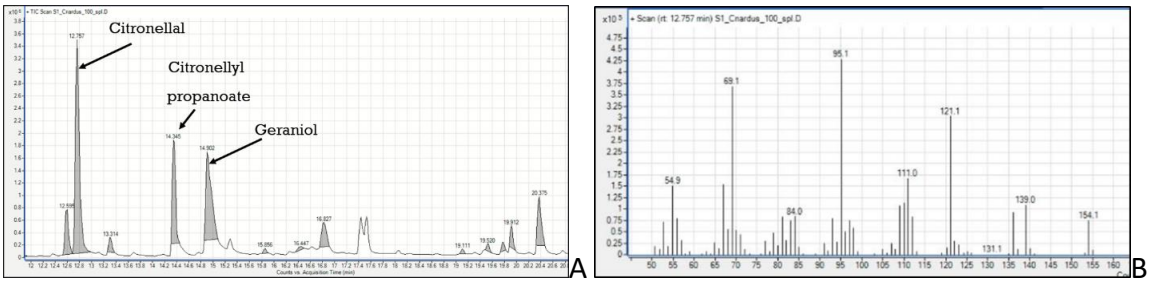

Figure A11: the base peak chromatogram of C.nardus (A) and GC-MS spectrum of citronellal which is the major component of CO (B).

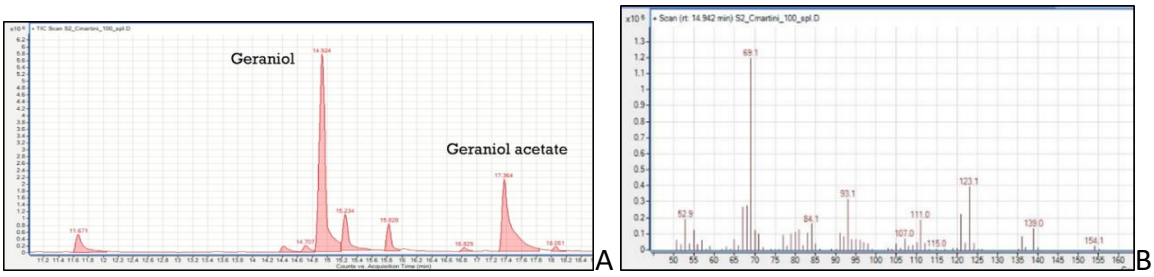

Figure A 12: the base peak chromatogram of C.martini (A) and GC-MS spectrum of geraniol which is the major component of PO (B).

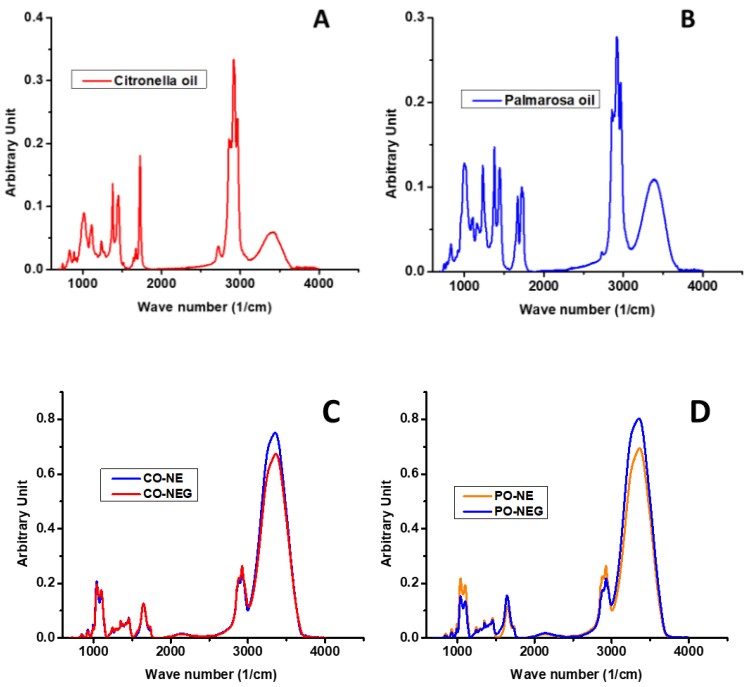

Figure A 13: FTIR spectra of CO (A), PO (B), CO NE and NEG (C) and PO NE and NEG (D).

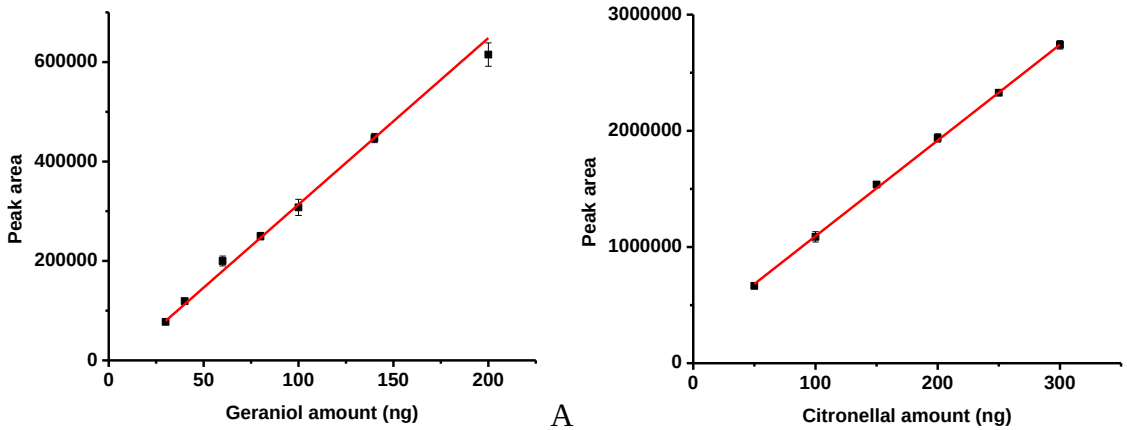

A

B

Figure A 14: calibration curves of geraniol (A) and citronellal (B).

Table A 1: Alkaline treatment conditions (temperature and time duration) of GELFs of the three plants.

Temperature (°C)	Reaction duration (h)
Room temperature	2, 3, 8, 18
80	2, 8
110	3, 6,
150	8

Table A 2: Accuracy and precision of AMD-HPTLC method for plant GlcCERs quantification (n=5).

Intra-day				Inter day			
	Accuracy		Precision	Accuracy		Precision	Acceptance range
Nominal amount (ng/band)	Calculated amount (ng/band)	% Recovered	% RSD	Calculated amount (ng/band)	% Recovery	% RSD	
50	51.94	103.89	11.87	49.54	99.09	10.44	<20%
100	105.39	105.39	10.10	106.58	106.58	13.17	<15%
400	411.28	102.82	7.69	412.72	103.18	6.98	<15%
800	802.40	100.30	4.89	780.72	97.59	6.76	<15%

RSD: relative standard deviation.

Table A 3: GlcCER species of Ethiopian plants identified after 4N NaOH treatment of GELFs at 80 °C for 2 h, using UHPLC-Triple Quadrupole MS/MS.

Source	GlcCERs species	t_R (min)	Precursor and product ion *m/z*				Target *m/z*
			$[M+H]^+$	$[M+H-H_2O]^+$	$[M+H-Glc]^+$	$[M+H-Glc-H_2O]^+$	
L, M	Glc-d18:2/h 16:0	9.5	714.5	696.5		534.4	262.9
N	Glc-d18:2/h 18:0	12.2	742.5	724.5		562.4	262.9
N	Glc-d18:2/h 20:0	14.6	770.4	752.6		590.6	262.9
L, N	Glc-d18:2/h 22:0	17.2	798.5	780.4		618.7	262.9
M, N	Glc-d18:2/h 24:0	18.6	826.7	808.6		646.6	262.9
L, M	Glc-d18:1/h 16:0	10.6	716.5		554.6	536.9	264.9
M, N	Glc-t18:1/h 22:0	15.9	816.5		654.5	636.7	262.9/280.7
M, N	Glc-t18:1/h 23:0	17.2	830.5		668.5	650.7	262.9/280.9
N	Glc-t18:1/h 24:1	16.1	842.5		680.5	662.8	262.9/280.8
M, N	Glc-t18:1/h 24:0	18.7	844.5		682.5	664.7	262.9/280.8
M, N	Glc-t18:1/h 26:0	21.7	872.5		710.5	692.6	262.9/280.8

L: lupin bean, M: mung bean, N: naked barley, $\mathbf{t_R}$: retention time.

Table A 4: Analysis of variance for NEs globule size (component proportions).

Source	DF	Seq SS	Adj	Adj MS	F	P
Regression	5	518.945	518.9452	103.7890	397.90	0.000
Linear	2	421.076	66.0613	33.0307	126.63	0.000
Quadratic	3	97.869	97.8690	32.6230	125.07	0.000
Oil*Smix	1	38.573	71.1469	71.1469	272.76	0.000
Oil*aqueous phase	1	49.969	48.5585	48.5585	186.16	0.000
Smix*aqueous phase	1	9.327	9.3267	9.3267	35.76	0.004
Residual Error	4	1.043	1.0434	0.2608		
Lack-of-Fit	3	1.023	1.0234	0.3411	**17.06**	**0.176**
Pure error	1	0.020	0.0200	0.0200		
Total	9	519.989				

Table A 5: globule size and PDI of NEs prepared at different HLB values of Smix from CO and PO (5% oil, oil: Smix, (1:1, *v/v*), 10 min ultrasonication) (n=3).

Oil type	HLB	Tween 80/Span 20 mixture		Tween 80/Transcutol P mixture	
		Globule size	PDI	Globule size	PDI
Palmarosa	11	275.85 ± 1.06	0.20 ± 0.00	175.06 ± 2.19	0.21 ± 0.01
	12	198.13 ± 3.11	0.12 ± 0.01	154.93 ± 3.08	0.17 ± 0.03
	13	208.37 ± 3.30	0.07 ± 0.02	185.10 ± 5.21	0.20 ± 0.00
	14	288.07 ± 0.99	0.08 ± 0.01	187.43 ± 5.67	0.51 ± 0.01
Citronella	11	154.51 ± 4.02	0.20 ± 0.09	134.87 ± 3.18	0.20 ± 0.02
	12	172.62 ± 2.70	0.15 ± 0.01	142.67 ± 1.86	0.17 ± 0.01
	13	185.07 ± 1.30	0.29 ± 0.01	155.97 ± 0.50	0.18 ± 0.01
	14	205.10 ± 2.31	0.24 ± 0.01	140.10 ± 1.57	0.16 ± 0.01

Mean ± SD

Table A 6: Accuracy and precision of GC-MS method for citronellal and geraniol quantification (n=3).

Standard	Nominal amount (ng)	Inter day			Intra day			
		Accuracy		Precision	Accuracy		Precision	Acceptance range
		Calculated amount (ng)	% recovery	RSD	Calculated amount (ng)	% recovery	RSD	
Citronellal	50	43.00	86.00	1.15	40.66	81.32	1.19	< 20%
	150	157.39	104.92	2.45	159.01	106.00	2.43	< 15%
	300	291.29	97.09	1.32	294.87	98.29	1.30	< 15%
Geraniol	30	24.28	80.93	16.89	25.53	85.10	4.29	< 20%
	100	102.40	102.40	7.32	99.17	99.17	5.27	< 15%
	200	202.30	101.15	5.89	197.00	98.50	3.83	< 15%

RSD: relative standard deviation